Stimuli-Responsive Polymer-Based Actuators and Sensors

by

Xue Li

A thesis submitted in partial fulfillment of the requirements for the degree of

Doctor of Philosophy

Department of Chemistry
University of Alberta

Abstract

This work covers the general scope of stimuli-responsive polymers, with the special focus on the thermoresponsive poly (*N*-isopropylacrylamide) (pNIPAm)-based hydrogels and particles (microgels) and their composites, humidity responsive polyelectrolyte-based bilayer devices, and their applications as artificial muscles, sensors and actuators.

In Chapters 3-5, a novel humidity responsive bilayer device was generated by combining poly (*N*-isopropylacrylamide)-co-acrylic acid (pNIPAm-co-AAc) microgel-based and polyelectrolytes. The two layers were used together as a glue to adhere them to a plastic substrate, which allowed them to lift weights (Chapter 3). The self-folding behavior of the bilayer devices was studied and mathematical models were built up to explain the behavior. The results showed that the model can describe the experimental data well. Accordingly, multiple 3D structures were obtained from the precisely designed 2D planar bilayer sheets (Chapter 4). Subsequently, the shape memory effect (SME) of the bilayer system was studied (in Chapter 5). The semi-crystallization of the polymer in the polyelectrolyte layer enables the SME of the device. Furthermore, the 'templated device' was obtained in order to assemble it with a strain sensor, which could serve as humidity sensors.

In the second part of the thesis, we describe the development of a semi-interpenetrated (semi-IPN) hydrogel-based bilayer actuator (Chapter 6). The polyelectrolyte is physically trapped in the chemically crosslinked pNIPAm-based

hydrogel network, which endows the bilayer with bi-directional deformations in response to pH and temperature in aqueous solution. Furthermore, they are specially designed to function as manipulators (or grippers) and small molecule release devices.

In the last part, Chapter 7 describes the synthesis of the *N, N'*-bis(acryloyl)cystamine (BAC) crosslinked pNIPAm microgels, where the crosslinking density can be altered by exposure to reducing reagents. 1D photonic crystals (etalons) are fabricated from these microgels, which show an approximately linear response to one reducing reagent dithiothreitol (DTT).

Preface

Chapter 3 of this thesis has been published as M.R. Islam, X. Li, K. Smyth, M.J. Serpe, "Polymer-Based Muscle Expansion and Contraction", *Angewandte Chemie International Edition,* 2013, 52, 10330-10333. I was responsible for the data collection and analysis (Figure 3-5, Figure 3-6), and investigation of the bending mechanism. M. R. Islam composed the manuscript and assisted in data collection. K. Smyth assisted in the data collection. M. J. Serpe was the supervisory author and was involved with the concept formation and manuscript composition.

Chapter 4 of this thesis has been published as X. Li, M. J. Serpe, "Understanding and Controlling the Self-Folding Behavior of Polymer-Based Muscles", *Advanced Functional Materials,* 2014, 24, 4119-4126. I was responsible for designing and executing experiments, data collection and analysis, and manuscript composition. M. J. Serpe was the supervisory author and was involved in the concept formation and manuscript composition.

Chapter 5 of this thesis has been published as X. Li, M. J. Serpe, "Understanding the Shape Memory Behavior of Self-Bending Materials and Their Use as Sensors", *Advanced Functional Materials,* 2016, 36, 3282-3290. I was responsible for designing and executing experiments, data collection and analysis, and manuscript composition. M. J. Serpe was the supervisory author and was involved in the concept formation and manuscript composition.

Chapter 7 of this thesis has been published as X. Li, Y. Gao, M. J. Serpe,

"Reductant-Responsive Poly (N-Isopropylacrylamide) Microgels and Microgel-Based Optical Materials", *Canadian Journal of Chemistry,* 2015, 93, 685-689. I was responsible for the data collection and analysis, and manuscript composition. Y. Gao assisted in the manuscript composition. M. J. Serpe was the supervisory author and was involved in the concept formation and manuscript composition.

Acknowledgement

First of all, I would like to express my deepest gratitude to my supervisor, Prof Michael J. Serpe for giving me the opportunity to work in his lab. He was always there to teach, guide, and support me to get through difficulties in my research. In the past five years' working, he offered me a lot of freedom to do researches I was interested in. He always offered me great advice on my future life and career plans. His great enthusiasm for both science and life strengthens my positive attitude towards my own. I thank him a lot for this. I would like to thank Serpe group members for your accompany and support.

I would like to show my great thanks to my supervisor committee members, Prof. Robert E. Campbell and Prof. Mark T. McDermott, for their valuable suggestions and comments on my research.

I would like to thank my dear parents and brother to support me throughout the years overseas. Last, but certainly not the least, I would like to thank my husband, Shengwang, who has sacrificed so much to make my career life go this far. His encouragement and advice really helps me out whenever I came across big challenges in my study. His unconditional love and support for my life truly brings me power and happiness.

Table of Contents

List of Figures

List of tables

List of Abbreviations

pNIPAm	poly (*N*-isopropylacrylamide)
LCST	lower critical solution temperature
PVCL	poly (*N*-vinylcaprolactone)
pDEAAm	poly (*N,N'*-diethylacrylamide)
p(DL)-HMPAMA	poly (*N*-(DL)-(1-hydroxymethyl) propylmethacrylamide)
ΔG	free energy of dissolution
ΔH	dissolution enthalpy
ΔS	entropy change
AAc	acrylic acid
MAAc	methacrylic acid
DMAEMA	*N, N'*-dimethyl aminoethyl methacrylate
VP	vinyl pyridine
EDC	1-ethyl-3-(3-dimethylaminopropyl) carbodiimide
CA	cinnamic acid
PAA	poly (acrylic acid)
EAPs	electroactive polymers
IPMCs	ionic polymer-metal composites
PPy	polypyrrole
GOx	glucose oxidase
ConA	concanavalin A
VPTT	volume phase transition temperature
BIS	*N, N'*-methylene-bis-acrylamide
APS	ammonium persulfate
TEMED	*N, N, N', N'*-tetramethylethylenediamine
DLS	dynamic light scattering

AFM	atomic force microscope
SMP	shape memory polymers
SME	shape memory effect
T_{tran}	transition temperature
T_g	glass transition temperature
T_m	melting temperature
CNTs	carbon nanotubes
PEG	polyethylene glycol
LCE	liquid crystal elastomers
1D	one dimensional
2D	two dimensional
3D	three dimensional
PCs	photonic crystals
m	diffraction order
h_l	thickness of the low refractive index material
h_h	thickness of the high refractive index material
n	refractive index
λ	the wavelength maximum of the peaks
d (in Chapter 2 and 7)	the spacing between the mirrors
θ (in Chapter 2 and 7)	incident angle
APBA	aminophenylboronic acid
pNIPAm-co-AAc	poly(*N*-isopropylacrylamide)-co-acrylic acid
PMMA	poly (methyl methacrylate)
SWNTs	single-wall carbon nanotubes
DEC	degree of electrostatic complexation
PILTf2N	poly(3-cyanomethyl-1-vinylimidazoliumbis-(trifuoromethanesulfonyl) imide)

C-pillar[5]arene	carboxylic acid-substituted pillar[5]arene
LCEs	liquid crystal elastomers
pHEMA	polyhydroxyethylmethacrylate
pHEMA-co-AAc	poly(hydroxyethylmethacrylate-co-acrylic acid)
pDADMAC	poly(diallyldimethylammonium chloride)
PSS	poly(sodium 4- styrene-sulfonate)
APMAH	*N*-3-aminopropyl methacrylamide hydrochloride
PEM	polyelectrolyte multilayer
PAH	poly (allylamine hydrochloride)
F_c	contracting forces
τ	torque
k	force parameter
θ (in Chapter 4)	bending angle
d (in Chapter 4)	thickness of layers
R	radius
PCL	polycaprolactone
rcf	relative centrifugal force
PDMS	polydimethylsiloxane
TEM	transmission electron microscopy
LED	light emitting diode
FESEM	field emission scanning electron microscope
XPS	X-ray photoelectron spectroscopy
IPN	interpenetrating polymer network
CV	crystal violet
DEAP	2, 2-diethoxyacetophenone
BAC	*N, N'*-bis(acryloyl)cystamine
DTT	dithiothreitol

DIC	differential interference contrast
PBS	phosphate buffer solution
GEMA	glucosyloxyethyl methacrylate
LBL	layer by layer assembly

Chapter 1: Introduction to Stimuli-Responsive Polymer Based Materials

Stimuli-responsive polymers are able to change their chemical and/or physical properties in response to small changes in their environment. They can exist as linear polymer chains in solution and surfaces, or can be crosslinked to generate polymer networks such as gels. In each case the polymers have different degrees of mobility, which directly impacts their properties, and ultimately their applications. This Chapter is intended as a general introduction to stimuli-responsive polymers and stimuli-responsive polymer-based materials. This Chapter is divided into three parts: 1) stimuli-responsive polymers; 2) stimuli-responsive polymer-based hydrogels; 3) stimuli-responsive polymer-based solids. As a majority of this thesis is focused on poly (*N*-isopropylacrylamide) (pNIPAm)-based materials, considerable time is focused on their discussion.

1.1 Stimuli-responsive polymers

Stimuli-responsive polymers are high molecular weight molecules (macromolecules), which undergo physical and/or chemical changes in response to

external stimuli.[1] For example, they can be made to respond to various stimuli, which could be classified as physical stimuli (temperature, light, and electricity),[2,3] chemical stimuli (pH, ionic strength, chemicals, and redox reagents),[4,5] or biochemical stimuli (antigen, glucose, ligands, and enzymes).[6,7]

1.1.1 Temperature responsive polymers

Of all the stimuli-responsive polymers, temperature responsive polymers are the most extensively studied. Of the various temperature-responsive polymers, those that exhibit a lower critical solution temperature (LCST) are the most prominent. Polymers that have a LCST are completely soluble in a particular solvent at temperatures below the LCST, while they are insoluble at temperatures above the LCST. This is known as a phase transition, where the polymer transitions from a random coil ("soluble") to a globular state ("insoluble"). The most extensively studied LCST polymers are water soluble, and include poly (*N*-isopropylacrylamide) (pNIPAm),[8,9] poly (*N*-vinylcaprolactone) (PVCL),[10,11] poly (*N,N'*-diethylacrylamide) (pDEAAm),[12] and poly (*N*-(DL)-(1-hydroxymethyl) propylmethacrylamide) (p(DL)-HMPAMA).[13] For most of the investigations in this thesis, pNIPAm was used. It has been reported in many publications that pNIPAm possesses a LCST of ~ 32 ºC where it undergoes a coil-to-globule transition in water. [9,14-18] A schematic depiction of pNIPAm can be seen in Figure 1-1. When pNIPAm is mixed with water, the free energy of dissolution (ΔG) can

be expressed as follows:

$$\Delta G = \Delta H - T\Delta S \qquad (1)$$

where ΔH is the dissolution enthalpy of pNIPAm and ΔS is the entropy change (mainly a result of water association with the polymer). ΔH favors dissolution due to hydrogen bonding of water with pNIPAm ($\Delta H < 0$),[2] as shown in Figure 1-1. Although, ΔS for dissolution of pNIPAm is unfavorable due to structuring of water around pNIPAm's isopropyl groups, and subsequently losing their ability to freely move in solution. This is shown schematically in Figure 1-1. [19] Therefore, at low temperature, pNIPAm is solvated with water and dissolves due to the favorable ΔH, which makes ΔG for dissolution negative. As the solution temperature gradually increases, ΔG becomes less negative. When the solution temperature surpasses the LCST, ΔG for dissolution of pNIPAm becomes positive, which makes dissolution unfavorable and pNIPAm undergoes the coil ("soluble")-to-globule ("insoluble") transition at the LCST.

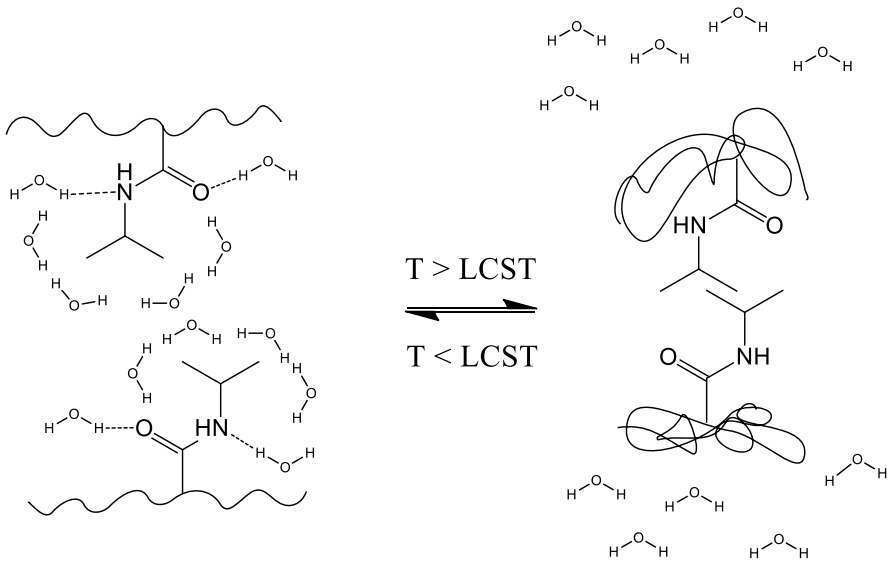

Figure 1-1 Structure of pNIPAm and illustration of pNIPAm's temperature induced phase transition in water.

1.1.2 PH- responsive polymer

The LCST of pNIPAm can be tuned as desired by copolymerizing hydrophobic, hydrophilic, and/or charged/ionizable monomers with *N*-isopropylacrylamide (NIPAm).[20] For example, pH responsive monomers that possess ionisable moieties can be copolymerized with pNIPAm to alter its responsivity. The comonomers can be either weak acids (such as acrylic acid (AAc) and methacrylic acid (MAAc)[21,22] or weak bases (such as *N, N'*-dimethyl aminoethyl methacrylate (DMAEMA) and vinyl pyridine (VP)).[23,24] In this dissertation, AAc, possessing a pKa of ~ 4.25, was selected to render pNIPAm-based materials sensitive to pH and ionic strength. Specifically, at pH > 4.25 the AAc groups are deprotonated making polymers negatively charged and leading to the

extension of polymer chains due to the charge-charge (Coulombic) repulsion along the polymer chain, while the polymer collapses at pH < 4.25 due to the protonation of AAc. Another advantage of AAc is that it allows the polymer to be modified with other small functional molecules due to their reactivity in the presence of 1-ethyl-3-(3-dimethylaminopropyl) carbodiimide (EDC). This approach is particularly appealing when delicate molecules (e.g., biomolecules) are to be covalently attached to polymers.[25-27]

1.1.3 Light responsive polymers

Light responsive polymers are typically equipped with photochromic functional groups, which undergo light induced reactions/responses that affect the polymer physical/chemical state. As shown in Figure 1-2, the most common photo-sensitive molecules are classified into three categories: 1) azobenzene derivatives which undergo reversible cis-trans photoisomerization;[28-30] 2) triphenylmethane leuco derivatives that undergo ionic dissociation under ultraviolet irradiation;[31] and 3) reversible photodimerization of the cinnamic acid (CA) group.[32] In this dissertation, we utilized the ability of azobenzene to undergo reversible cis-trans isomerization in response to light of specific wavelengths.[33] The isomerization gives rise to the changes in molecular size (the distance between the 4 and 4' carbons decreases from 0.9 nm to 0.55 nm), shape (rodlike to bent) and polarity.[34] The responsive nature of azobenzene has been applied in

photoinduced deformation of liquid crystalline polymers.[35,36] It has been incorporated into a variety of other polymer systems as well, including pNIPAm,[37] pDMAEMA,[38] and poly (acrylic acid) (PAA).[29]

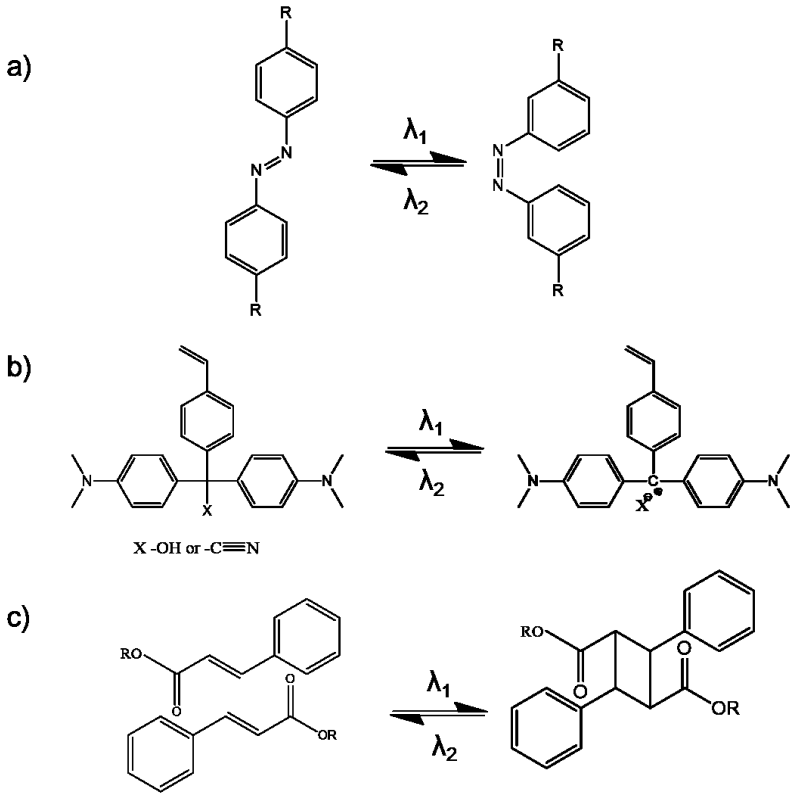

Figure 1-2 Schematic illustration of light-induced isomerization and photochemical reactions. a) Trans–cis photoisomerization of azobenzene groups; b) Photoinduced ionic dissociation of triphenylmethane leuco derivatives; c) Photodimerization of the cinnamic acid.

1.1.4 Electricity responsive polymers

Electricity responsive polymers (or electroactive polymers (EAP)),[39] can be

subdivided into two groups: ionic EAPs and electronic EAPs.[40] Ionic EAPs include ionic polymer-metal composites (IPMCs)[41] and conjugated polymers,[42] and their response depends on ion and solvent transport in fluids to effect volume changes of polymers. Electronic EAPs include piezoelectric polymers, electrostrictives, and dielectric elastomers,[43] which require high voltages and must therefore be shielded from the fluid environment.[40] A common example of an ionic EAP is the conjugated polymer polypyrrole (PPy), which was utilized in this dissertation.[44] PPy is characterized by alternating single and double bonds along the polymer backbone, as shown in Figure 1-3. PPy can be either p- or n- doped by chemical and/or electrochemical processes during which the number of electrons associated with the polymer backbone changes.[45] Specifically, positive charges are delocalized along the polymer chains after removal of electrons (oxidation) by the application of a positive potential or reacting with oxidants. To maintain charge neutrality of the polymer chains, negatively charged anions are incorporated into the polymer to compensate for the delocalized positive charges, which is called p-doping. The positively charged polymer backbones can be rendered neutral when a potential is applied to reduce the polymer. Therefore, the small, mobile anions will be expelled from the polymer resulting in the collapse of the polymer. However, when large, immobile anions are incorporated in the polymer, the reduction results in swelling of the polymer chains due to the higher osmotic pressure of the more highly charged species.[46-48] PPy possesses many advantageous properties that allows them to be used in myriad applications, e.g., artificial muscles and actuators,[49] biomimetic devices,[50]

and biomedical applications.[51] Specifically, they are light weight, exhibit a large strain, can be operated in liquid electrolytes at room temperature, and can be activated by applying low voltages.

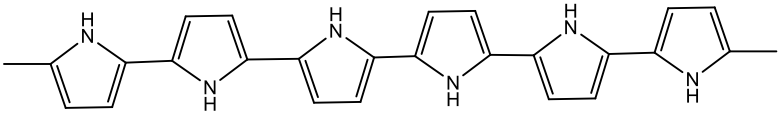

undoped

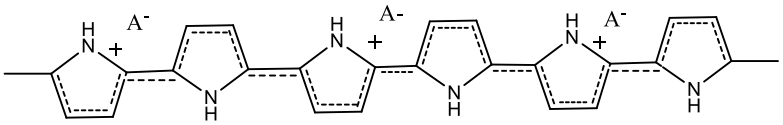

p-doped

$$P^{+}(A^{-}) + M^{+}(aq) + e^{-} \longleftrightarrow P^{0}(A^{-}M^{+}) \quad \text{(large anion doped)}$$

$$P^{+}(A^{-}) + e^{-} \longleftrightarrow P^{0} + A^{-}(aq) \quad \text{(small anion doped)}$$

Figure 1-3 Structures of undoped and p-doped PPy and the reduction of PPy doped with large anion and small anion respectively.

1.1.5 Biomolecule responsive polymers

Smart polymers are becoming very important for biomedical applications, such as biosensing, controlled drug delivery, and tissue engineering.[52-56] Therefore, it is often advantageous to develop polymers to detect biological stimuli (biomolecules), such as glucose, DNA, antigen, and redox/thiols (e.g. Glutathione), which offers the possibility of early disease diagnosis and hence the chance to improve public health.[57]

Due to their potential applications for both glucose sensing and controlled insulin

delivery, polymers that respond to glucose have been widely studied. This is also a topic studied in this dissertation. A majority of studies related to glucose responsive polymers are based on glucose oxidase (GOx)-catalyzed reaction of glucose with oxygen. In this case, instead of directly responding to the concentration of glucose, the response comes from the interaction of the by-products (e.g. gluconic acid and H_2O_2) with the polymer.[58-60] Therefore, a pH responsive polymer loaded with GOx can be used to detect pH drop of the solution upon gluconic acid generation.[58,59] Another type of glucose responsive polymer system utilizes competitive binding of glucose with glycopolymer-lectin complexes.[61] The lectin most commonly employed to sense glucose is concanavalin A (ConA). Glycopolymers tend to crosslink in the presence of ConA due to their multivalency. However, these crosslinks can be disrupted in the presence of glucose. [62,63]

The very specific interaction of antibodies and antigens can also be used to introduce bioresponsivity into polymers. For example, chemical conjugated antibody-antigen pairs can serve as reversible crosslinkers within polymer networks. Upon the addition of a free antigen, the competitive binding of antibody results in the loss of antibody-antigen crosslinks and concomitant swelling of the polymer network.[64-66]

Finally, polymers which are responsive to both reductants and/or oxidants (redox responsive polymers) could also be used to yield bioresponsive polymers. In one example, the interconversion of thiols and disulfides plays an important role in many biological process, and can be exploited for bioresponsivity.[67,68] Therefore, redox/thiol responsive

polymers have been widely studied, especially in fields of biosensors and controlled drug delivery.[69,70] Disulfide bonds can be reversibly converted to thiols by exposure to various reducing agents and/or undergo disulfide exchange in the presence of other thiols, polymers containing disulfide linkages can be considered both redox and thiol responsive.[71,72]

1.2 Stimuli-responsive hydrogels

Hydrogels are defined as chemically and/or physically crosslinked hydrophilic polymer networks, which are able to swell with water many times their dry mass.[73-75] Physical hydrogels are formed by dynamic crosslinking of polymer chains, which are held together by non-covalent interactions such as hydrogen bonding, hydrophobic interaction and electrostatic interactions.[76-79] Chemical hydrogels are formed by covalent crosslinks between the polymer blocks, which is achieved by reacting monomers in the presence of a monomer containing two or more polymerizable groups (crosslinker). Compared with physical crosslinked hydrogels, chemical hydrogels are inherently more stable in a variety of environmental conditions, such as pH and ionic strength changes which may weaken the physical interactions. Therefore, chemically crosslinked hydrogels have a permanent structure, which has allowed them to be used for numerous applications such as sensors, actuators, and drug delivery devices.

A stimuli-responsive hydrogel is a polymer network that is completely (or partially)

composed of units (monomers, or polymers), e.g., see section 1.1. They can also be made to respond to multiple physical, chemical and biochemical stimuli.[80-84] That is, hydrogels capable of responding to many different stimuli can be generated. The responsivity of hydrogels arises from the reversible changes in solvation of the polymer chains constituting the hydrogel network when exposing them to the respective stimuli. The most widely used theory to explain the swelling of neutral hydrogels is the theory of Flory and Rehner.[85] Specifically, the swelling degree of a hydrogel network is determined by the free energy for the network expansion in solvent, which depends on the free energy of mixing between solvent and polymer chains, and the crosslinking density of the hydrogel networks. Whereas the crosslinking density of the hydrogel network remains unchanged, the free energy for the network expansion depends mainly on the hydrogel components. Thus, the response of a hydrogel to external stimuli is determined by the hydrogel composition, and the degree of crosslinking. They can undergo reversible volume phase transitions, such as swelling, collapse, and solution-to-gel transitions, upon exposure to stimuli due to the molecular interactions.

The most commonly studied hydrogel systems are composed of thermoresponsive pNIPAm. As mentioned in section 1.1.1, linear pNIPAm possesses the ability to respond to temperature changes in aqueous media by undergoing a coil-to-globule transition. Likewise, pNIPAm hydrogels show temperature dependent deswelling when the temperature is higher than the LCST. The transition temperature for hydrogel is usually called volume phase transition temperature (VPTT). The deswelling behavior can be

explained by competing solvation mechanisms, where at high temperature above VPTT the favorable polymer-water interactions are disrupted and polymer-polymer interactions begin to dominate, causing the polymer network to deswell therefore expelling its retained water.[86,87] Generally, pNIPAm-based hydrogels are crosslinked with *N*, *N*′-methylene-bis-acrylamide (BIS) or dihydroxyethylene-bis-acrylamide by redox polymerization at room temperature using ammonium persulfate (APS) and *N, N, N', N'*-tetramethylethylenediamine (TEMED) as a pair of redox initiators.[88,89] These structures can be seen in Figure 1-4. They have also been prepared by a radiation-induced polymerization technique, which allows the degree of crosslinking to be easily controlled by irradiation conditions.[90] A variety of hydrophilic or hydrophobic monomers with other functional groups can be added to the pNIPAm-based hydrogel structure and render them responsive to many other stimuli, such as pH, light, electricity, and biomolecules.[65,91-93] The mechanisms corresponding to their responsivity to these stimuli have been detailed in section 1.1.

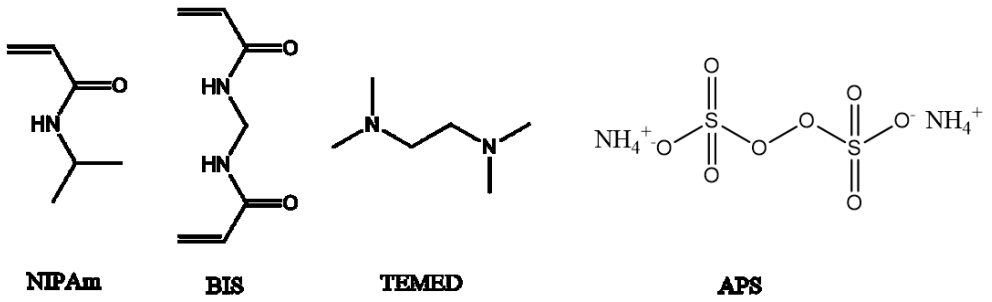

Figure 1-4 Chemical structures of NIPAm, BIS, TEMED, and APS.

Colloidally stable hydrogels (microgels or nanogels depending on their diameter) could also be generated, and have found numerous applications.[94,95] PNIPAm-based microgels have the same temperature dependent swelling/deswelling behavior as the corresponding hydrogels,[96] yet they respond with faster kinetics due to their smaller dimensions.[97] Over the past few decades, pNIPAm-based microgels have gained considerable attention as “intelligent” materials for many applications. These include their uses in fabrication of photonic crystals,[98,99] drug delivery,[100,101] and cell culture.[102,103] PNIPAm-based microgels can be synthesized using a variety of approaches, although our group uses temperature induced free-radical precipitation polymerization.[98,104-106] Typically, as shown in Figure 1-5a the main monomer NIPAm and crosslinker BIS are dissolved in water, and O_2 is removed from the mixture by purging with N_2 gas. This solution is allowed to stir and heat to 70 ºC. Then comonomers (e.g. AAc) can be added to the reaction mixture, followed up by addition of the free-radical initiator APS, which produces free radicals due to its cleavage in solution at high temperature. The free radicals cause pNIPAm chains to grow in a homogeneous fashion until they reach a critical chain length, after which the growing chain collapses to become a colloidally unstable "precursor particle". Then, the precursor particles serve as nuclei for particle growth into a colloidally stable microgels.[96] This growing process of microgels is demonstrated in Figure 1-5b.

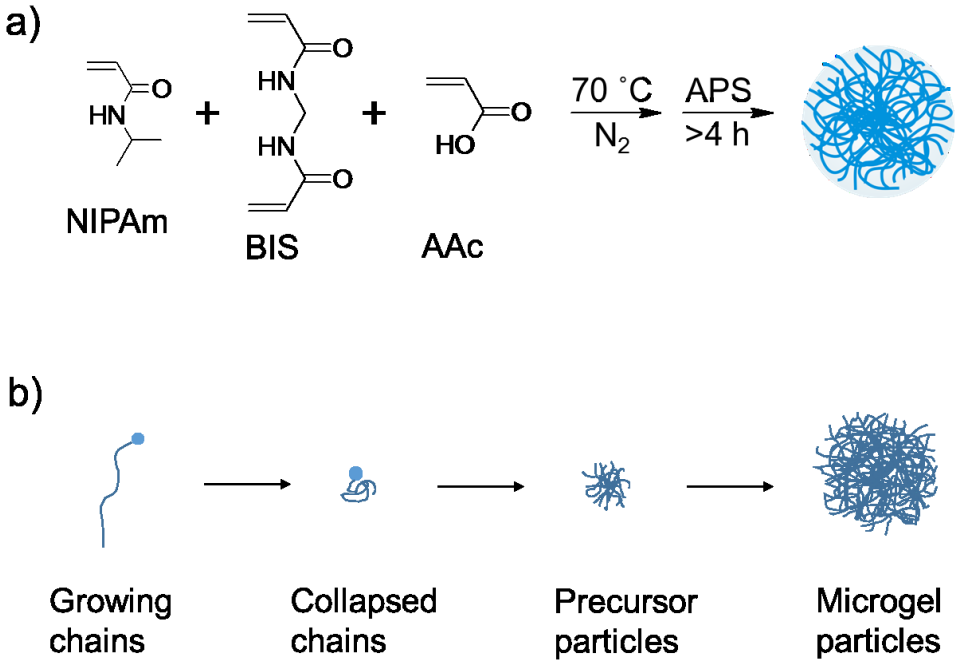

Figure 1-5 a) Schematic of the synthesis of microgels, b) Growth of microgels during the free radical precipitation polymerization.

PNIPAm-based microgels are able to decrease/increase size respectively in response to increase/decrease in temperature. This process is highly reversible. Visibly, a dilute aqueous solution of microgels appears to be clear at low temperature due to the high water retention in the microgel network. When the temperature of the system is increased to above the LCST of pNIPAm, the microgel network deswells by expelling most of the water from their network structure and the resultant microgel solution appears cloudy. The swelling and deswelling of microgel particles can be characterized by dynamic light scattering (DLS). DLS is able to give particle size, in a dilute solution, by monitoring fluctuations in the scattered light intensity as a function of time. In addition, microgels can also be characterized by rheology, atomic force microscope (AFM) and electron

microscopy.[107,108]

1.3 Stimuli-responsive solids

The stimuli-responsive materials introduced above have focused on materials interactions in solvent rich environment. In this section, stimuli-responsive solids, such as shape memory polymers and shape memory polymer-based devices, will be introduced.

Shape memory polymers (SMPs) are defined as polymers, which are able to "memorize" a permanent shape. Under appropriate conditions of temperature and stress they can be manipulated in such a way that a specific temporary shape can be "fixed" by shape programming (such as by twisting, spinning, stretching, and/or pressing). Subsequently, triggered by stress-free external stimuli (heat or light) they will transform from their temporary to permanent shape. This is called the shape memory effect (SME).[109] These types of SMPs are considered as classical SMPs ("one way SME"), which requires a new programming step to reestablish the temporary shape once the permanent shape is recovered from the last deformation. In contrast, some SMPs or SMPs-based devices, which don't require repeated programming but show reversible shape changes in response to external stimuli, are emerging as an interesting class of SMPs. They exhibit so-called "two way or reversible SME". A schematic illustration of one way SME and two way SME is shown in Figure 1-6. In one way SME, the blue represents the permanent state of SMPs. Upon exposure to stimuli, the temporary state is

formed by programming. The yellow represents the temporary state of SMPs after exposure to stimuli. Likewise, in two way SME, the blue is the permanent state of SMPs, and the yellow represents the temporary state of SMPs.

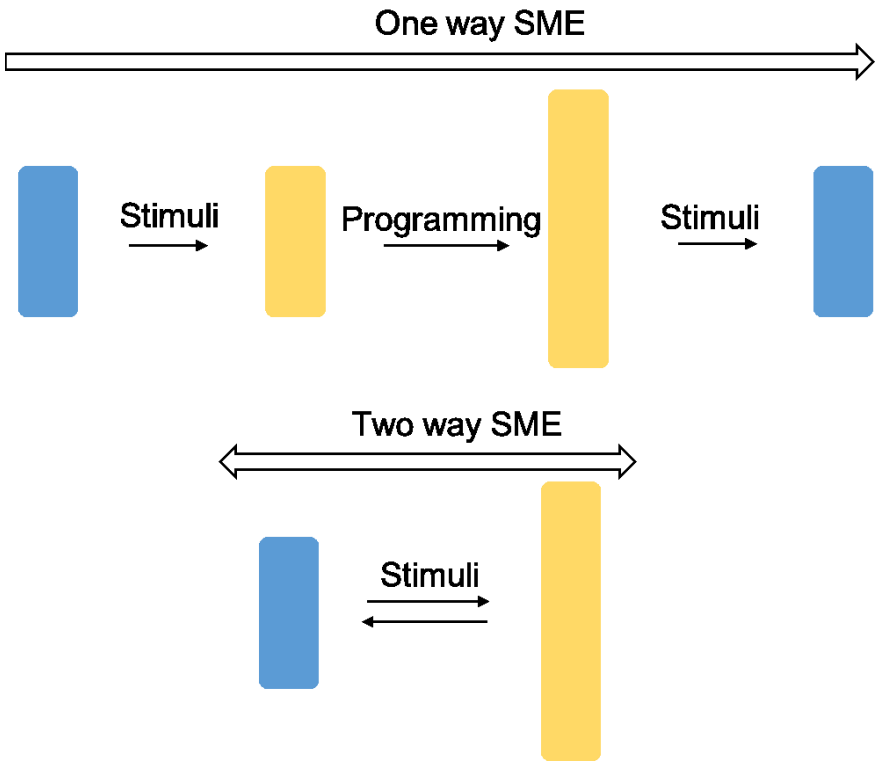

Figure 1-6 Schematics of one way and two way SME.

1.3.1 Shape memory polymers with one way SME

Generally, SMPs contain at least two different phases, a “hard” phase (provides the stable polymer network) and a “soft” phase (provides the reversible switching transition). The hard phase dictates the original shape and serves as the driving force for the shape recovery. The hard phase can be achieved via chemical crosslinks (e.g. covalent bond),

physical crosslinks (e.g. molecule entanglement), crystalline phases, and/or interpenetrating networks.[110-113] The "soft" phase is responsive to the external stimuli and responsible for fixing the temporary phase, which can undergo crystallization-melting transition, vitrification-glass transition, liquid crystal anisotropic-isotropic transition, and/or reversible molecule crosslinking (such as photodimerization and Diels-Alder reaction).

For example, thermally induced one way SMPs contain both a hard phase and a soft phase. At room temperature, the SMPs are rigid plastics. Upon heating above the transition temperature (T_{tran}) (a melting temperature T_m or a glass transition temperature T_g), of the soft phase, the material becomes an elastomer. This heating allows the easy macroscopic deformation when the external force is applied. When it is cooled to a temperature below the T_{tran}, the deformation will be maintained even after the removal of the external force. When heating the material again above T_{tran}, SMP will recover its original shape in the absence of external force.[114] Most investigated thermal transition-based SMPs are based on polyethers, polyester and polyolefins.[113,115-120] The soft phases of all these SMPs reveal a low T_m or relatively high T_g, which could be tuned in a wide range depending on the degree of branching as well as the crosslinking density of the polymer.[121,122] In most cases the hard phase of the T_m based SMPs is achieved by crosslinks or crystalline phases, therefore these SMPs possess a higher stiffness than other SMPs as well as faster shape recovery from the temporary shape.[109] Compared with the T_m based SMPs, T_g based SMPs show a slower shape recovery due to the broad glass

transition of the soft phase.[110] The soft phases are amorphous domains in the polymer, while the hard phases could be achieved by crosslinks and crystalline domains.[123-126]

Although the transition temperature can be tuned by chemical modification of SMPs, direct heating is required in most cases. In contrast, physically doped T_{trans} -based SMPs with specific fillers enable the shape memory effect without direct utilization of heat.[127] Electric field responsivity can be achieved if SMPs are doped with enough electrical conductive fillers, such as carbon nanotubes (CNTs), polypyrrole, Ni powders and nanorods.[128-132] When applying voltage to these conductive filler doped SMPs, the internal resistance-induced Joule heating will increase the temperature of the polymer and trigger the SME. Various strategies have been developed to improve the electricity conductivity of the fillers inside SMPs, such as new filler content and shape, adjusting voltage applied, and SMPs' modification.[133-135]

On the other hand, for T_g based SMPs, although the transition temperature of SMPs can be tailored by chemical modification, it's not easy to produce SMPs with functionally gradient recovery temperatures below the room temperature. However, it may be realized by penetrating solvent molecules into the amorphous phase area of SMPs.[136-139] The solvent molecules serve as plasticizers in the polymer and increase the flexibility of the polymer chains in this phase. Therefore, the T_g of the SMPs may gradually drop to temperatures below room temperature with different amounts of solvent molecules trapped inside. This will lead to the shape recovery of the deformed SMPs without external heat. For example, to make SMPs water responsive, hydrophilic materials, such

as polyethylene glycol (PEG) and chitosan, were introduced in the SMP networks.[137,140]

To make SMPs light responsive, one simple method is to incorporate light responsive fillers in SMPs, which is a similar concept to electricity responsive SMPs. The fillers may be gold nanoparticles, CNTs, et al.[141,142] They are able to absorb a specific wavelength of light (e.g. near-infrared light) and convert it to heat (so called photothermal effect), which increases the temperature of SMPs to trigger shape recovery. Secondly, SMPs can be equipped with functional groups undergoing reversible photodimerization or metal-ligand coordination, which effects the shape recovery, in response to light irradiation. This method, which is not the investigation in this dissertation, will not be discussed in deep detail.

1.3.2 Shape memory polymer with two way SME

Two way SMEs (or reversible SMEs) are able to switch between two shapes (memorized shape and temporary shapes) many times upon exposure to external stimuli without the requirement of external mechanical work (shape programming). However, in order to achieve the reversible SME, an internal “driving force” for the shape recovery (back transformation) is required.

Reversible SMPs can be split into two categories: free-standing reversible SMPs (fabricated from two-way SMPs) and engineered (e.g. laminated) SMPs based devices (fabricated from one-way or two-way SMPs). The first category is based on the

molecular designs of the polymers, which contains liquid crystal elastomers (LCE), liquid crystal monomer included polymer network, or bidirectional SMPs. LCE undergoes transition between the anisotropic and isotropic phase depending on the change of the order of mesogens in LCE in response to temperature.[143,144] The most important fact is that mesogens in LCE are uniformly aligned. Macroscopically, the LCE will be effected to expand/contract reversibly when the temperature becomes higher/lower than the transition temperature. Instead of depending on temperature regulated phase changes, the azobenzene included LCE are capable of reversible shape changes in response to light of specific wavelength.[145] Polymer networks incorporating liquid crystal monomers have been utilized to fabricate reversible SMPs as well.[146] Moreover, bidirectional SMPs are designed by generating two transition switches (e.g. two crystalline domains) in the polymer. The domain with high T_m determined the original state, while the domain with low T_m is responsible for the reversible shape changes of the polymer.[147]

Reversible SMPs based devices are engineered from the classic SMPs or reversible SMPs by e.g. laminating or patterning. Typically, bilayer devices are formed after laminating a layer of SMPs with a passive elastic polymer. The imbalance of the internal stresses in the two layers as a result of external stimuli can produce a driving force for reversible SMEs.[148,149] The introduction of the bilayer systems allows for many possible reversible shape transformations of SMPs without the need of external forces. The bilayer system featured with the reversible SME is extensively investigated in the dissertation.

This Chapter described the general behavior of “smart” polymers exposed to

different stimuli. This dissertation is focused mainly on pNIPAm-based hydrogels and microgels, and shape memory polymers. They are fabricated into one dimensional (1D) photonic crystals by thin film deposition, and bilayer systems fabricated from the shape memory polymer are used for artificial muscles, generating three dimensional (3D) structures, sensors and actuators. The next Chapter will give an introduction to photonic crystals fabricated from microgels, shape memory polymer-based bilayer actuators, and their potential applications.

Chapter 2: Stimuli-Responsive Polymer Based Photonic Crystals and Actuators

Much of this thesis is focused on stimuli-responsive polymer-based layered structures, spanning from one-dimensional (1D) photonic crystals to laminated polymer actuators. Therefore, this Chapter will serve as an introduction to these topics.

2.1 Photonic crystals

Photonic crystals (PCs) are materials composed of building blocks of various refractive indexes organized in some fashion in space. The building blocks can be planar layers, pillars, or spherical colloids. These building blocks can interact with impinging electromagnetic radiation to yield interference between specific wavelengths of the impinging radiation, which can yield color if the periodicity in the PC is on the same length scale as visible light wavelengths. There are many examples of natural PCs, including butterfly wings, peacock feathers, and the opal gemstone.[150,151] Various materials, such as metals, semiconductors, ceramics and polymers have been used to fabricate PCs with periodicity in one-, two-, and three-dimensions (1D, 2D, 3D). As shown in Figure 2-1a, the periodicity exists in one dimension for 1D PCs, which are typically produced by layer-by-layer deposition, and spin-coating.[152,153] 2D PCs display

periodicity in two spatial directions. Top-down methods, such as photolithography and etching, are primarily used to produce 2D PCs, and the schematic representation of 2D PCs is shown in Figure 2-1b. The Asher group is well known for generating and exploiting 2D PCs for various applications.[154,155] 3D PCs exhibit periodicity in three dimensions, as shown in Figure 2-1c. The primary method to fabricate 3D PCs is the self-assembly of monodispersed nano-spheres in a host.[156-158]

By interacting with the incident light (via reflection, refraction, and diffraction), the ordered material will produce interesting optical properties, e.g. color. The wavelength of light (color of light) that is reflected from a PC depends primarily on the distance between the ordered features/building blocks, thus PCs can exhibit specific color. If the distance between the PCs building blocks is changed, for example, by a chemical or physical stimulus, the wavelength of reflection (and color) will also change. Therefore, this effect enables photonic crystals a wide range of applications, such as sensing, displays, and telecommunications.[56,159-167]

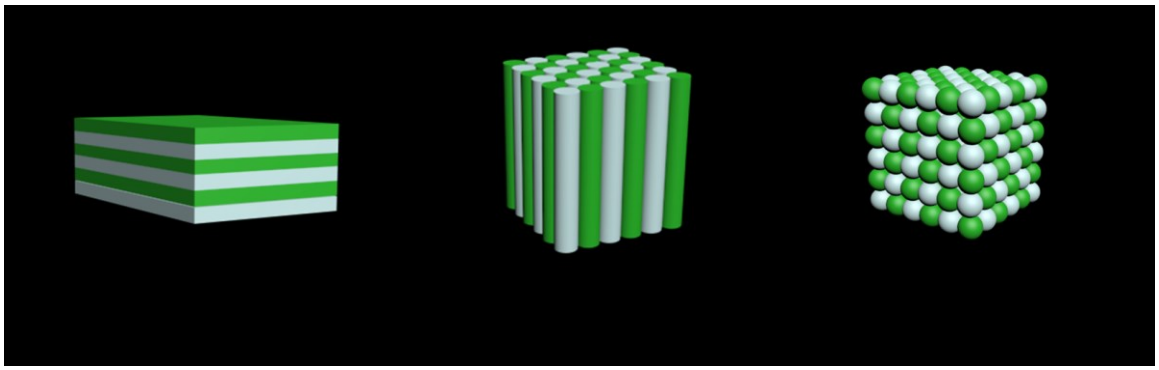

Figure 2-1 The schematic representation of three kinds of photonic crystals.

Many investigations have focused on assembling 2D or 3D photonic crystals, while 1D photonic crystals are far less studied. 1D PCs offer many advantages compared to their 2D/3D counterparts, including ease of fabrication, reduced direction-dependent optical properties, and a less dimensional change of PCs. In this section, 1D PCs are introduced in detail with a particular focus on microgel-based 1D devices (etalons) developed by our group.

2.1.1 1D photonic crystals

Generally, 1D PCs are composed of alternating layers of high-and low-refractive index materials. A common example of a 1D photonic crystal is a Bragg stack that has been used extensively for light filtration. Light impinging on these materials interacts with each of the layers, where light is reflected and transmitted. At each interface, this same process occurs, and as long as the distance between the two layers is on the order of the wavelength(s) of light being used, there will be some constructive and destructive interference of specific wavelengths of light. For example, if the layer thicknesses are in the range of visible light, then color will be observed.

The wavelength position of the Bragg-diffraction maximum can be predicted using the Bragg-Snell law (equation 1) which holds for normal incidence and non-absorbing materials:[168]

$$m\lambda_{max} = 2(n_l h_l + n_h h_h) \qquad (1)$$

where m is the diffraction order, h_l and h_h are the thickness of the low- and high-refractive-index materials, respectively, while n_l and n_h are the respective refractive index. Therefore, a change in either the layer thicknesses and/or refractive indexes will lead to a shift in the wavelength of light reflected from the Bragg stack. Specifically, if the layer thickness and/or the refractive index of the layers increases, a red shift in the position of Bragg diffraction peak will be observed. There are two other characteristic parameters for the Bragg diffraction peak: the bandwidth (full width at half maximum), and the reflectivity of the photonic crystals, which will not be discussed in detail here.[168,169] By modifying the composition of the deposited materials and their porosity, the refractive index can be tuned; while by the control of fabrication methods (e.g. by spin coating at various rates), the physical thickness of films can be modulated. More importantly, the thickness can also be tuned by the use of materials which exhibit expansion/contraction in response to certain external stimuli. One of the most important classes of materials that exhibit this behavior are stimuli responsive materials/hydrogels, which were introduced in the Chapter 1. Hydrogel based PCs are usually constructed from a combination of inorganic materials (e. g. SiO_2 or polystyrene colloids) and hydrophilic or hydrophobic polymers. A significant amount of research has been conducted on 2D or 3D PCs composed of hydrogels and microgels for sensing,[99,170-177] while a few polymer films based 1D PC sensors have been established.[178-181]

2.1.2 Etalon

The Serpe Group developed a novel, yet simple, 1D PC, which is similar to a Bragg stack. However, instead of consisting of multiple alternating layers of two materials, our device is formed by creating a cavity of one material (microgels) between two reflective surfaces (Au), as shown in Figure 2-2a.[104] This structure is similar a Fabry-Pérot etalon or

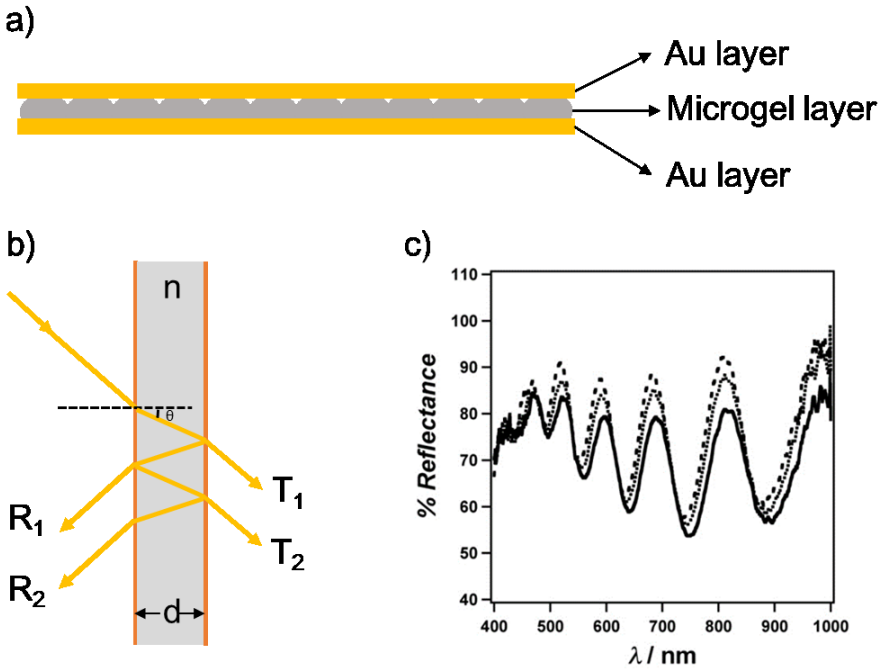

Figure 2-2 a) The structure of the etalon (two Au layers and microgel layer); b) Schematic of a traditional Fabry-Pérot etalon (n, refractive index of the dielectric; d, distance between two mirrors); c) representative reflectance spectra.

interferometer, which consists of a dielectric layer between two reflective surfaces or mirrors. Consequently, we refer to our devices simply as etalons. Like Bragg stacks, when light impinges on an etalon, the refractive index contrast/reflectivity at the

mirror/dielectric interface yields light interference (Figure 2-2b), which results in a characteristic multipeak reflectance spectrum (Figure 2-2c). The spectrum that results can be described by the equation for the interference of light in an optical cavity, and the maxima of reflected light intensity is described by the following equation:

$$m\lambda = 2ndcos\theta \qquad (2)$$

where λ is the wavelength maximum of the peak(s), m is the peak order, n is the refractive index of the dielectric, d is the spacing between the mirrors, θ is the incident angle.[105]

To construct these devices, we deposited 2 nm of Cr (as an adhesion layer) followed by 15 nm of Au onto 25 mm^2 precleaned glass coverslips via thermal evaporation. The Au-coated substrates were annealed at 250 °C for 3 h followed by cooling to room temperature before use, and the substrates were rinsed with ethanol, and dried with N_2. Then a 40 μL aliquot of concentrated microgels was added onto the Au-coated glass and spread toward each edge using the side of a micropipette tip. The film was rotated 90º, and the microgel solution was spread again. The spreading and rotation continued until the microgels covered the entire substrate and became too viscous to spread further. [182,183] The microgels were allowed to dry completely on the substrate for 2h, on a hot plate with its temperature set to 35 °C. Then the dry film was rinsed with DI water to remove excess microgels not bound directly to the Au and soaked in DI water overnight on a hot plate set to 30 °C. Then the films were then dried with N_2 gas, and an additional 2 nm Cr and 15 nm Au deposited onto the microgel thin film. After soaking these assemblies in DI

water, they exhibit the color and multipeak reflectance spectra mentioned above. As mentioned in Chapter 1, pNIPAm-based microgels can be made responsive to a variety of stimuli (such as pH, ionic strength, humidity, and biomolecules) in addition to temperature, by simply incorporating the desired functionality into the microgels at the time of synthesis by adding the appropriate comonomers. For our etalons, the thickness of the microgel film sandwiched between two Au layers can be changed, leading to a shift in the peaks of the reflectance spectra and a change in the device color. Consequently, the device can serve as an excellent platform for sensors.[182,184-189] For example, we reported a proof of concept experiment showing that the etalon structure could be used for sensing glucose. Aminophenylboronic acid (APBA)-functionalized pNIPAm-co-AAc microgels were synthesized, followed by the fabrication etalons from the microgels. The reaction mechanism between APBA and glucose is shown in Figure 2-3a. In a basic buffer the boronic acid moieties on the APBA (pK_a = 8.2) are hydroxylated such that the boron possesses a negative charge. The binding of diols, like glucose, is favored for boronic acid in the charged state. As glucose binds, more boronic acid groups must convert to the charged state in order to maintain the equilibrium, which effectively lowers the pK_a. As more boron atoms become charged, more glucose can bind until equilibrium is reached, which leads to an increase in the Coulombic repulsion inside the microgel, which results in a swelling response, as shown in Figure 2-3b. In the etalons, this will be observed as a red shift, according to the equation (2). Furthermore, we have shown that this technology is capable of detecting

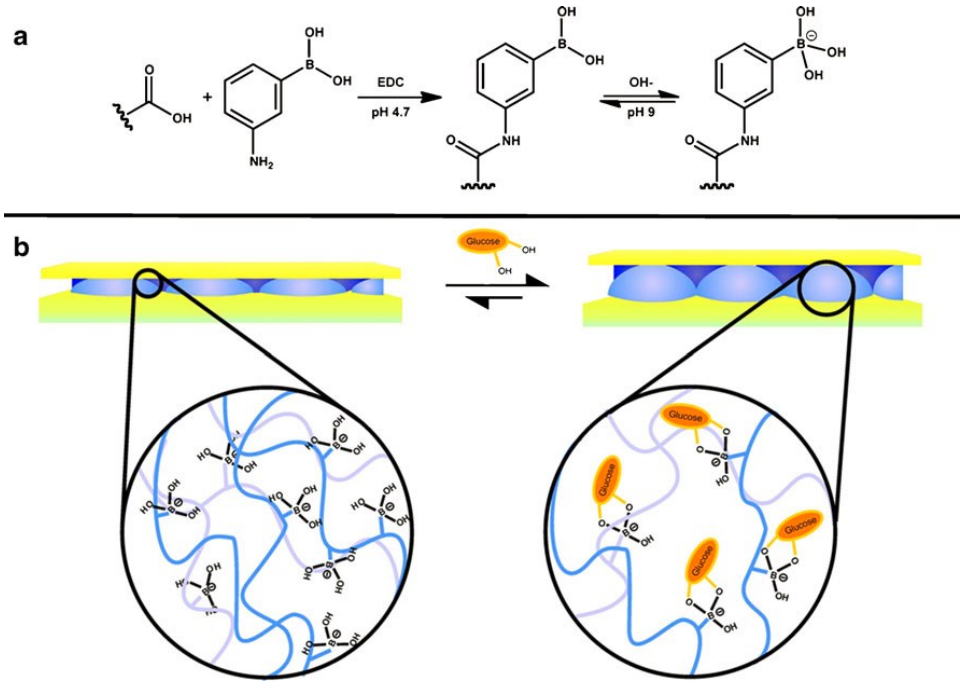

Figure 2-3 Reaction scheme for (a) the functionalization of the acrylic acid moieties on the microgel with APBA followed by the activation of the boronic acid with base and (b) a cartoon depiction of the glucose responsivity of an APBA-functionalized microgel etalon at pH 9. Reprinted with permission.[185] Copyright 2012, Springer-Verlag.

micromolar concentrations of target DNA in solutions containing two and four base pair mismatch sequences without the use of labels.[183] Positively charged microgel-based etalons were fabricated, and we showed that when negatively charged DNA is added to the etalon, the microgels are crosslinked and collapse due to electrostatics, and the device exhibits a spectral blue shift. Briefly, in this work the residual “probe” DNA was combined with different concentrations of "target" and the excess probe DNA was isolated and detected by the etalons, as shown in Figure 2-4. It was shown that the excess

of probe DNA that was detected was inversely related to the concentration of target DNA.

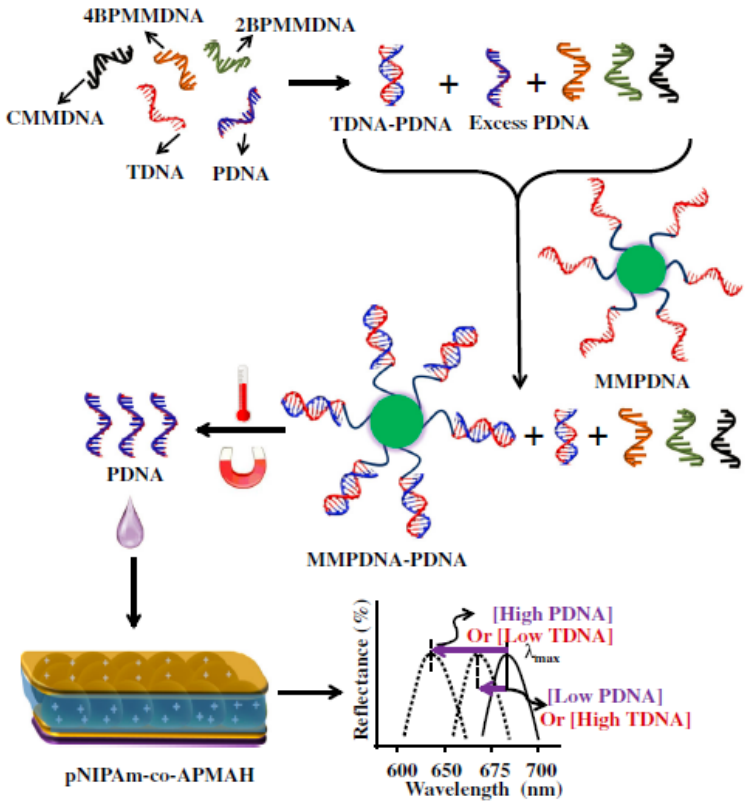

Figure 2-4 The protocol used for indirect sensing of target DNA, by sensing probe DNA by etalon. Reprinted with permission.[183] Copyright 2014 Springer-Verlag Berlin Heidelberg.

2.2 Polymer actuators

Polymer actuators are materials capable of converting energy from external stimuli (e. g. heat, light, and electricity) to mechanical forces, thus exhibiting shape changes. There are many kinds of polymer-based actuators composed of a variety of materials. For example, actuators can be generated from hydrogels that rely on their reversible volume

changes,[190,191] liquid crystal polymers, where actuation is a result of cooperative reorganization of mesogen groups;[192,193] and shape memory polymers, where the actuation relies on temperature induced relaxation,[194,195] Polymers can be soft (viscoelastic) and hard (glassy) depending on their physical and chemical structures, which allows them to be used for many applications spanning from the microscale to macroscale. The most common and useful actuation behavior is the reversible transformation between two dimensional (2D) polymer sheets and three-dimensional (3D) structures. 2D polymer sheets, which can transform into 3D structures, can be divided into two categories. The first generates microscopic surface topography (e.g. wrinkles) in response to external stimuli. [196-198] This category of material will not be discussed here as it is outside of the scope of the work presented here. The second category exhibits dramatic macroscopic 3D shape changes by bending, twisting, or folding upon exposure to external stimuli. In order to create a 3D structure from a 2D planar sheet, it's necessary to engineer the planar sheet such that it is able to generate differential stress either along its thickness or lateral dimensions so that bending or folding occurs. For instance, stimuli responsive polymer-based bilayers (Figure 2-5a), or polymers with differential crosslinking density along its thickness, (Figure 2-5b), bend or fold due to the relaxation of internal stresses originated from dissimilar properties of the two layers, such as swelling and thermal expansion.

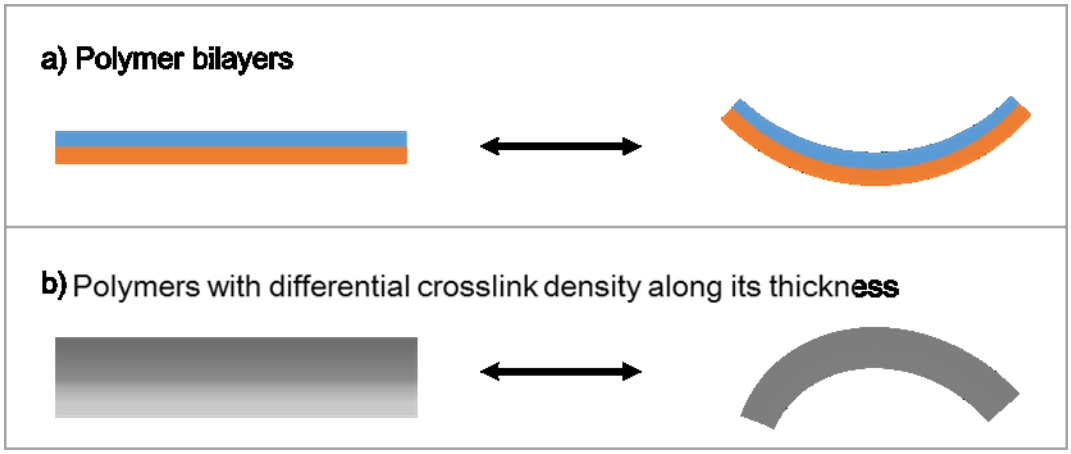

Figure 2-5 Schematic illustration of the design of the polymer layers enabling the stimuli responsive deformation.

Many methods, such as photolithography, molding, and imprinting, have been used to fabricate 2D planar bilayers, which can fold into various 3D structures, such as tubes, cubes, and capsules[199] Bending or folding occurs when one of the polymer layers swells or contracts more than the other, in response to a specific stimulus. The general theory of bilayer bending originates from the model of a bi-metallic strips developed by Timoshenko,[200] which is a structure featuring two layers of metal with different thermal expansion coefficients. The bilayer bends in response to high temperature since one layer expands more than the other. The curvature of the deflected bilayer is dependent on the composition, modulus, and thickness of the bilayers. It was also demonstrated that the resulting shape of the bent or folded 3D object can be controlled by the shape of the original 2D bilayer.[201,202] In addition, bending or folding can also be achieved by two other means: fabrication of locally responsive hinges using materials which are different

from the rest of the polymer sheet (Figure 2-6a); application of stimuli to only required regions on a polymer sheet (Figure 2-6b).

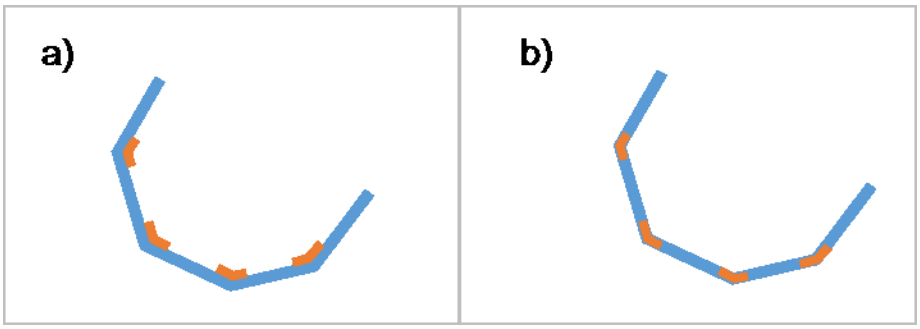

Figure 2-6 Schematic depiction of two additional folding strategies.

Smart hydrogels are often used for the fabrication of planar 2D sheets because: 1) they undergo dramatic expansion and contraction in response to external stimuli (such as temperature, pH, and the type of solvent); and 2) they can generate strong internal stresses necessary to effect the bending of 2D planar polymer sheet.[203] As illustrated in Figure 2-5, to make 3D structures from hydrogel based 2D planar sheet, there are two fabrication strategies. One approach is making hydrogel-based bilayers (one layer or both layers are hydrogels), which respond to the same stimuli differently. The bending/unbending of the hydrogel-based bilayer system is the result of inhomogeneous swelling/deswelling of the two layers. For example, a laminate structure consisting of two layers of photo-crosslinked hydrogels, the active layer being a thermoresponsive copolymer poly (*N*-isopropylacrylamide)-co-acrylic acid (pNIPAm-co-AAc) and the passive layer being poly (methyl methacrylate) (PMMA), can direct folding in a

sophisticated manner leading to the generation of complex 3D shapes in response to temperature changes in the environment.[204] They elucidated empirical rules by analyzing the folding patterns and performing finite-element simulations, which allowed the pre-determination of folding conformation of the pNIPAm-co-AAc-based hydrogel bilayers in response to changes in pH and ionic strength.[205] In addition, the bending of hydrogels can also be achieved by patterning crosslinks in a hydrogel, which generates hydrogels with inhomogeneous structure.[206-210] For example, "halftone" photolithography was utilized to photo-crosslink pNIPAm based copolymers containing pendent benzophenone moieties, which serve as photoactive crosslinkers. The density of crosslinks in the gel matrix can be tuned by using different irradiation doses, which leads to highly cross-linked regions distributed in a lightly cross-linked matrix. The stress generated in the system leads to the deformation with nearly constant Gaussian curvature.[211] Moreover, actuator hinges made from single-wall carbon nanotubes (SWNTs)-pNIPAm hydrogels were generated on the polyethylene (PE) substrates.[212] Up to 5 times enhancement to the thermal response time of the SWNTs-pNIPAm hydrogels was achieved due to the enhanced mass transport of water molecules. Complex shapes, such as cubes and flowers, can be fabricated by programming the SWNTs-pNIPAm hydrogels.

The main advantage of hydrogel-based actuators are their simplicity and their ability to be operated in aqueous solutions in which they exhibit considerable volume changes in response to changes in solution conditions.[213,214] Hydrogel actuators with different shapes

and manner of actuation can easily be fabricated using photolithography and other molding methods. Furthermore, many hydrogels are biocompatible and biodegradable, which allows their applications in biomedicine.[215,216] Compared with shape memory polymer-based actuators, the main drawback of hydrogel actuators is that they require solvation, and do not actuate in a dry state.

Generally, shape memory polymer (SMPs) actuators are of two types: one-way SMPs and two-way SMPs, as detailed in Chapter 1. Typical thermoresponsive SMPs yield a one-way shape change material, yet certain types of SMPs exhibit two-way shape changes, as discussed in Chapter 1. Unlike working with one-way SMPs, thermoresponsive two-way SMPs are considerably more challenging, although Lendlein and coworkers reported the synthesis of polymers with two different melting points, which leads to the two way shape memory actuation.[147,217] In contrast, the laminated two way SMPs-based actuators are easy to be fabricated from either one way or two way SMPs. Furthermore, large shape changing strain can be easily achieved and controlled by selecting suitable materials for the bilayers, tuning the thickness and the aspect ratio of the bilayer system. For example, a two-way SMP was prepared by laminating a thermoresponsive one-way SMP with an elastic polymer or a shape memory alloy.[218,219] [149] The imbalance of the internal stress in the composite as a result of heating or cooling produce the driving force for the two-way reversible shape memory effect (SME) (reversible conversion between 2D and 3D structures).

Some of the thermoresponsive SMPs possessing a glass transition temperature (T_g)

have been observed to have water or solvent driven shape memory effect.[136,220] Instead of triggering shape recovery at high temperature, the solvent, which may penetrate into the SMPs and reduce the T_g of SMPs, may lead to the shape recovery of SMPs without heat. Solvent-responsive two-way shape memory polymer-based actuators have been recently reported.[140,221,222] In addition, more and more solvent responsive laminates, which are fabricated from novel polymer composites (either one-way or two-way SMPs) exhibit two way SME, which serves as reversible polymer actuators.[223-226] For example,[139] a mixture of solution of cationic poly (ionic liquid), poly (3-cyanomethyl-1-vinylimidazolium bis (trifuoromethanesulfonyl) imide) (PILTf_2N, Tf_2N donates the counter anion) and a carboxylic acid-substituted pillar[5]arene (C-pillar[5]arene) that bears 10 acid groups in DMSO was cast on a glass substrate and dried. Then, the membrane was soaked in ammonia solution, which diffuses into the membrane from top to bottom. The deprotonation of COOH into $COO^-NH_4^+$ triggers the electrostatic complexion between the negatively charged C-pillar[5]arene and the imidazolium cation from PILTf_2N forming a gradient in the degree of electrostatic complexation (DEC) along the membrane cross-section, as shown in Figure 2-7a. The electrostatic complexion maintains the membrane to be intact and stable in organic solvents. When the membrane is placed in acetone vapour, the solvent molecules diffuse rather rapidly into the porous membrane from both the top and bottom surfaces and interacts with the Tf_2N, which has a higher concentration on the top surface compared to the bottom. This will induce the fast bending (actuation) of the membrane in response to

acetone vapour, as shown in Figure 2-7. Furthermore, the membrane returns to its initial position once the device is placed in air.

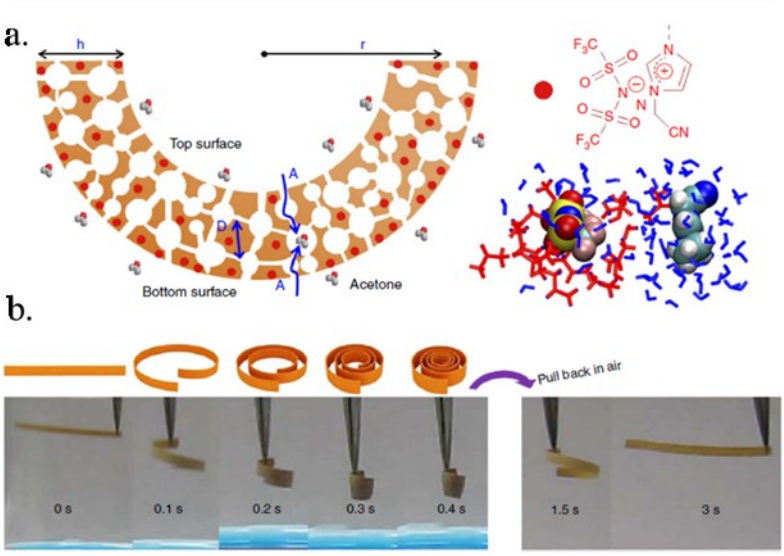

Figure 2-7 a) A scheme of the porous membrane actuator; b) Adaptive movement of a PILTf2N/C-pillar[5]arene membrane placed in acetone vapour and then back in air. Reprinted with permission.[139] Copyright 2014 Nature Publishing Group.

Liquid crystal elastomers (LCEs) are another popular shape memory polymer, which combine oriented liquid crystals and polymeric elastomers. In a liquid crystal polymer network-based actuator, the oriented liquid crystals stretches or contracts anisotropically as the order parameter changes, for instance, as a result of a change in temperature or light stimulation with specific wavelengths, thus inducing shape change of the actuators.[148,227,228] Recently, humidity responsive LCEs-based actuators were fabricated. The uniaxially aligned liquid crystal polymer network is formed based on the hydrogel bonding between the aligned mesogens. The polymer swells anisotropically when water

penetrates into the LCEs network. The one-layer actuators can be tailored to either bend, fold, or curl when bringing only one side of the actuator to contact aqueous solution.[229]

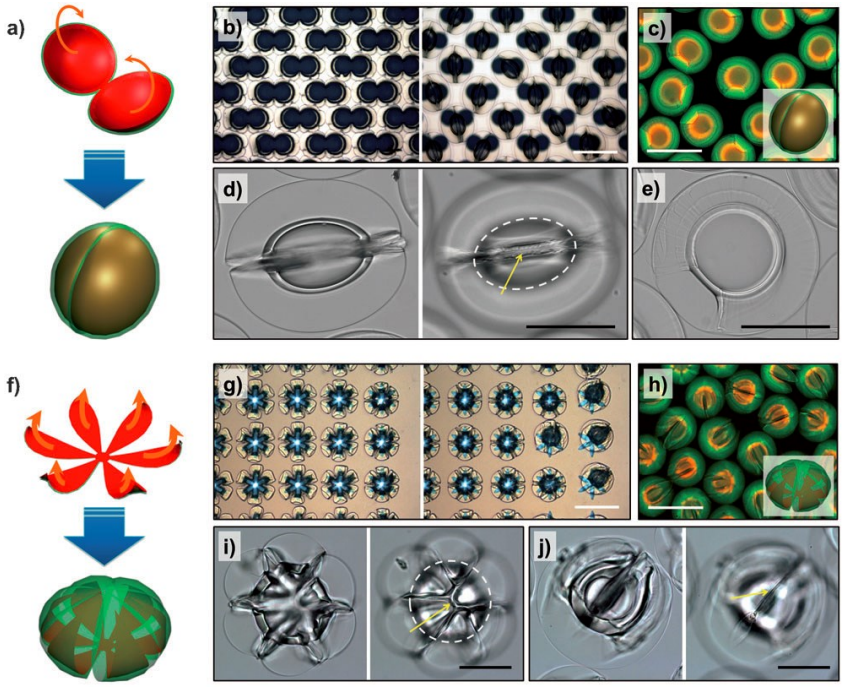

Figure 2-8 a) Transformation of snowman-shaped microparticles to a microcapsule. b) Optical microscope images of arrays of bilayer microparticles on a photomask and transformed microcapsules at pH 9. c) Confocal microscope image of microcapsules, inner layer consisting of R6G-tagged p(HEMA) and outer layer consisting of FITC-tagged p(HEMA-co-AA). d) Magnified optical microscope images of microcapsules in top view at two different focal planes and e) side view. f–j) A set of a scheme and optical and confocal microscope images of flower-shaped microparticles. Scale bars indicate 500 mm for b, c, g, and h, and 200 mm for d, e, i, and j, respectively. Reprinted with permission.[230] Copyright 2012 Wiley-VCH Verlag GmbH & Co. KGaA, Weinheim.

There are many application possibilities of polymer-based actuators. Firstly,

hydrogel-based actuators can be utilized as biomedical devices and containers for drug delivery applications.[231-235] For example, pholithographically fabricated planar bilayer microparticles, composed of polyhydroxyethylmethacrylate (pHEMA) and poly (hydroxyethylmethacrylate-co-acrylic acid) (PHEMA-co-AAc), showed a structural transformation to microcapsules with a closed compartment in response to a pH change.[230] The transformation was highly reversible, and this bilayer structure was therefore used for in situ encapsulation and the triggered release of active ingredients, as shown in Figure 2-8. The soft hydrogel materials enabled the formation of curved surfaces and tight contact between patches, facilitating the complete closure of compartments in the resultant microcapsules. Secondly, polymer-based actuators can be used as biomimetic actuators, sensors, grippers and soft robotics.[236-241] Lee et al. used the inhomogeneous deformation of hydrogels and fabricated pH-sensitive hydrogel actuators mimicking the shape and swimming motion of an octopus,[242] as shown in Figure 2-8.

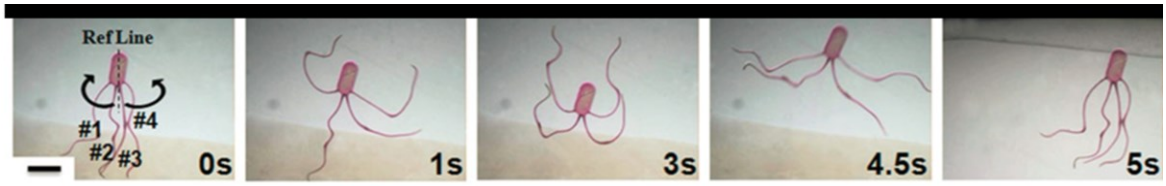

Figure 2-9 Locomotion of octopus aquabot under an electric field. Initial angles of tentacles 1 and 2 are each in the clockwise direction relative to the "Ref Line," while tentacles 3 and 4 are bent in the counter-clockwise direction. During the receding phase, all four tentacles were slowly bent upward, ready to propel; during the propelling phase, the aquabot rapidly moved upward by the propulsion of all four tentacles (scale bar¼1 mm).

Reprinted with permission.[242] Copyright 2008 Wiley-VCH Verlag GmbH & Co. KGaA, Weinheim.

Furthermore, hydrogel actuators, exhibiting changes in macroscopic shapes in response to stimuli, can readily be used for the design of sensors. One possible approach is to use AFM cantilevers, which are coated on one side with a stimuli responsive polymer and are able to bend in response to external stimuli. The bending is detected by the change in the reflection of the laser beam from the surface of the cantilever.[243]

Furthermore, another group of polymers called conjugated polymers, which were introduced in Chapter 1, have been developed into artificial muscles (soft and wet actuators).[236,244-246] Natural muscles are biological tissues to transform from chemical or electrical energy into mechanical energy and heat. It involves the aqueous media, electric pulse from the brain, liberation of ions inside the sarcomere, chemical reactions (ATP hydrolysis), and conformational changes along the natural polymer chains. Similarly, the chemical nature of the artificial muscle based on conducting polymers, e.g. PPy, provides motors with the unique sensing of electrical pulses. For example, a triple layer is fabricated from PPy/non-conducting and adhesive film/PPy). The PPy layer is doped with small ions ClO_4^- As the current flows, the left PPy film acts as the anode and swells, and the right PPy acts as the cathode and shrinks in aqueous solution. The triple layer muscle was immersed in an aqueous solution of 1 M $LiClO_4$ and initiates its movement under a constant current of 5 mA as a consequence of the electrochemical reactions and changes

of volume. The angular movement allows the muscle to overcome the border of the obstacle and the free movement continues until the current stops. Moreover, conjugated polymer based actuators have reached the early stage to be used in biomedical devices.[40,247,248]

The projects presented in this were conducted to understand the properties of stimuli-responsive polymers, mainly focusing on temperature responsive pNIPAm and humidity responsive poly (diallyldimethylammonium chloride) (pDADMAC) and how they can be used for actuators that respond to humidity levels in the atmosphere. The devices were specifically able to bend in response to environmental humidity and used as humidity responsive artificial muscles and sensors. The other objective of this thesis was to design and develop pNIPAm based soft actuators, which can be used in the future for grippers and drug delivery devices.

Chapter 3: Polymer-Based Muscle Expansion and Contraction[1]

3.1 Introduction

This Chapter describes the assembly of novel humidity responsive polymer bilayer-based muscle-like actuators. Of specific interest to the investigations in this Chapter are responsive polymer-based systems that are able to do work, i.e., lift masses.[249,250] These systems, often referred to as artificial muscles, have been the subject of intense research owing to their potential to control movements in mechanical motors.[251,252] In this Chapter we show that the devices are lightweight and exhibit large strain, which allows them to lift weights many times their own mass.

Polymer-based stimuli-responsive polymers and materials have been of considerable interest for many years owing to their ability to convert a chemical or physical stimulus into an observable change in a system, as detailed in Chapter 2. Polymer gel-based thin films, assemblies, and particles (microgels and nanogels) have been designed to respond to a variety of stimuli for a number of potential applications in tissue engineering, artificial muscles, valves, and actuators.[210,224,253-259] Hydrogels are of particular interest owing to their mechanical properties, chemical diversity, and hydration properties, which allow them to interface well with biological systems. Recently, responsive hydrogels and

[1] This Chapter has been adapted from a previously published article; Islam, M.R., Li, X., Smyth, K., Serpe, M. J., *Angew. Chem. Int. Edit.,* 2013, 52, 10330.

polymer- based thin films have been developed as programmable soft matter or motors by exploiting conformational changes of the polymer that affects the system.[210,224,256]

Thermoresponsive pNIPAm shows a random coil to globule transition at temperature above 32 °C (LCST). Charged pNIPAm-based microgels have been synthesized and used for various applications.[260-262] In this Chapter, we describe the synthesis of pNIPAm-co-AAc microgels. AAc is a weak acid, having a pK_a of approximately 4.25. Therefore, at pH > 4.25 the AAc groups are deprotonated, thus making microgels negatively charged (polyanionic), as mentioned in Chapter 1.

3.2 Experimental section

Materials: *N*-Isopropylacrylamide (NIPAm) was purchased from TCI (Portland, Oregon) and purified by recrystallization from hexanes (ACS reagent grade, EMD, Gibbstown, NJ) prior to use. *N, N*-methylenebisacrylamide (BIS) (99%), acrylic acid (AAc) (99%), and ammonium persulfate (APS) (98+ %) were obtained from Sigma-Aldrich (Oakville, Ontario) and were used as received. N-(3-Aminopropyl) methacrylamide hydrochloride (APMAH) were purchased from Polysciences, Inc. (Warrington, PA). Poly (diallyldimethylammonium chloride) solution (pDADMAC) of MW (10,0000 ~ 20,0000) (20% in water); as well as poly (sodium 4- styrene-sulfonate), (PSS, MW 70,000) were purchased from Sigma-Aldrich (St. Louis, MO). Deionized (DI) water with a resistivity of 18.2 MΩ●cm was used. Cr/Au annealing was done in a Thermolyne muffle furnace

from Thermo Fisher Scientific (Ottawa, Ontario). Anhydrous ethanol was obtained from Commercial Alcohols (Brampton, Ontario). Fisher's finest glass coverslips were 25×25 mm^2 and obtained from Fisher Scientific (Ottawa, Ontario). Cr was 99.999% and obtained from ESPI (Ashland, OR), while Au was 99.99% and obtained from MRCS Canada (Edmonton, AB).

Microgel Synthesis: microgels composed of poly (*N*-isopropylacrylamide)-co-acrylic acid (pNIPAm-co-AAc) were synthesized via temperature-ramp, surfactant free, free radical precipitation polymerization as described previously. The monomer mixture, with a total concentration of 154 mM, was comprised of 85% (mole/mole) NIPAm, 10% AAc, and 5% BIS as the crosslinker. NIPAm (17.0 mmol), and BIS (1.0 mmol) were dissolved in deionized water (100 mL) with stirring in a beaker. The mixture was filtered through a 0.2 μm filter affixed to a 20 mL syringe into a 200 mL 3-neck round-bottom flask. The beaker was rinsed with 25 mL of deionized water and then filtered into the NIPAm/BIS solution. The flask was then equipped with a temperature probe, a condenser and a N_2 gas inlet. The solution was bubbled with N_2 gas for ~1.5 h, while stirring at a rate of 450 rpm, allowing the temperature to reach 45 °C. AAc (2.0 mmol) was then added to the heated mixture with a micropipette in one aliquot. A 0.078 M aqueous solution of APS (5 mL) was delivered to the reaction flask with a transfer pipet to initiate the reaction. Immediately following initiation, a temperature ramp of 45 to 65 °C was applied to the solution at a rate of 30 °C/h. The reaction was allowed to proceed overnight at 65 °C.

After polymerization, the reaction mixture was allowed to cool down to room temperature and filtered through glass wool to remove any large aggregates. The coagulum was rinsed with deionized water and filtered. Aliquots of these microgels (12 mL) were centrifuged at a speed of ~8500 relative centrifugal force (rcf) at 23 °C for ~ 40 minutes to produce a pellet at the bottom of the centrifuge tube. The supernatant was removed from the pellet of microgels, which was then re-suspended to the original volume (12 mL) using deionized water. This process was repeated until the microgels were cleaned a total of six times to remove any unreacted monomer and/or linear polymer from the microgel solution.

Fabrication of Au coated substrate: Briefly, 25 × 25 mm pre-cleaned glass coverslips or transparent flexible plastic sheet were rinsed with DI water and ethanol and dried with N_2 gas, and 2 nm of Cr followed by 15 nm or 50 nm of Au were thermally evaporated onto them at a rate of ~0.2 Å s^{-1} and ~0.1 Å s^{-1}, respectively, using a Torr International Inc. model THEUPG thermal evaporation system (New Windsor, NY). The Cr acts as adhesion layer to hold the Au layer on the glass/plastic. The Au coated glass substrates were annealed at 250 °C for 3 h and then cooled to room temperature prior to use. An aliquot of about 12 mL of previously purified microgel solution was centrifuged for 30 min at 23 °C at ~8500 rcf to pack the microgels into a pellet at the bottom of the tube. After removal of the supernatant solution, the microgel pellet was vortexed and placed onto a hot plate at 30 °C. A previously coated Cr/Au substrate was rinsed with ethanol,

dried with N_2, and then placed onto hot plate (Corning, NY) set to 30 °C. An aliquot (40 μL for each 25 × 25 mm area) of the concentrated microgels was put onto the substrate and then spread toward each edge using the side of a micropipette tip. The substrate was rotated 90 °, and the microgel solution was spread again. The spreading and rotation continued until the microgel solution became too viscous to spread due to drying. The microgel solution was allowed to dry completely on the substrate for 2 h with the hot plate temperature set to 35 °C. After 2 h, the dry film was rinsed copiously with DI water to remove any excess microgels not bound directly to the Au. Microgel painted substrate was then placed into a DI water bath and allowed to incubate overnight on a hot plate set to ∼30 °C. Following this step, the substrate was again rinsed with DI water to further remove any microgels not bound directly to the Au substrate surface. The microgel painted Au coated substrate was dried with N_2 gas and used for the experiment.

Bending Experiment: Au coated microgel painted substrates were placed on to a Petri dish. A specific amount of pDADMAC solution (20% in water) was spread onto the microgel layer. The whole set up was undisturbed and dried at ambient temperature. After the complete drying of the film, the humidity response was tested either in a humidity chamber or in air. Load and release test was done in a humidity chamber and the paper clips experiment was done in air. In both cases Air-O-Swiss AOS 7145 Cool Mist Ultrasonic humidifier (manufactured by Swiss Pure Air) was used.

3.3 Results and discussion

The device is constructed by depositing a monolayer of poly (*N*-isopropylacrylamide)-co-acrylic acid, pNIPAm-co-AAc microgels on an Au-coated substrate. Once deposited, the microgels form a homogenous layer with the thickness defined by their diameter in solution. The pNIPAm-co-AAc microgels used herein had a solution diameter of (1.55 ± 0.07) μm (measured using differential interference contrast microscopy); the films typically have a thickness of approximately 0.5 of the solution diameter.[105] Subsequently, a solution containing oppositely charged poly (diallyldimethylammonium chloride) (pDADMAC), the structure of which is shown in Figure 3-1a, is added to the microgel-coated substrate and allowed to dry. The pDADMAC solution had a pH of 6.55, which rendered the microgel layer polyanionic. The pDADMAC layer contracts when it dries, owing to water evaporation enhancing hydrophobic interactions between the pDADMAC chains. Since the electrostatic interactions between pDADMAC and the microgels, and the interaction between microgels and the Au layer, are strong, the substrate bends when the polymer dries (Figure 3-1b).

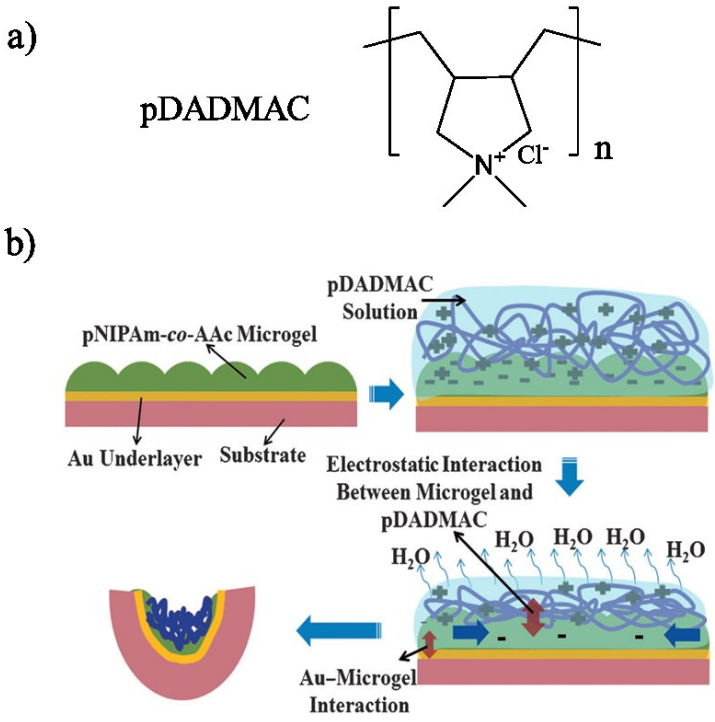

Figure 3-1 a) Structure of pDADMAC, b) A flexible plastic substrate (transparency film) was coated with an Au/Cr layer. Cr acts as an adhesion layer such that the Au adheres to the plastic. PNIPAm-co-AAc microgels were deposited on this substrate, to yield a monolithic monolayer of microgels on the Au. Addition of a pDADMAC solution renders the pNIPAm-co-AAc microgel negatively charged owing to the deprotonation of AAc moieties in the microgel initiating the electrostatic interaction between the microgels and polyelectrolyte. Upon drying, the pDADMAC layer contracts bending the substrate owing to the strong interactions between the microgels and pDADMAC and the microgels and Au.

When this process is conducted using a standard microscope glass coverslip as the substrate, the bending forces are so strong that the coverslip is shattered. This is shown in Figure 3-2a along with the results for control experiments conducted by drying the

pDADMAC solution on bare glass and unmodified Au-coated glass substrates. When the pDADMAC solution is dried on an Au-coated glass substrate, with microgels painted on the Au, the glass substrate bends so much that the glass shatters (Figure 3-2a). This was repeated many times, which showed that 80% of the Au-coated microgel-painted substrates shattered after drying. When the same experiment is conducted on a bare glass substrate, no bending is observed, while slight bending, and even occasional substrate cracking (ca. 20% of the samples) takes place on Au-coated glass substrates without microgels present. When a microgel-modified, Au-coated plastic substrate (simple transparency slide) is exposed to pDADMAC, and the pDADMAC solution is allowed to dry, the plastic substrate can curl up significantly into a tight scroll structure (Figure 3-2b).

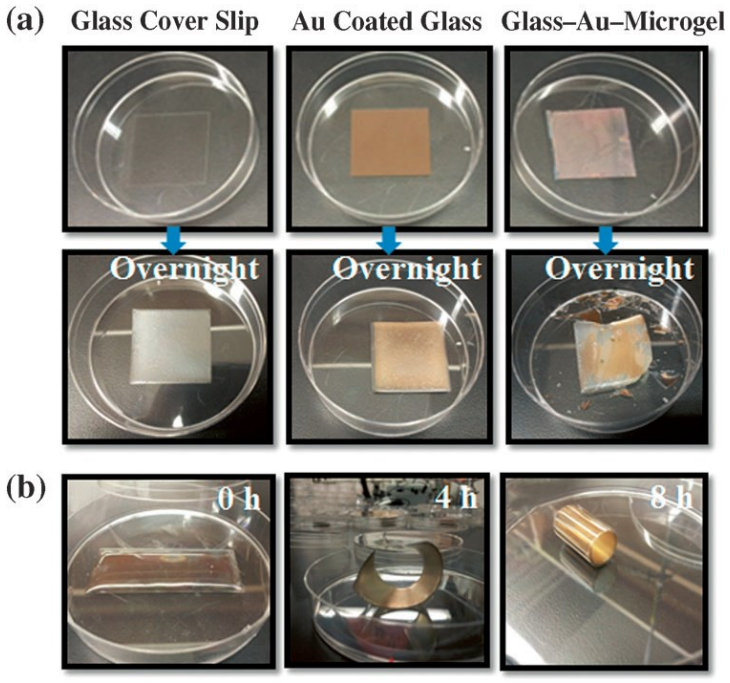

Figure 3-2 Electrostatic interaction and substrate bending mediated by pDADMAC drying. In each case, a fixed amount of pDADMAC solution was added and dried at ambient condition. a) (left column) bare glass cover slip, (middle column) Au-coated glass and (right column) microgel painted on Au-coated glass. b) Flexible Au-coated substrate with microgels deposited bends and eventually curls upon drying over 8 h.

In all the cases above, we hypothesize that the microgels serve as glue that allows the contraction of the pDADMAC layer to be translated to the substrate below. Our previous studies have shown that the microgel-Au interaction is strong. Furthermore, we have shown that there are multiple, electrostatic interactions between pDADMAC and the charged microgels.[263] Therefore, the contraction of the pDADMAC layer upon drying can be translated to the solid substrate through its interaction with the microgels, and the microgels transfer the contraction to the Au-coated surface, thereby pulling the sides of the substrate up. Depositing Cr as an adhesion layer between the Au and the substrate strengthens the Au-substrate bond. Drying pDADMAC on an Au-coated substrate without the microgels present does not yield a strong enough bond to the surface to allow for consistent substrate bending/breaking. Similarly, simply drying microgels on a surface does not bend the substrate, because when the microgels dry, there are no long range interactions between them, hence they dry “locally” without long-range deformations that are translated to the substrate.

To further prove our hypothesis that the electrostatic interactions between the

microgels and the pDADMAC lead to the observed bending, we designed a flexible substrate with numerous arms. The arms were coated with Au and painted with pNIPAm-co-AAc microgels and alternate arms were exposed to the same pDADMAC solution used above while keeping the other arms empty (Figure 3-3). The arms exposed to the pDADMAC solution curled up (Figure 3-3). When the empty arms were exposed to polyanionic poly (sodium 4-styrenesulfonate) (PSS) solution (20 wt%) and dried at ambient condition, they did not bend at all. This proves that the polyanionic PSS deposited on the polyanionic microgels cannot yield the necessary interactions with the microgels bound to the Au-coated substrate to bend the plastic substrate. Furthermore, this experiment shows that by controlling the shape of the flexible substrate, we are able to devise complex constructs, in this case a "hand" capable of grasping an object.

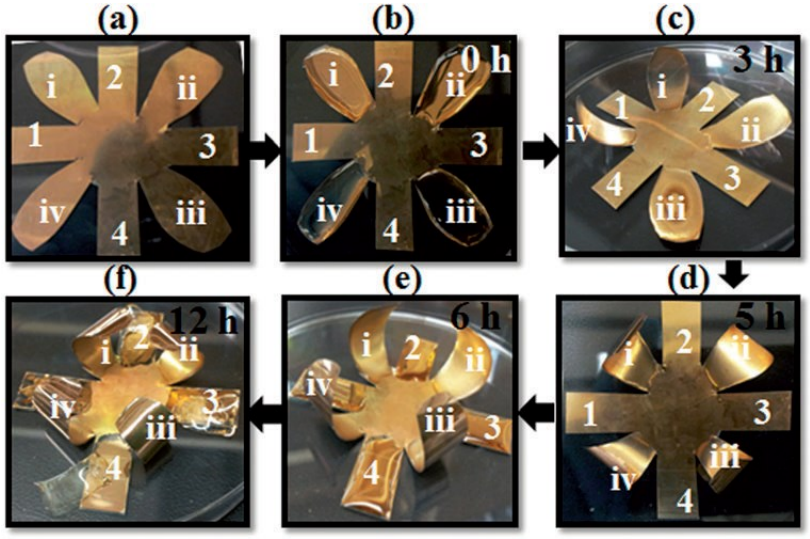

Figure 3-3 A specially cut Au-coated plastic substrate, with the Au containing pNIPAm-based microgels. Arms i–iv were exposed to the pDADMAC solution while Arms 1–4 were exposed to the PSS solution. The arms that were exposed to pDADMAC

clearly bend upon solution drying, while the PSS arms are unresponsive to drying. Drying of the pDADMAC solution took place over 6 h. After this time, (e) the PSS solution was added to the arms and allowed to dry overnight.

If our above hypothesis is correct, and the bending of the substrates is a result of the dehydration-mediated contraction of the pDADMAC layer, the process should be reversible upon rehydration of the devices, as shown in Figure 3-4. To illustrate this, we introduced our device to a humidity chamber (Figure 3-5), which allowed for atmospheric temperature and humidity to be controlled and maintained.

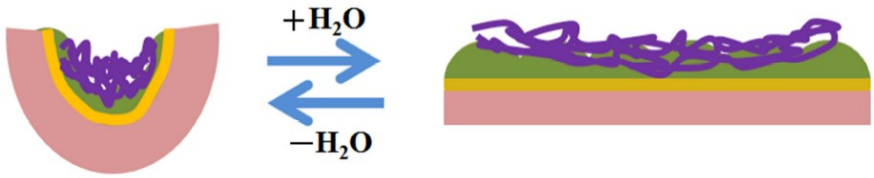

Figure 3-4 Schematic demonstration of bending and flattening of flexible substrate supported microgel assembly. When the bent substrate is exposed to humidity, the pDADMAC layer rehydrates, causing it to become less contracted due to pDADMAC rehydration, and the plastic substrate flattens out. Reducing the humidity causes the pDADMAC layer to recontract, bending the substrate again, which can be repeated over many cycles.

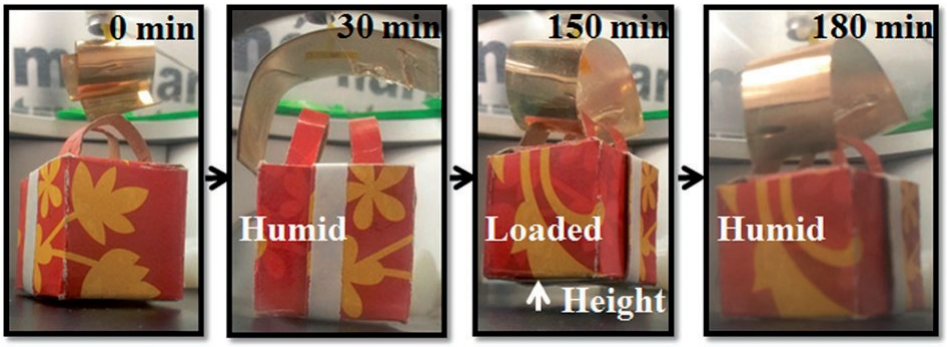

Figure 3-5 The curled substrate was hung from a string into a humidity chamber (0 min). The humidity of the environment was then increased to 80%, and the device uncurled, which was then lowered close to a box (30 min). The humidity was reduced to 10% and the substrate recurled, grasping the box. While maintaining this humidity, the box was lifted off the chamber surface (150 min). A subsequent increase in the humidity allowed the device to reopen, and drop the box (180 min). Here, the masses of the device and the box were 0.2 g and 4.8 g, respectively.

The device was connected to a string, which was extended out of the chamber top. Initially, under low humidity, the device was fully closed (Figure 3-5) but opened up after the humidity of the environment was increased to 80%. The open arm was then lowered to a box that was in the chamber, and the humidity was subsequently decreased to 10%. After this decrease, and waiting (ca. 2.0 h), the device curled back up, but in this case it clamped onto the box. To illustrate the strength of the clamping, the box was lifted off the chamber‘s bottom surface. Finally, the humidity was increased to 70%, which caused the device to open again, thus dropping the box. The mass of the box was 4.8 g, while that of the polymer-based device was only 0.2 g. That is, the mass of the box was 24 times the mass of the device.

We further studied whether the device can be used as an artificial muscle to lift weight and release it in response to humidity. To do this we loaded paper clips onto a curled substrate and exposed the setup to a humid environment (Figure 3-6). Paperclips (used as weights) were hung off the end of the device, and the device opened up upon increasing the humidity and curled back up when the humidity was decreased. This is similar to an arm curling a mass, but in this case, the mass that is being lifted is 14 times the mass of the device. Given that a human arm is approximately 6.5% of the total mass of the human body, this is equivalent to a 75 kg human with a single arm that is capable of lifting 68.3 kgs.

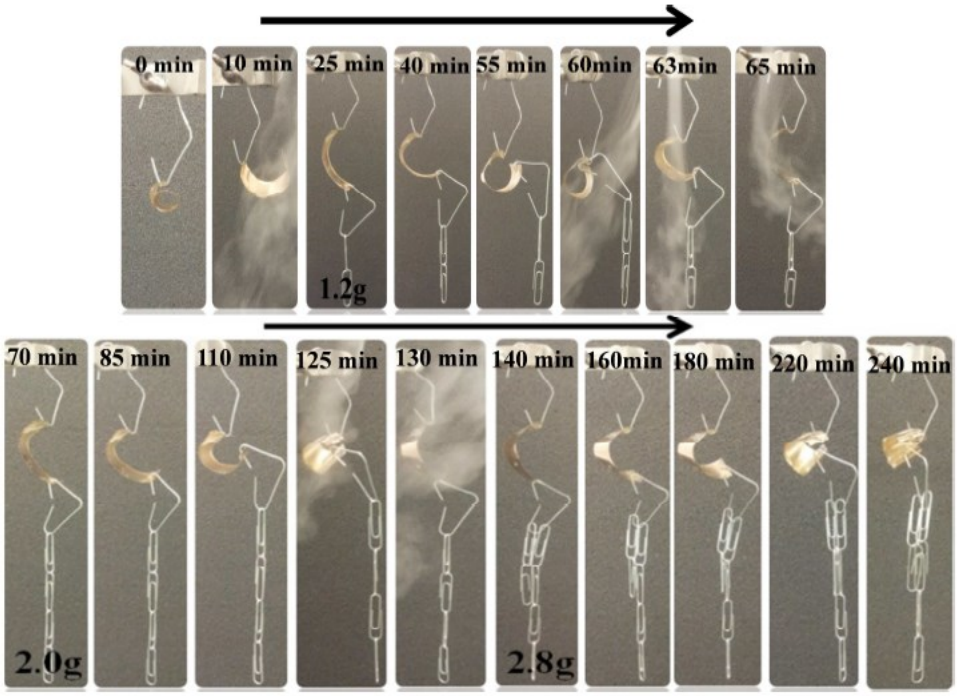

Figure 3-6 Use of the polymer-based devices as artificial muscles. Here, a small curled substrate was hanged from an arm and cycled between low and high humidity. In each case,

the device was able to recontract, and curl up even though the mass was increased to 2.8 g.

Finally, we showed that dried substrates can resist opening when a force is applied to them. This is illustrated in Figure 3-7, where weights were hung from the end of a suspended device showing that even with 52.50 g hanging from the end of the dried device it is not significantly unwound. Using the same numbers as above for the mass of a human arm, this is equivalent to a 75 kg human that has an arm capable of resisting a force of 1280 kgs pulling on the arm.

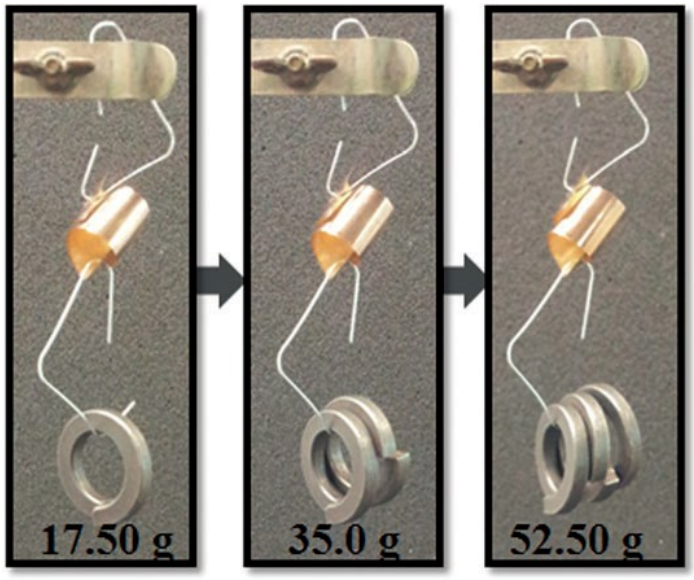

Figure 3-7 A dry polymer-based device resisting uncurling as masses are hung from the end of the device.

3.4 Conclusion

In summary, we found that polyelectrolyte-mediated crosslinking of microgels

painted on Au-coated substrates are able to actuate, and act as muscles or arms in response to humidity. These arms are able to lift relatively large masses, and resist forces many times its own mass. Given this, we strongly believe that this device can be further developed to optimize its capability as artificial arm. This study is very promising to realize responsive-polymer-based materials for applications in soft robotics and artificial muscles.

Chapter 4: Self-Folding Polymer-Based Materials[2]

4. 1 Introduction

This Chapter describes the study of the self-folding behavior of bilayer materials mentioned in Chapter 3. The materials are composed of a semi-rigid polymer substrate coated with a thin layer of Au; the Au layer is subsequently coated with a pNIPAm-based microgel layer and finally covered with a solution of pDADMAC. By varying the size and aspect ratio of the polymer substrate, a set of empirical rules were developed and applied to predict the material's self-folding behavior. From these rules, materials, which self-fold from two-dimensional, flat objects into discrete three-dimensional structures, can be designed. They are fully capable of unfolding and folding multiple times in response to humidity.

Materials that spontaneously undergo a change in structure, e.g., from a two dimensional (2D) to three dimensional (3D) structure in response to external stimuli have been of great interest as artificial muscles, and for fabricating novel actuators, switches, valves and in robotics.[204,257,261,264-266] Various stimuli responsive polymers have been identified, which exhibit responses to electric fields, temperature, light, pH, ionic strength, humidity and/or solvent composition.[195,267-270] Recently, responsive hydrogels and

[2] This Chapter has been adapted from a previously published article. Li, X., Serpe, M. J., *Adv. Funct. Mater.,* 2014, 24, 4119.

polymer-based films have been used as materials capable of converting chemical or physical energy into mechanical forces, which can lead to macroscopic changes to a material's conformation.[211] Specifically, temperature responsive pNIPAm based hydrogel sheets capable of transforming from a planar state to a 3D structure have been developed by tuning the concentration of monomers and crosslinking density in the hydrogel sheets.[271] Regions with different polymer content went through differential deformation upon heating allowing the formation of unique 3D structures. Wang et al. recently fabricated near-infrared light-driven hydrogel actuators by interfacing reduced-graphene oxide sheets with protein-based polymers. These hydrogels showed rapid, reversible bending motion at specific positions where near-infrared laser was applied.[259] Another system composed of a soft poly (butadiene) phase and a hard metal – ligand phase was developed, which exhibited shape-memory properties in response to external stimuli.[272] In this case, the key component in fulfilling the shape change is the metal – ligand phase which can become soft when exposed to a variety of stimuli (e.g., light, heat, chemicals).

Of recent, several types of humidity responsive polymers have also been used to fabricate actuators. For example, Langer and coworkers[224] recently developed a polymer composite of rigid polypyrrole (PPy) embedded with a flexible polyol-borate network. PPy can absorb water and change its shape, while the soft polyol-borate network is also sensitive to water, undergoing hydrolysis and reformation of the borate ester crosslinker upon water absorption and desorption, respectively. By breaking and reforming intermolecular hydrogen bonding between PPy and the polyol-borate network and the

borate ester within the polyol-borate network upon water sorption and desorption, the film shows expansion and contraction, resulting in the film's rapid and continuous locomotion. In another example, Sun and coworkers developed one bilayer film consisting of a polyeletrolyte multilayer (PEM) film and a layer of UV-cured prepolymer.[273] The PEM is a film of thermally crosslinked poly (acrylic acid) (PAA) / poly (allylamine hydrochloride) (PAH). The PAA/PAH is able to absorb/desorb water with increasing/decreasing environmental humidity, which resulted in swelling/shrinking of the layer. They fabricated an energetic walking device driven by the powerful humidity responsive PEM.

Layer-by-layer assembled films of alternating polyanions and polycations is an important soft materials which showed repeated deformation in response to different stimuli.[260,274] PDADMAC is a homopolymer of diallyldimethylammonium chloride (DADMAC) and a high charge density cationic polymer (polycation), which has been applied to fabricate various advanced materials by layer-by-layer self-assembly.[261]

4.2 Experimental section

Materials: *N*-isopropylacrylamide (NIPAm) was purchased from TCI (Portland, Oregon) and purified by recrystallization from hexanes (ACS reagent grade, EMD, Gibbstown, NJ) prior to use. *N, N*-methylenebisacrylamide (BIS) (99%), acrylic acid (AAc) (99%), and ammonium persulfate (APS) (98+ %) were obtained from Sigma-Aldrich (Oakville,

Ontario) and were used as received. Poly (diallyldimethylammonium chloride) solution, pDADMAC of MW (100,000 ~ 200,000) (20% in water) were purchased from Sigma-Aldrich (St. Louis, MO). Deionized (DI) water with a resistivity of 18.2 MΩ●cm was used. Cr/Au annealing was done in a Thermolyne muffle furnace from Thermo Fisher Scientific (Ottawa, Ontario). Anhydrous ethanol was obtained from Commercial Alcohols (Brampton, Ontario). Fisher's finest glass coverslips were 25×25 mm and obtained from Fisher Scientific (Ottawa, Ontario). Cr was 99.999% and obtained from ESPI (Ashland, OR), while Au was 99.99% and obtained from MRCS Canada (Edmonton, AB).

Microgel Synthesis: Microgels composed of poly (*N*-isopropylacrylamide)-co-acrylic acid (pNIPAm-co-AAc) were synthesized via radical precipitation polymerization as described previously.[105] The monomer mixture, with a total concentration of 154 mM, was comprised of 85% (mole/mole) NIPAm, 10% AAc, and 5% BIS as the crosslinker. NIPAm (17.0 mmol), and BIS (1.0 mmol) were dissolved in deionized water (100 mL) with stirring in a beaker. The mixture was filtered through a 0.2 μm filter affixed to a 20 mL syringe into a 200 mL 3-neck round-bottom flask. The beaker was rinsed with 25 mL of deionized water and then filtered into the NIPAm/BIS solution. The flask was then equipped with a temperature probe, a condenser and a N_2 gas inlet. The solution was bubbled with N_2 gas for ~1.5 h, while stirring at a rate of 450 rpm, allowing the temperature to reach 45 °C. AAc (2.0 mmol) was then added to the heated mixture with a micropipette in one aliquot. A 0.078 M aqueous solution of APS (5 mL) was delivered to

the reaction flask with a transfer pipet to initiate the reaction. Immediately following initiation, a temperature ramp of 45 to 65 °C was applied to the solution at a rate of 30 °C/h. The reaction was allowed to proceed overnight at 65 °C. After polymerization, the reaction mixture was allowed to cool down to room temperature and filtered through glass wool to remove any large aggregates. The coagulum was rinsed with deionized water and filtered. Aliquots of these microgels (12 mL) were centrifuged at a speed of ~8500 relative centrifugal force (rcf) at 23 °C for ~ 40 minutes to produce a pellet at the bottom of the centrifuge tube. The supernatant was removed from the pellet of microgels, which was then re-suspended to the original volume (12 mL) using deionized water. This process was repeated until the microgels were cleaned.

Fabrication of plastic substrates: Transparent flexible plastic sheets (transparency films for high temperature laser copiers from 3M company, Canada) were rinsed with DI water and ethanol and dried with N_2 gas, and 2 nm of Cr followed by 50 nm of Au were thermally evaporated onto them at a rate of ~0.2 Å s^{-1} and ~0.1 Å s^{-1}, respectively, using a Torr International Inc. model THEUPG thermal evaporation system (New Windsor, NY). The Cr acts as adhesion layer to hold the Au layer on the plastic. An aliquot of about 12 mL of previously purified microgel solution was centrifuged for 30 min at 23 °C at ~8500 rcf to pack the microgels into a pellet at the bottom of the tube. After removal of the supernatant solution, the microgel pellet was vortexed and placed onto a hot plate at 30 °C. A previously coated Cr/Au substrate was rinsed with ethanol, dried with N_2, and then placed onto hot plate (Corning, NY) set to 30 °C. Aliquots (40 µL for each 25 × 25

mm area) of the concentrated microgels were put onto the substrate and then spread toward each edges using the side of a micropipette tip, as previously described.[275] The microgel solution was allowed to dry completely on the substrate for 2 h with the hot plate temperature set to 35 °C. After 2 h, the dry film was rinsed copiously to remove any unreacted monomer and/or linear polymer from the microgel solution. Then the substrates were washed copiously with DI water to remove any excess microgels not bound directly to the Au. Microgel painted substrate was then placed into a DI water bath and allowed to incubate overnight on a hot plate set to ~30 °C. Following this step, the substrate was again rinsed with DI water to further remove any microgels not bound directly to the Au substrate surface. The microgel painted Au coated substrate was dried with N_2 gas and used for the experiment.

Self-folding devices: A specific amount of pDADMAC solution (pH 6.5, 20 wt% in water) was spread onto the microgel layer. The whole set up was undisturbed and dried at ambient temperature/humidity. After the complete drying of the film, the devices were moved into the chamber, which can control the environmental humidity. Air-O-Swiss AOS 7145 Cool Mist Ultrasonic humidifier (manufactured by Swiss Pure Air) was used to control the humidity in the chamber with an electronic feedback mechanism to maintain a steady humidity.

4.3 Results and discussion

4.3.1 Mechanism

To explain how the device bends/deforms, the device can be thought of as two separate layers (Figure 4-1a). The pDADMAC-microgel composite (upper layer) serves as the device's active layer, while the Au-plastic substrate (lower layer) is the passive layer. Two assumptions were made in this investigation: (1) the pDADMAC–microgel composite is homogeneous and stress along the layer either linearly increases or decreases; (2) the Au-plastic substrate is not contractible and stress along the layer either linearly increases or decreases. The interface between the two layers can be thought of as being made of an infinite number of points, which do not change location because of assumption (2). Each point is defined as a fulcrum, one of which is shown in Fig. 1a; the two layers are connected at that/those small region(s). In the active layer, we have shown that dehydration leads to contraction, presumably due to enhanced hydrophobic interactions between the pDADMAC. This contraction leads to contracting forces (F_c), which are shown as black vectors in Figure 4-1a. The strong forces pull all parts of the Au-plastic lower layer in the direction of force. Meanwhile the lower layer connected to the upper layer by the fulcrum will be pulled in the opposite direction by the torque (τ) generated from the contraction of the upper layer.

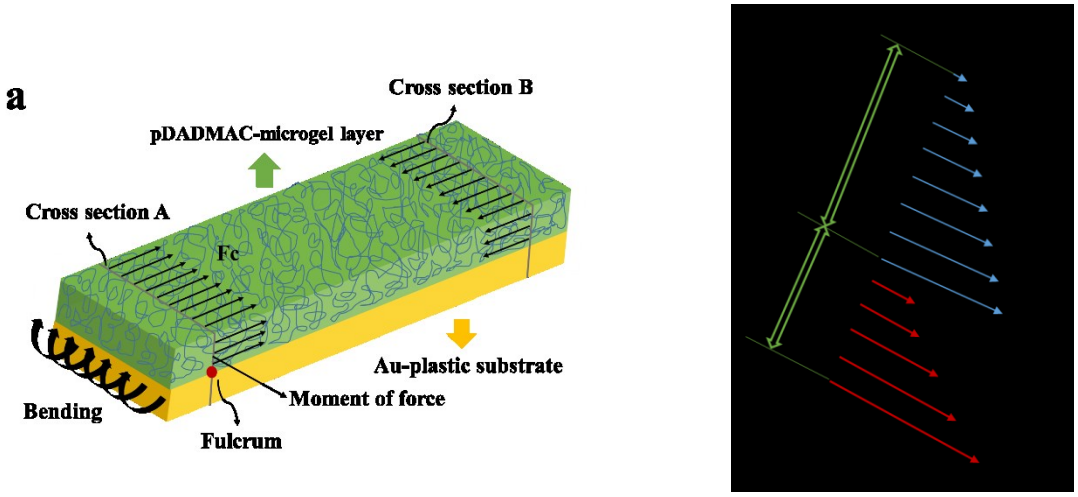

Figure 4-1 Mechanical model used to describe the devices. a) A detailed view of the device showing the stress generated in the upper layer (Fc), which leads to device bending. The device is considered to be two separate layers, the top layer defined by the pDADMAC-microgel layer and the bottom layer defined by the Au/Cr-coated plastic substrate. b) A single portion of the device in a). The dashed line represents the initial state of the two layers, while the solid line represents the final state after bending is complete. F_1^i are the stresses at different points on the Au-plastic substrate, while F_2^j are the stresses at different points on the microgel-pDADMAC layer. d_1 is the thickness of Au-plastic substrate, while d_2 is the thickness of the microgel-pDADMAC layer. θ is microscopic bending angle. The blue vectors (force vectors in upper layer) represent the contraction forces in the microgel-pDADMAC layer, while the red vectors (force vectors in lower layer) represent the restoring forces in the Au-substrate layer after the bending is complete.

To further explain the bending/folding process and to identify the governing parameters, we developed a mathematical model. To make the model less complex, we concentrated on only a "microscopic" portion of the assembly. As shown in Figure 4-1b, the two layers are represented by two lines connected by one fulcrum. The dashed line

represents the initial state of the portion of the assembly considered, while the solid line represents the final state after bending is complete. After bending is complete, the force at the fulcrum (at the interface between the pDADMAC and the microgel-Au-plastic layers) is a maximum, which gradually decreases as the distance from this point increases through the upper layer. The forces are noted as F_2^j indicated by the blue vectors in Figure 4-1b. This is the case because we assume that the plastic layer is not contractible (assumption 2), therefore we assume that the interface is likewise not contractible. Therefore, the polymer at the interface has more of a restoring force than the fully contracted polymer layer far away from the interface -- much like a spring. F_2^j in the upper layer depends on three factors: the microscopic bending angle θ, a material related force parameter k_2 and the thickness d_2 of the upper layer. The fulcrum point shown is common to both layers. Based on the fact that the contraction force in the upper layer is relatively large and that the lower Au – plastic layer isn't contractible (F_1^i at the interface is 0), we assume that the stress at the fulcrum at the interface is only from the contraction of the upper layer. Then the stress on this point is equal to the remaining contracting force at the bottom of the upper layer and we note it as F_2^0. And the remaining contracting force on the top of the upper layer can be expressed as ($F_2^0 - k_2\ \theta\ d_2$). Based on assumption 1, the *average* stress along the upper layer after bending is complete can be expressed as equation (1):

$$F_{2\ average} = \frac{(F_2^0 - k_2\,\theta\,d_2) + F_2^0}{2} \qquad (1)$$

Likewise, the forces on the plastic-Au layer increase as the distance from the interface increases. Again, this can be related to a spring; at the interface where bending is most complete there is little restoring force, while there is still significant forces at the bottom where bending is less complete. These forces are noted as F_1^i (red vectors), which are in the same direction of the remaining contraction forces in the upper layer, which oppose bending due to the fulcrum. The bending angle θ together with material related force parameter k_1 and thickness d_1 of the lower layer determines the restoring forces along the lower layer. As shown in Fig. 2b, the stress at the bottom of the lower layer was noted as F_1^0, which can be expressed as (k_1 θ d_1). Because the Au-plastic layer is not contractible, the stress on the fulcrum from the bottom layer is 0. Thus, the average stress in this layer can be expressed as equation (2).

$$F_1^{\,average} = \frac{k_1\,\theta\,d_1 + 0}{2} \qquad (2)$$

Due to stresses on both layers two torques are formed on both layers separately, which are expressed mathematically below:

$$\tau_1 = F_1^{\,average} \times r_1 = \frac{k_1\,\theta\,d_1 + 0}{2} \times \frac{d_1}{2} \qquad (3)$$

$$\tau_2 = F_2^{\,average} \times r_2 = \frac{(F_2^{\,0} - k_2\,\theta\,d_2) + F_2^{\,0}}{2} \times \frac{d_2}{2} \qquad (4)$$

r represents the distance from the point where the torque is measured to the point where the force is applied in the respective layers, while d is the thickness of the respective layers. In each equation, r is equal to half of the thickness of each layer. At the final state of bending ("equilibrium"), the two torques are equal to maintain a steady bent state,

otherwise, the assembly will continue to bend until this is the case. As such, after complete bending equations (3) and (4) are equal leading to equation (5):

$$\frac{k_1\,\theta\,d_1+0}{2}\times\frac{d_1}{2}=\frac{F_2{}^0-k_2\,\theta\,d_2+F_2{}^0}{2}\times\frac{d_2}{2} \qquad (5)$$

Then the microscopic bending angle θ can be expressed as equation (6):

$$\theta=\frac{2\,d_2\,F_2{}^0}{k_1\,d_1{}^2+k_2\,d_2{}^2} \qquad (6)$$

Again, this is the "microscopic" bending angle, which leads to macroscopic device bending. Macroscopically the device will show specific curvature after bending is complete. Theoretically, we can represent the curvature by the radius (R) of rolls or incomplete rolls after bending. In this case, microscopically $F_2{}^0$ in equation (6) can be expressed as one force (between the upper layer and the lower layer), which is determined by another force parameter, the interfacial force parameter (k) multiplied by a length (L), which represents the length of the interfacial layer exerting forces on the fulcrum on the microscopic level. Furthermore, L can be expressed as the bending angle θ multiplied by $(R - d_1)$. Therefore, $F_2{}^0$ can be represented by equation (7):

$$F_2{}^0=k\,\theta\,(R-d_1) \qquad (7)$$

Subsequently, equation (6) can be rewritten as equation (8):

$$\theta=\frac{2\,d_2\;k\theta\,(R-d_1)}{k_1\,d_1{}^2+k_2\,d_2{}^2} \qquad (8)$$

Finally, the macroscopically observed R can be expressed as equation (9):

$$R=\frac{k_1\,d_1{}^2/_k+k_2\,d_2{}^2/_k}{2\,d_2}+d_1 \qquad (9)$$

As k, k_1, k_2 are force parameters (constants) determined by the materials themselves, from equation (9) we conclude that the radius after bending is only related to the thickness of each layer d_1 and d_2.

To test our mathematical model, we fabricated rectangular devices of different dimension, but containing the same upper and lower layer thicknesses. As predicted from equation (9), these devices should self-fold to yield similar values for R. There is a precedent for this result; in a previous study, Li and coworkers[276] observed that the curvature of rolls after bending of rectangular bilayers depended on the thickness of the layers and strain, but not the bilayer dimensions. While this is the case, our investigation is the first to develop and test a mathematical model that is capable of predicting the self-folding behavior of such materials. Furthermore, we investigated how the bending of a single device, with given dimensions, depended on the upper layer thickness (d_2) to determine if equation (9) could indeed be used to predict R.

4.3.2 Self - folding behavior of rectangular devices

Self-folding is a term used to describe materials that transform autonomously from two-dimensional materials into three dimensional structures such as spirals, tubes, corrugated sheets or polyhedron.[277] Self-folding can take place on many length scales -- from meters to nanometers.[278,279] Here, we show that the self-folding behavior of materials with centimeter-scale dimensions can be predicted using equation (9). To

accomplish this, we fabricated rectangular devices with four different aspect ratios.

b

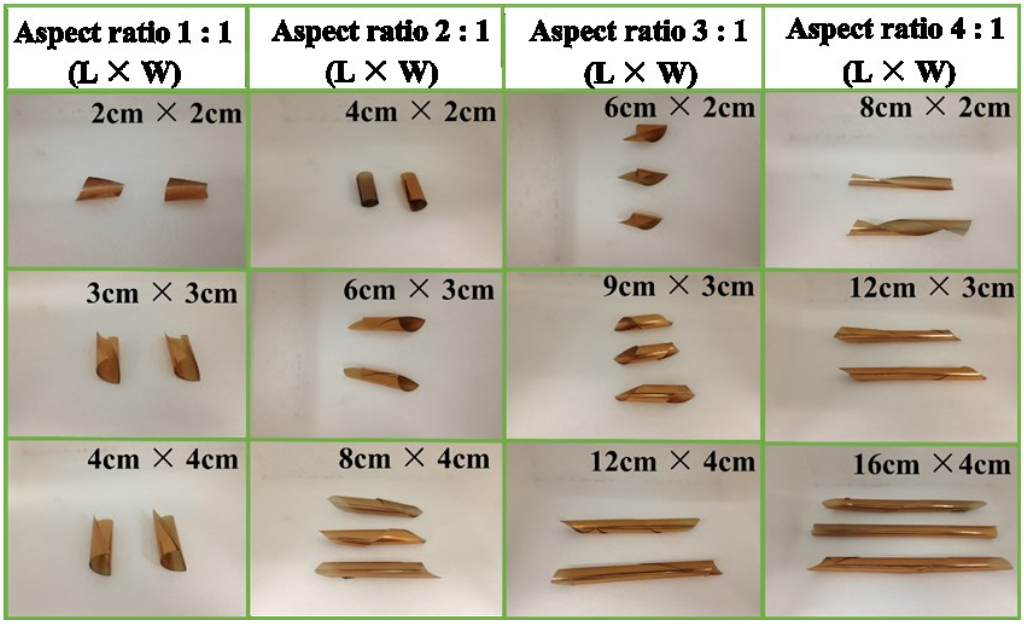

Figure 4-2 Images of devices before and after bending. a) A photograph of a device with dimensions of 3 cm × 9 cm before bending. b) Devices of different aspect ratio and dimensions after bending. As can be seen, the devices form different 3D structures after bending dependent on the aspect ratio and size of the devices. L represents the length of the device, while W is the width.

Furthermore, for each aspect ratio, we fabricated devices of different overall dimensions. In each case, the amount of pDADMAC added to each device was scaled for their individual dimensions such that the amount of pDADMAC on a given device area was

the same from device to device. Therefore, the thickness of the upper layer (d_2) was constant. Furthermore, the devices were constructed from the same lower layer material, maintaining the same lower layer thickness (d_1) from device to device. Figure 4-2a is a photograph of a representative device (3 cm × 9 cm) with pDADMAC deposited in its unfolded state (high humidity), while Figure 4-2b shows the final state of the devices dried under the same conditions. It is interesting to note that the devices tend to self-fold into unique three-dimensional structures after drying, which will be the subject of a future investigation. Here, we were interested in the radius of curvature (R in equation (9)) and how that depended on the device's aspect ratio and size. To measure the radius of curvature, we used the approach shown schematically in Figure 4-3. The circle in Figure 4-3 represents a device in its final state. If two lines are drawn (AB and A'B), perpendicular to the radii (OA and OA') they intersect at point B. As a result, two triangles are formed. In Δ OAB, the length AB can be measured using two rulers placed on the tangents to the curvature of the device -- the "length" at the intersection point is AB. Furthermore, the angle between the two rulers at that condition is also measured. With this information, the radius OA could be determined using equation (10) and equation (11):

$$\tan\frac{\alpha}{2} = \frac{OA}{AB} \quad (10) \qquad OA = AB \times \tan\frac{\alpha}{2} \quad (11)$$

For each device, we measured the radius at 5 different locations at a humidity of 19.7% and temperature of 23 °C and plotted the average radius as a function of the area (length × width) for each aspect ratio. The data is shown in Figure 4-5. As can be seen, while the

individual devices may self-fold into different structures (tubes/spirals), the radius of curvature for all the devices, regardless of overall size or aspect ratio, is in the range of 0.75 ~ 0.85 cm. From these results, we conclude that the final radius of the devices only depends on the thickness of the two layers. Again, investigations into the self-folding into different structures will be the subject of a future publication.

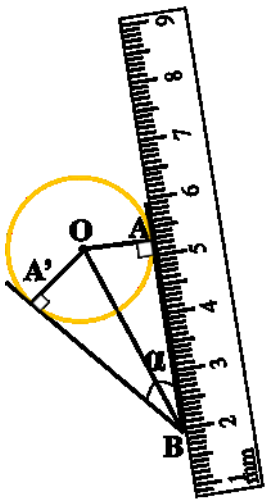

Figure 4-3 Protocol used for measuring the radius of the devices after bending. AB and A'B are two tangents perpendicular to the radius of a device OA and OA', respectively. B is the intersection of the two tangents. α is the angle between the two tangents. Two rulers were used to measure AB and A'B, while a protractor was used to measure the angle between the rulers to determine α.

In addition, using devices with dimensions of 9 cm × 3 cm, the thickness of the upper layer d_2 was systematically varied by depositing different amounts of pDADMAC

solution on the surface of the microgel-Au-plastic substrate. In this case, the thickness of Au-plastic substrate was kept constant. The volumes of pDADMAC used were 1 - 10 mL, which yielded a range of d_2, and two devices of each thickness were prepared for each volume, as shown in Table 4-1.

Table 4-1 The thickness of the pDADMAC layer after deposition and drying of different volumes on a substrate. These are the actual measured thicknesses that were used in Figure 4-6 in the main text.

Following drying of the pDADMAC layer, its thickness was measured using a digital caliper and the radius of curvature was measured for each device using the same protocol as above. The data is plotted in Figure 4-4. As can be seen, the radius of curvature depends dramatically on the thickness of the upper layer. Subsequently, by knowing the thicknesses of both layers, we could fit equation (12) to the data in Figure 4-5, and the best fit values for A and B determined. It should be pointed out here that equation (12) is the same as equation (9) with the constants A and B representing the individual k-containing terms in equation (9). As a result of the fit, the best fit values for A and B in equation (12) were found to be 3.6 ± 0.4 and 15.1 ± 2.4, respectively.

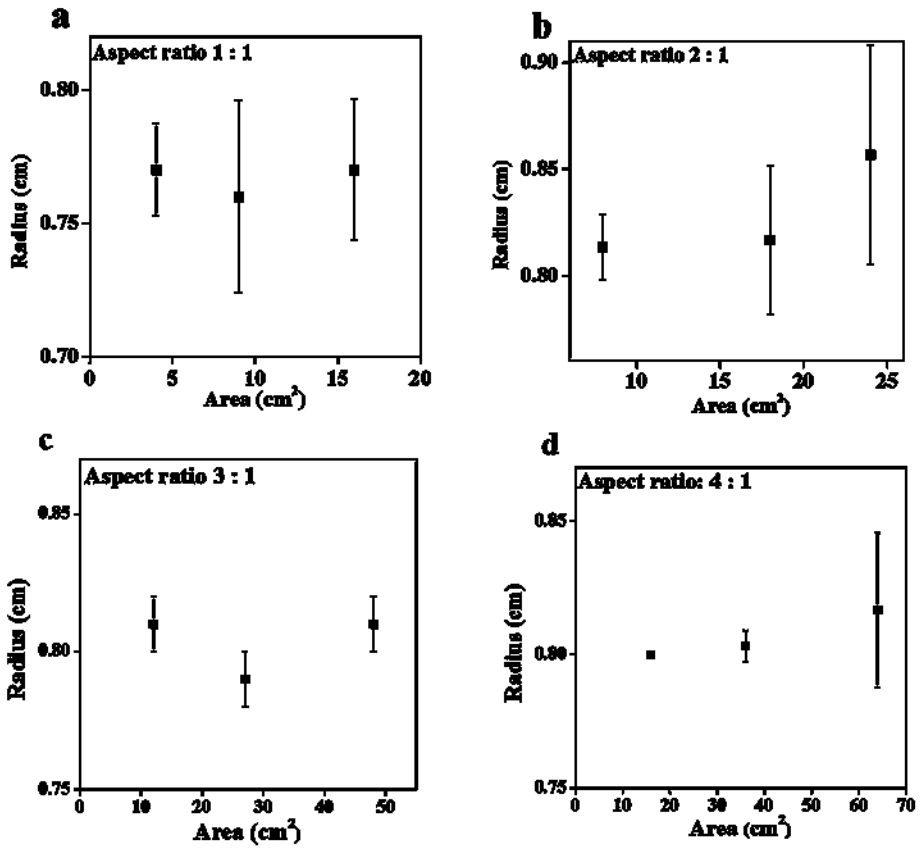

Figure 4-4 The measured radius of the devices as a function of their size and aspect ratio. As can be seen, the measured radius of the devices didn't depend strongly on their size and aspect ratio. Three devices were made at each size and aspect ratio and the radius determined at 5 different locations for each device. Each point is therefore the average of 15 radius values measured from 3 devices at 5 different locations. The error bars indicate the standard deviation.

$$R = \frac{A + B\,{d_2}^2}{2\,d_2} + 0.1016 \quad (12)$$

Further, we tested the model by fabricating device with given d_2 and comparing the predicted and measured R values. For d_2 of 0.45 mm, and 0.72 mm, the model predicts an

R of 7.40 mm and 8.02 mm. This is in comparison to the measured values of 6.63 mm and 8.43 mm, as can be seen the model closely predicts the experimental R.

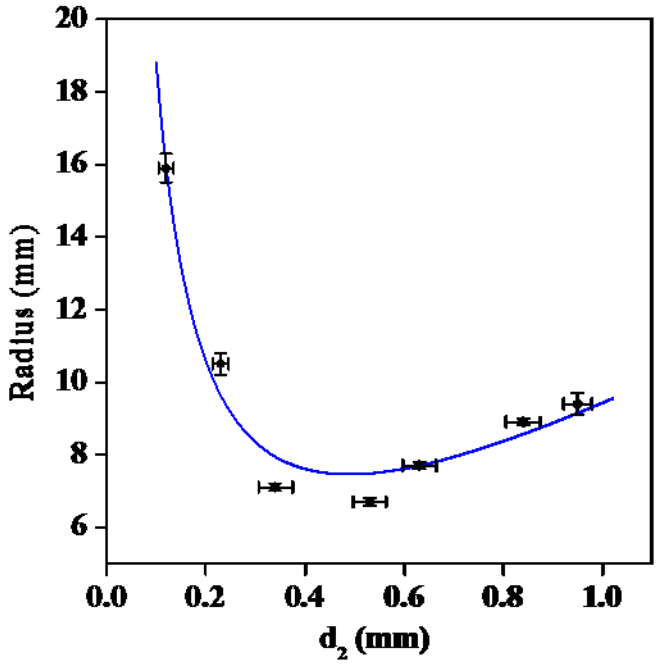

Figure 4-5 Dependence of device radius on pDADMAC layer thickness. The data points are real data obtained by measuring the radius of two separate devices with a given d_2. Each point is the average of 10 radii determined at 5 different locations of the two separate devices. The error bars are the standard deviations of the measured d_2 and radius. The blue curve is the best fit of equation (12) to the data yielding values for A and B of 3.6 ± 0.4 and 15.1 ± 2.4, respectively. The equation was fit to the data using Matlab software.

4.3.3 Controlling the self-folding process

Using our mechanical and mathematical models above to predict important design

parameters, we created materials that are capable of self-folding into desired 3D structures. To accomplish this, an empirical rule was developed to calculate the amount of pDADMAC-microgel composite needed to be added to the Au – plastic substrate to make the whole device self-fold by a specific angle α. Equation (13) was developed to predict this behavior:

$$\overset{\frown}{AA'} = \frac{180^0 - \alpha}{360^0} \times 2\pi \times OA \quad (13)$$

Wherein, $\overset{\frown}{AA'}$ is the length of the arc AA' in Figure 4-3, while OA is the radius of the self-folded structure at a specific humidity and temperature. 2π × OA is the circumference of the self-folded device. For example, at humidity of 19.7% (dry) and temperature of 23ºC, if we want a structure with a curling angle α of 90º, we need the length of $\overset{\frown}{AA'}$ to be ~ 1.25 cm according to the equation (13). That means, if we want the device to bend to yield a right angle, we need to deposit a layer of pDADMAC onto the device with a width of ~ 1.25 cm along the direction of bending. The volume of pDADMAC added to the device should yield the same d_2 as used above. Following this rule, we designed devices capable of self-folding into discrete and predetermined 3D structures. As can be seen in Figure 4-6, the width and direction of the deposited pDADMAC layer depends on how we want the device to self-fold, and through this, we have great control over the device's reversible self-folding behavior.

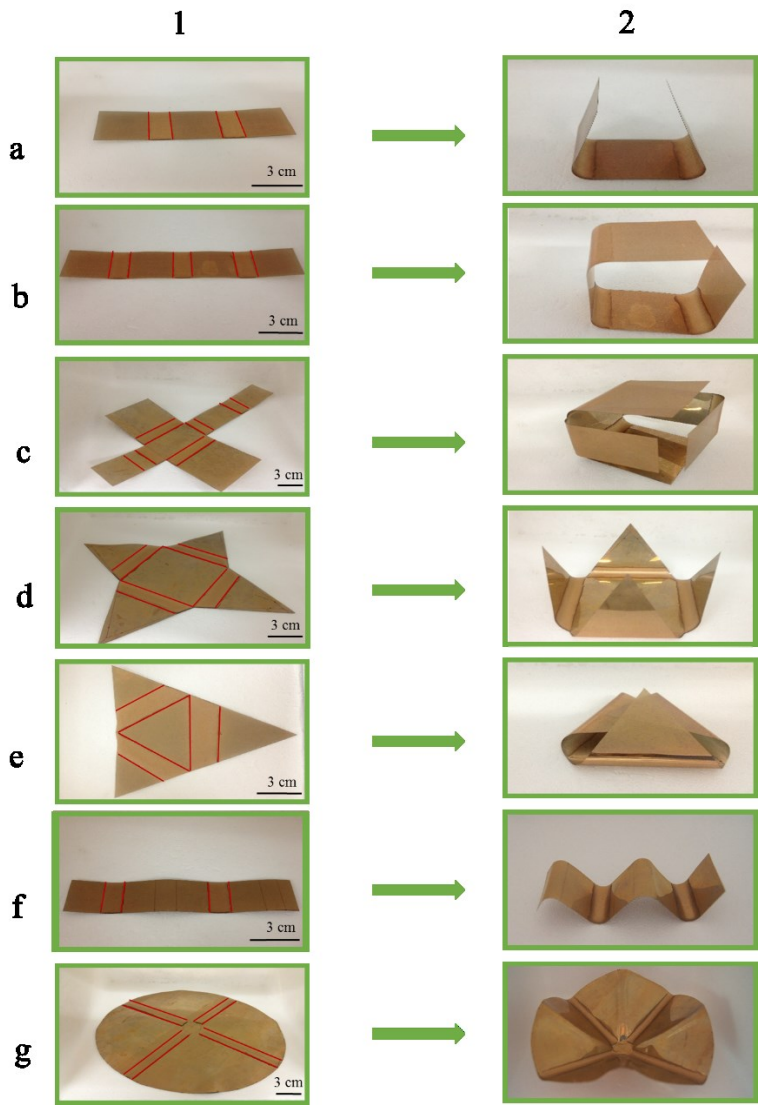

Figure 4-6 Rationally designed devices capable of self-folding into three-dimensional structures. Column 1) Specially designed microgel coated Au/plastic substrates with a given width of pDADMAC deposited at specific locations (red outlined areas) to yield the desired 3D structure Column 2) after drying. For devices a, b, c, and d the width of the pDADMAC solution deposited in each red frame was around ~1.25 cm. For device e, the width of the pDADMAC solution was ~2 cm. For devices f and g both sides of the plastic substrates were coated with Au and microgels, and pDADMAC subsequently deposited on specific locations with a width of ~1.25 cm.

4.4 Conclusion

In summary, we investigated in detail the self-folding behavior of rectangular humidity-responsive microgel-based polymer composites deposited on a substrate of varying dimensions and aspect ratios. We detailed a mechanical and mathematical model that is capable of describing the self-folding characteristics of these bilayer devices. Furthermore, using this information, we were able to devise an approach for fabricating devices that self-fold into predetermined 3D structures with varying complexities. We hypothesize that the material parameters defined in the presented model is one that can be generalized to essentially any bilayer material, and similar studies can be completed. This work paves the way for producing stimuli responsive adaptive polymer materials, which have potential applications in actuation, sensing, artificial muscles and robotics.

Chapter 5: Understanding the Shape Memory Behavior of Self-Bending Materials and Their Use as Sensors[3]

5.1 Introduction

In this Chapter, we show that the bending conformation/direction of the bilayer systems presented in Chapter 3 and 4 could be templated, and they are capable of exhibiting shape memory. Our bilayer system is examined in detail, which led to an understanding of the phenomena leading to shape memory. By close examination of microscopy images and diffraction patterns, it is concluded that the dried polymer-based layer was composed of both amorphous and crystalline phases — the amorphous phase can readily absorb water, which results in actuation, while the crystalline phases template the bending characteristics of the device. With an understanding of the bending behavior of the devices, humidity sensors are generated by interfacing them with stretchable strain sensors, which were also developed here specifically for the bendable materials here.

Actuators composed of responsive (i.e., smart or stimuli responsive) polymers/materials are capable of reversibly changing their shape, size, and/or mechanical properties in response to external stimuli. Actuators have found applications as/in sensors,[280-282] artificial muscles,[283,284] controlled encapsulation/delivery vehicles,[191]

[3] This Chapter has been adapted from a previously published article. Li, X., Serpe, M. J., *Adv. Funct. Mater.* 2016, 26, 3282.

biomimetic actuating systems,[285] and soft robotics.[237] A variety of stimuli responsive polymers and materials, such as liquid crystalline polymers, hydrogels, shape memory polymers (SMPs), and elastomers have been fabricated to make sensors and actuators.[112,143,286,287]

So called "shape memory polymers" (SMPs) are another interesting class of stimuli responsive materials that have been used for actuation.[127] As mentioned in Chapter 1, a conventional SMPs exists in some initial (or permanent) shape, which can be changed when exposed to specific environmental conditions (typically high temperature). With the material trapped (typically physically) in the temporary state, the environmental conditions can be returned back to their initial state, which traps the material in its temporary state. The SMPs can return to its permanent shape once the environmental conditions return to the state where the temporary state was formed.[288-290] Recent results have shown that shape memory materials can be achieved without the use of standard SMPs. For example, Ionov and coworkers reported on a polymer-based actuator composed of biodegradable polycaprolactone (PCL)-gelatin bilayers, which are unfolded at room temperature and folded at temperature above PCL's T_m.[291] This is because PCL is crystalline and stiff at low temperature, which prevents any shape change of the material. Heating the PCL above its T_m allows the material to deform due to the melting of the polymer. Cooling down leads to the recrystallization of the PCL and induces the polymer film to recover its unfolded shape.

Strain sensors, with high flexibilities and stretchability, have the ability to transduce

physical forces (including bending and twisting) and chemical stimuli into electrical signals.[292-295] These devices play a key role in many emerging technologies, such as: intelligent robotic sensing systems,[296] human motion and health monitoring,[297,298] and electronic skin.[299,300] One typical approach to fabricating strain sensors is to impregnate flexible/stretchable polymer materials with conductive species. Nanoscale fillers (e.g., carbon nanotubes, graphene, metal nanowires, and metal nanoparticles) incorporated into flexible polymers have been shown to be effective for producing these devices. Several reviews have been published that illustrate how conductive nanostructures can be used for strain sensing applications.[294,301-303] However, in many cases they exhibit high electrical resistivity that may change significantly under strain and the conductivity is typically too low to be useful, leading to poor performance and reliability.[304] One alternative is to deposit thin films of highly conductive metal or alloy onto elastomeric substrates and those metal films on elastomeric substrates are sensitive to strain by fracturing or buckling, while retaining relatively high conductivity.[305]

5.2 Experimental section

Materials: *N*-isopropylacrylamide (NIPAm) was purchased from TCI (Portland, Oregon) and purified by recrystallization from hexanes (ACS reagent grade, EMD, Gibbstown, NJ) prior to use. *N, N′*-methylenebisacrylamide (BIS) (99%), acrylic acid (AAc) (99%), and ammonium persulfate (APS) (98+%) were obtained from Sigma-Aldrich (Oakville,

Ontario) and were used as received. Poly (diallyldimethylammonium chloride) solution (pDADMAC) with a MW 100,000 ~ 200,000 (20 wt% in water) was purchased from Sigma-Aldrich (St. Louis, MO). Sylgard 184 silicone elastomer base and Sylgard 184 silicone elastomer curing agent were purchased from Dow Corning Corporation, Midland, MI, USA. Deionized (DI) water with a resistivity of 18.2 MΩ•cm was used. Cr/Au annealing was done in a Thermolyne muffle furnace from Thermo Fisher Scientific (Ottawa, Ontario). Anhydrous ethanol was obtained from Commercial Alcohols (Brampton, Ontario). Cr was 99.999% and obtained from ESPI (Ashland, OR), while Au was 99.99% and obtained from MRCS Canada (Edmonton, AB).

Microgel Synthesis: Microgels composed of poly (*N*-isopropylacrylamide)-co-acrylic acid (pNIPAm-co-AAc) were synthesized via free-radical precipitation polymerization as described previously.[104] The monomer mixture, with a total concentration of 154 mM, was comprised of 85% (mole/mole) NIPAm, 10% AAc, and 5% BIS as the crosslinker. NIPAm (17.0 mmol), and BIS (1.0 mmol) were dissolved in deionized water (100 mL) with stirring in a beaker. The mixture was filtered through a 0.2 μm filter affixed to a 20 mL syringe into a 200 mL 3-necked round-bottom flask. The beaker was rinsed with 25 mL of deionized water and then filtered into the NIPAm/BIS solution. The flask was then equipped with a temperature probe, a condenser and a N_2 gas inlet. The solution was bubbled with N_2 gas for ~1.5 h, while stirring at a rate of 450 rpm, allowing the temperature to reach 45 °C. AAc (2.0 mmol) was then added to the heated mixture with a micropipette in one aliquot. An aqueous solution of APS (0.078 M, 5 mL) was delivered

to the reaction flask with a transfer pipet to initiate the reaction. Immediately following initiation, a temperature ramp of 45 to 65 °C was applied to the solution at a rate of 30 °C/h. The reaction was allowed to proceed overnight at 65 °C. After polymerization, the reaction mixture was allowed to cool down to room temperature and filtered through glass wool to remove any large aggregates. The coagulum was rinsed with deionized water and filtered. Aliquots of these microgels (12 mL) were centrifuged at a speed of ~8500 relative rcf at 23 °C for ~ 40 minutes to produce a pellet at the bottom of the centrifuge tube. The supernatant was removed from the pellet of microgels, which was then resuspended to the original volume (12 mL) using deionized water. This process was repeated until the microgels were cleaned.

Fabrication of Self-Bending Bilayers: Transparent flexible plastic sheets (transparency films for high temperature laser copiers from 3M company, Canada) were rinsed with DI water and ethanol and dried with N_2 gas, and 2 nm of Cr followed by 50 nm of Au were thermally evaporated onto them at a rate of ~0.2 Å s^{-1} and ~0.1 Å s^{-1}, respectively, using a Torr International Inc. model THEUPG thermal evaporation system (New Windsor, NY). The Cr acts as adhesion layer to hold the Au layer on the plastic. An aliquot of about 12 mL of previously purified microgel solution was centrifuged for 30 min at 23 °C at ~8500 rcf to pack the microgels into a pellet at the bottom of the tube. After removal of the supernatant solution, the microgel pellet was vortexed and placed onto a hot plate at 30 °C. A previously coated Cr/Au substrate was rinsed with ethanol, dried with N_2, and then placed onto a hot plate (Corning, NY) set to 30 °C. Aliquots (40 μL for each 25 × 25

mm area) of the concentrated microgels were put onto the substrate and then spread toward each edge using the side of a micropipette tip, as previously described. The microgel solution was allowed to dry completely on the substrate for 2 h with the hot plate temperature set to 35 °C. Then the substrates were washed copiously with DI water to remove any excess microgels not bound directly to the Au. The microgel painted substrates were then soaked in DI water bath and allowed to incubate overnight on a hot plate set to ~30 °C. Following this step, the substrate was again rinsed with DI water to further remove any microgels not bound directly to the Au coated substrate surface. The microgel painted Au coated substrate was dried with N_2 gas and a specific amount of pDADMAC solution (pH 6.5, 20 wt% in water) was deposited onto the microgel layer. The whole set up was undisturbed and dried at ambient temperature/humidity. After complete drying of the pDADMAC layer, the devices were placed into a humidity controlled chamber. The humidity was controlled with an electronic feedback mechanism to maintain a steady humidity -- humidity was modulated using an Air-O-Swiss AOS 7145 Cool Mist Ultrasonic humidifier (manufactured by Swiss Pure Air).

Fabrication of Au-PDMS Hybrid Strain Sensors: A PDMS film with a thickness of 0.5 mm was made by mixing silicone elastomer base and curing agent (from Dow Corning) in volume ratio of 10:1. Then the resulting film was rinsed with DI water and ethanol and dried with N_2 gas, and 2 nm of Cr followed by 50 nm of Au were thermally evaporated onto the PDMS at a rate of ~0.2 Å s^{-1} and ~0.1 Å s^{-1}, respectively, using a Torr International Inc. model THEUPG thermal evaporation system. The sensor devices were

evaluated by measuring their resistance using a multimeter. To evaluate the sensor resistance as a function of stretching, the electrodes of a multimeter were continuously in contact with the two ends of the device. To evaluate the sensor resistance as a function of bending (when coupled to the self-bending devices), one end of the sensor was clamped, and attached to the multimeter electrode, while the other electrode was only attached to the sensor device after it completed bending at a given humidity. Additionally, the sensor devices were incorporated in a circuit composed of a battery and a green LED (~532 nm emission center) — the resistance of the sensor device could control the intensity of the LED. Similar to the above approach, the LED was continuously connected to the sensor device for the stretching experiments, while the LED was only connected to the sensor devices after complete bending. We quantified the intensity of the LED using a fiber optic probe to collect the light, which was coupled to a USB2000+ spectrophotometer all from Ocean Optics (Dunedin, FL).

X-ray Diffraction: A polymer film sample was prepared by dropping 0.5 mL pDADMAC solution on a silicon (100) substrate. Then we placed it in a humidity chamber held at 5% humidity until the layer dried. A Rigaku XRD Ultima IV using CuKα X-ray source (40 kV, 44 mA) and continuous scan mode was used to collect data, which was examined using JADE software.

Transmission Electron Microscopy and Electron Diffraction: The dried pDADMAC layer was first microtomed into thin films with a thickness of 100 nm by a LEICA EM UC6 and the thin films were floated onto acetone. Then the thin films were placed on

carbon-coated, copper grids. Within a short time, the acetone evaporated and the thin films were well attached onto the grids. Then TEM images and electron diffraction on specific areas were obtained by CM20FEG/STEM, operated at 200 kV.

5.3 Results and discussion

5.3.1 Shape memory effect study of bilayer systems

A schematic of the devices used in this investigation is shown in Figure 5-1. Specifically, onto circular plastic substrates (5.5 cm diameter) 2 nm Cr and 50 nm Au were deposited via thermal evaporation followed by painting pNIPAm-co-AAc microgels onto the resulting substrate, and finally a solution containing positively charged pDADMAC (20 wt% in water) was added onto the microgels and allowed to dry.[284] Importantly, the pDADMAC solution has a pH of ~ 6.5, which renders the pDADMAC positively charged, while the AAc in the microgels is deprotonated and hence negatively charged. The many electrostatic interactions between these species allows the

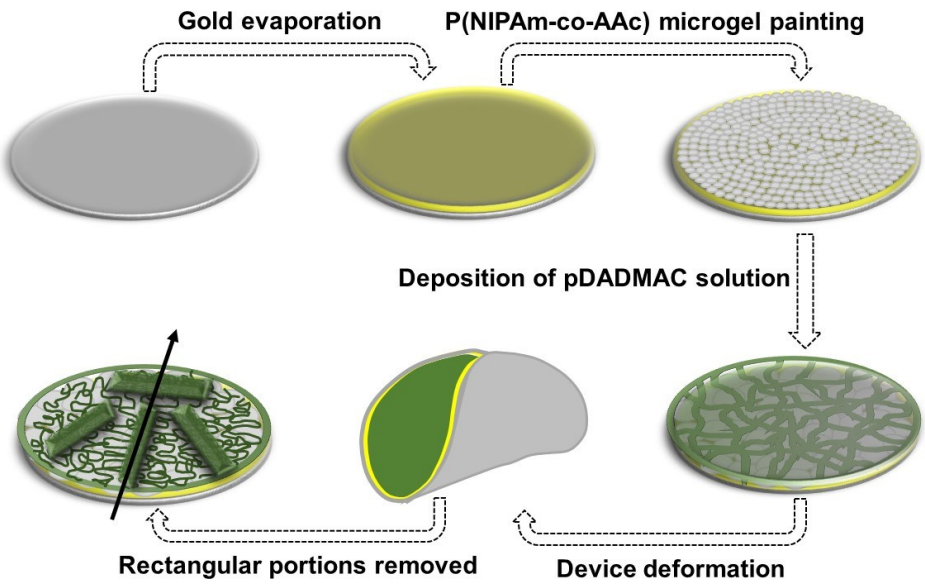

Figure 5-1 Bilayer fabrication process showing the bending behavior, and the bending axis (black arrow). Rectangular pieces can be cut from this bilayer at various orientations relative to the bending axis.

pDADMAC layer to strongly adhere to the microgel layer. Furthermore, since the microgel layer is strongly adhered to the Au-coated flexible substrate, the contraction of the pDADMAC layer upon drying is translated into bending of the flexible substrate. We consider the resulting devices as bilayers — the top layer being composed of pDADMAC and microgels and the bottom layer is the Au and plastic. Upon drying the pDADMAC layer at 5% relative humidity, the device bends along one central axis and the resultant shape and degree of bending depends on the size/shape of the flexible substrate, and the amount of pDADMAC deposited on the microgel coated flexible substrates. It is also important to note that pDADMAC itself doesn't bend significantly upon drying, and the fact that it is strongly bound to the flexible substrate allows the contraction upon drying

to be translated into device bending. The device subsequently opens (unbends) when it is exposed to an environment with a relative humidity of 55%; this is due to the pDADMAC layer absorbing water from the environment, hydrating, and expanding. The bending and unbending process can be repeated many times and each time the device bends along the central axis that was formed during the initial bending. Thus the devices exhibit shape changing behavior and *shape memory* since the bent and unbent conformations are reproducible over many cycles.

Figure 5-2a shows a photograph of a typical bent circular device that was fabricated as part of this investigation. For this investigation, three devices were fabricated in the same way, with the same dimensions and each showed the same bending behavior as the device shown in Figure 5-2a. When each of the three devices was opened, rectangular portions (0.8 cm × 3 cm) were cut out of each device, with different orientations relative to the bending axis; this is shown in Figure 5-2 (b-d) — these are referred to as templated devices. As can be seen in Figure 5-2e, each of the rectangular portions bend into a specific conformation defined by where they were cut from the circular device, and the cutting orientation/direction relative to the bending axis. In other words, they bend into a conformation that exactly matches how they would have bent if they were still part of the circular device they were cut from. For comparison, three separate rectangular devices (untemplated devices) with the same dimensions of those in Figure 5-2e (0.8 cm × 3cm) were fabricated in the same way as the circular devices, although the devices were not prebent prior to their generation. The rectangular devices were allowed to bend under the

same conditions as the devices in Fig 5-2e, and as can be seen in Figure 5-2f, the devices bend in a completely different manner relative to those devices cut from the circular

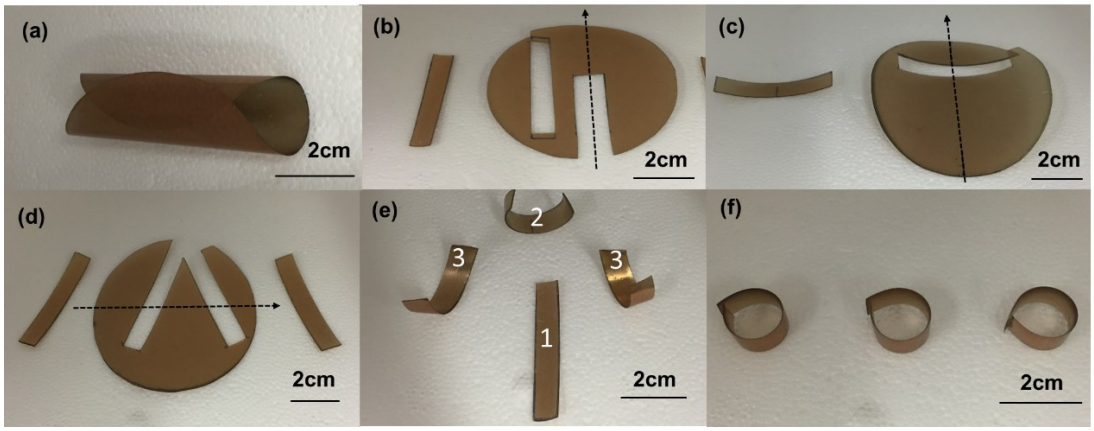

Figure 5-2 (a) A bent circular device; (b, c, d) Rectangular pieces cut from three different opened circular devices — the arrows indicate the bending axis on each device; (e) Bent rectangular devices cut from prebent circular bilayers — e1 is from b, e2 is from c, e3 are from d; (f) Bent rectangular devices with the same dimensions of the devices in (e), but these devices were cut from pieces that were not prebent.

"parent" devices. In fact, the bending behavior of the devices in Figure 5-2f can be predicted from our previously developed models, while our current models could not explain the bending behavior of the devices in Figure 5-2e. We also point out that all the respective devices bend in the same way over many bending/unbending cycles, suggesting that the bending direction is permanently templated into the devices.

To explain the bending of the untemplated devices in Figure 5-2f, we consider some recently published examples of self-bending bilayers.[203,306-308] Many bilayers constructed

from inorganic and polymer-based materials exhibit self-bending behavior due to the relaxation of internal stresses that originate from dissimilar properties of the two layers, e.g., lattice mismatches, thermal expansion coefficients, and swelling abilities. The size and shape of the bilayers also have a significant effect on the bending behavior that can yield "long-side", "short-side" and "diagonal" bending.[276,309,310] In other words, the way devices bend depends on the dimensions of the devices, and their specific aspect ratios. Thus, the bending behavior of the untemplated devices is directly related to their shape, size, and aspect ratio; the devices will bend in the direction (and into a shape) that minimizes resistance to bending. In the case of the untemplated devices here, long-side bending is the preferred bending direction, as can be seen in Figure 5-2f. On the other hand, the templated devices show completely different bending behavior, allowing them to bend in ways that are not preferred (Figure 5-2e), and into configurations that require bending in directions/conformations of high resistance. In order to explain this behavior, we defined the shape of the circular device after bending in low humidity as the "permanent shape" (also called "memorized shape"). Since the circular device is symmetric, it always bends into a tube configuration, which yields the minimum resistance to bending. By exposing the devices to high humidity, they can be fixed into unbent "temporary states". They have the ability to bend back to the permanent shape when the humidity is again decreased. Therefore, any portion of the circular device will be templated to bend in the direction that was originally dictated by the "parent" circular device, thus allowing the materials to reproducibly change shape with changes in

humidity. This reproducible bending behavior can be considered to impart shape memory to our materials, although it is for different reasons than what is seen in typical shape memory polymers.

To explain the shape memory function of our devices (and the templating effect), we investigated the properties of the pDADMAC layer via X-ray diffraction (XRD) analysis. XRD was performed on a pDADMAC film deposited on (100) silicon substrate, and the obtained XRD pattern is shown in Figure 5-3a. We have assigned the broad and strong peaks at $2\theta = 16.19^{o}$, 21.80^{o}, and 34.05^{o} to the polymer itself, showing both crystalline and amorphous phases. The rest of the diffraction peaks could be attributed to sodium chloride (NaCl), which exist in the polymer solution. Furthermore, we

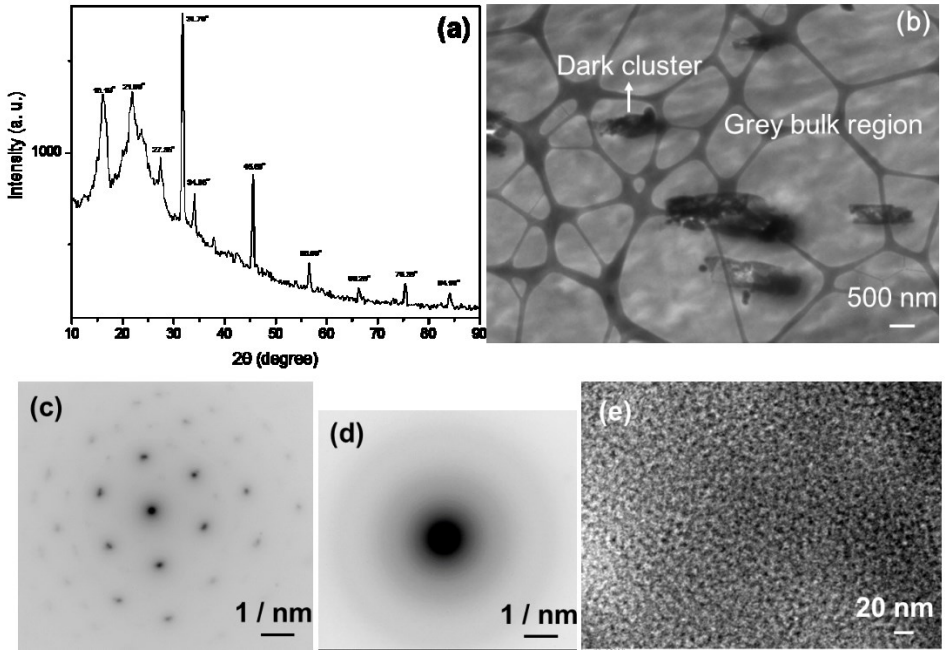

Figure 5-3 (a) X-ray diffraction pattern of pDADMAC layer; (b) TEM image of

pDADAMAC layer — dark "web-like" features are from the TEM grid; (c) Electron diffraction pattern of cluster of the microtomed thin pDADMAC film; (d) Electron diffraction pattern of polymer portion of the film; (e) TEM image of the polymer portion of the film.

investigated whether crystalline phases can be observed throughout the thickness of the polyelectrolyte layer. To investigate this, we microtomed the pDADMAC layer into thin polymer slices, each with a thickness of 100 nm and analyzed the film structure by transmission electron microscopy (TEM). From the TEM images in Figure 5-3b, it can be seen that there are two distinct regions — a grey bulk region and small dark clusters dispersed in the film. Electron diffraction analysis was performed on these two regions, and as can be seen in Figure 5-3c, the diffraction pattern for the dark clusters was proven to be NaCl while the diffraction pattern for the grey bulk region shows weaker (although present) features, as can be seen in Figure 5-3d. These further prove the semicrystallization of the polyelectrolyte layer. The TEM image (Figure 5-3e) of the grey bulk film in large magnification reveals that there are density differences on the polymer film, which is indicative of two distinct regions in the layer. This could be a proof that the film contains both crystalline and amorphous phases.

Based on above results, we propose the observed shape memory bending/unbending behavior of our templated devices is a result of the formation of both crystallized and amorphous phases in the pDADMAC layer. Specifically, upon deposition of the pDADMAC solution onto the microgel layer, the chains are in a fully extended state, as a

result of the highly charged monomer units in the polymer backbone repelling each other via electrostatic repulsion, and resultant electrostatic double layer-like effects. At low humidity, the pDADMAC solution dries, and the concentration of both the pDADMAC and the counterions in solution increases. The increase in counterion concentration increases the screening effect of pDADMAC's charged units — this allows the polymer chains to contract, and get closer to one another. Under these conditions, strong intermolecular interactions and entanglements between polymer chains can result in the formation of both crystalline and amorphous phases in the pDADMAC layer. We point out that NaCl crystals can serve as nucleation sites for pDADMAC crystallization, but this is not required for crystalline phase formation. In fact, Lu and coworkers have shown that crystallization could be observed in pure pDADMAC thin films.[311]

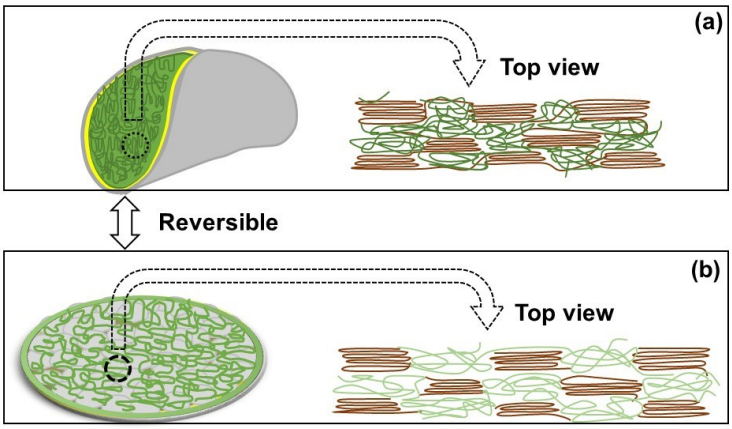

Figure 5-4 (Left) Schematic of the bent and unbent circular devices and (right) the corresponding proposed pDADMAC phases. Top views are the x-y of each circled region.

While the discussion above details how crystalline phases are formed, it still does not account for the observed shape memory. To explain this, we show a schematic of a bent device in Figure 5-4a. As can be seen, the device bends along one central axis into a tubular structure. As a result of drying, the device bends and crystalline phases are formed throughout the pDADMAC layer (described above), separated by amorphous phases; the crystalline phases are *hypothesized* to align perpendicular to the bending axis. We propose that it is the alignment of the crystalline phases with the bending axis that locks the bending direction of the devices in place. When exposing the bent device to high humidity, the amorphous phases swell more readily than the crystalline phases, leading to unbending of the device. This is shown schematically in Figure 5-4b. It is important to note that the crystalline phases retain their structure at high humidity, while the amorphous phases become soft and swollen — it is the retention of the crystalline phases that templates the shape memory. This concept is supported by previous studies that show that water may serve as a plasticizer of pDADMAC, which decreases its glass transition temperature (T_g), which is 70 °C for pDADMAC.[312] Therefore, as water is sorbed, the amorphous phases become soft and swollen, allowing the device to unbend. At the humidity required for unbending, the crystalline phases remain intact, which is also supported by literature precedent.[313,314] Finally, any portion cut from the prebent circular device will likewise retain these crystalline structures and orientations, which allows them bend/unbend in the same manner each time. Therefore, the individual portions cut from the prebent circular device will bend as it would if it were never cut

from the circular "parent" device, exhibiting a shape memory-like effect. We point out again that pDADMAC itself is not a shape memory polymer, although our bilayer devices allow it to bend flexible substrates into specific shapes, and these devices exhibit shape memory. This concept is illustrated schematically in Figure 5-5. As can be seen schematically in Figure 5-5a, when the rectangle is cut perpendicular to the bending axis, the device bends along the long axis, while it bends on the short axis if the rectangle is cut parallel to the original bending axis, as shown schematically in Figure 5-5b. Similar arguments can be made for any other devices (rectangular or otherwise) cut from different parts of the original circular device, and with any orientation relative to the bending axis.

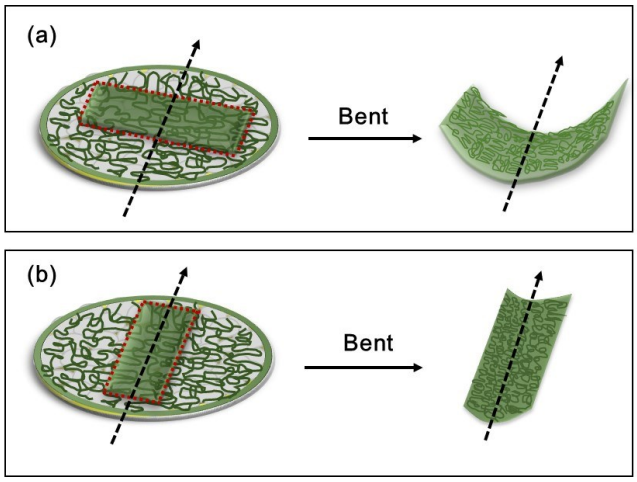

Figure 5-5 Schematic of the bent rectangular portions cut from the shaded regions of the (left) circular devices. (a) Rectangular device's long axis cut perpendicular to the bending axis; (b) Rectangular device's long axis cut parallel to the bending axis.

It is worth noting that the mechanism of shape memory that we describe here is much different than for common temperature triggered shape memory polymers, which relies on increasing and decreasing their temperature above and below the material's melting or glass transition temperature to yield material deformation. To the best of our knowledge, this is the first time that the crystallization of polyelectrolytes has been used to explain the shape memory behavior and deformation of devices.

5.3.2 Applications

With the shape memory behavior of our systems described, we used these devices to construct novel humidity sensors. Specifically, we cut rectangular pieces from a circular device (as above) and coupled them to strain sensors that are capable of changing their electrical properties (resistance/conductivity changes) upon stretching and/or bending. We also used these sensors as an electrical component in a circuit that was coupled to a light emitting diode (LED). This allowed the resistance changes of the strain sensors to modulate the intensity of the light emitted from the LED.

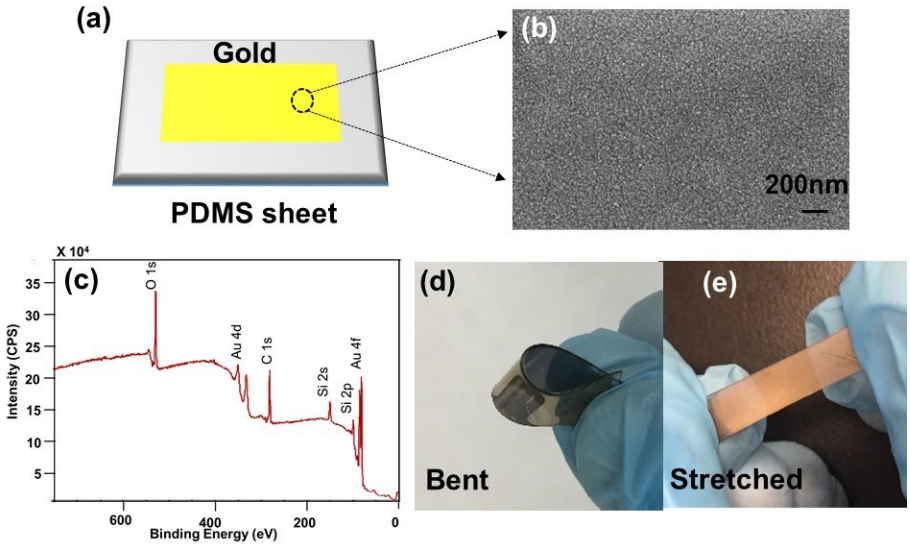

Figure 5-6 (a) Schematic depiction of the strain sensor; (b) FESEM images of the surface of the strain sensor after fabrication; (c) XPS of the gold coated PDMS substrate; (d, e) bent and stretched strain sensors.

First, we fabricated the strain sensor as shown schematically in Figure 5-6a. A 0.5 mm thick polydimethylsiloxane (PDMS) film was generated by mixing commercially available silicone elastomer base gel and curing agent in a 10:1 volume ratio and curing overnight at 70 °C on a plastic substrate. A thermal evaporator was then used to deposit 2 nm of Cr followed by 50 nm Au onto the PDMS. The resultant material was then cut into 10 mm wide x 25 mm long pieces. Figure 5-6b shows the field emission scanning electron microscope (FESEM) image of the surface of the hybrid material, which revealed connected Au "islands" with an average grain size of ~13 nm. Figure 5-6c shows the X-ray photoelectron spectroscopy (XPS) analysis of the surface, which reveals characteristic signals for Au, O and Si. Finally, we show that the devices are bendable and

stretchable, as shown in Figure 5-6d and 5-6e.

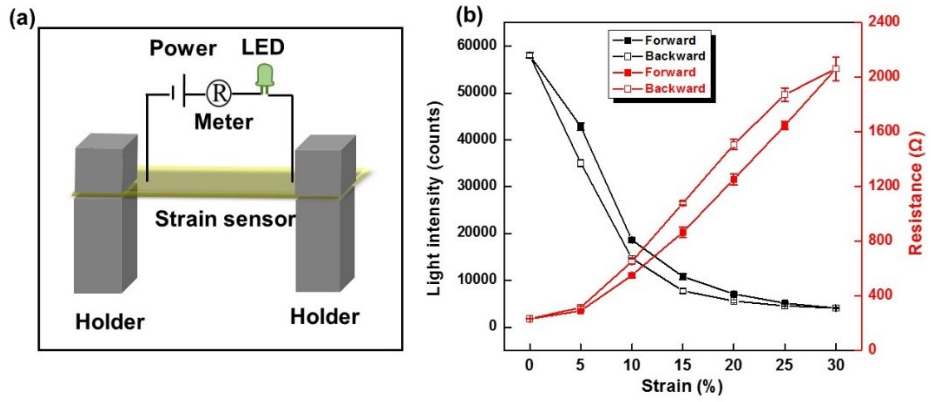

Figure 5-7 (a) Schematic depiction of the setup used to monitor resistance (and LED intensity) as a function of strain. (b) LED light intensity (left axis) resistance (right axis) and as a function of strain. In all cases, each data point is the average signal obtained from a single device measured three times, while the error bars is the standard deviation.

Figure 5-7a shows schematically how the resultant device was used as a strain sensor. Both ends of the device were clipped to electrical connectors, and a multimeter was used to determine the resistance of the devices as a function of applied strain, i.e., length increase compared to original length. Specifically, we determined the resistance as a function of stretching degree for strains of 0, 5, 10, 15, 20, 25, and 30% — the resistance was recorded for both stretching and unstretching. The stretching/unstretching was repeated three times and the results are shown in Figure 5-7b. Furthermore, we introduced this device as a component of an electrical circuit composed of a LED and a battery and showed that the light intensity could be modulated by stretching/unstretching

the hybrid material in the same manner as above. The intensity of the LED light at the different strains is shown in Figure 5-7b. We quantified the intensity of the LED using a fiber optic probe to collect the light, which was coupled to a USB2000+ spectrophotometer. As can be seen, there is some hysteresis between multiple stretching and unstretching cycles, although the distinct strains can be measured.

We point out that the mechanical properties and conductive behavior of PDMS coated with Au was reported previously, although no systematically study exists on the reversibility and precision of the response over many stretching cycles.[305,315,316] Here we further examined the morphology of the gold surface of the Au-coated PDMS using atomic force microscopy (AFM) and FESEM to understand why the electrical properties of the hybrid depended on the strain. Figure 5-8a shows schematically how the Au structure changes with strain, while Figures 5-8b and c are the corresponding AFM and FESEM images of the strained device. Before stretching the "as-deposited" Au layers appeared to be flat, consisting of islands with nanoscale dimensions. When the device was imaged while being held in a stretched state (15% strain), small lateral and transversal microcracks appear in the Au layer, which explained the increase in electrical resistance upon stretching the device. When the strain was increased near 30%, the crack number increased, with a concomitant increase in crack width. The combination of the increase in lateral and transversal cracks directly leads to the increased electrical resistance. When the strain is reduced, the Au film nearly flattens out, and the cracks disappear, leading to the decrease in resistance. This behavior explains the reversibility of

the electrical properties of the hybrid during the strain cycles.

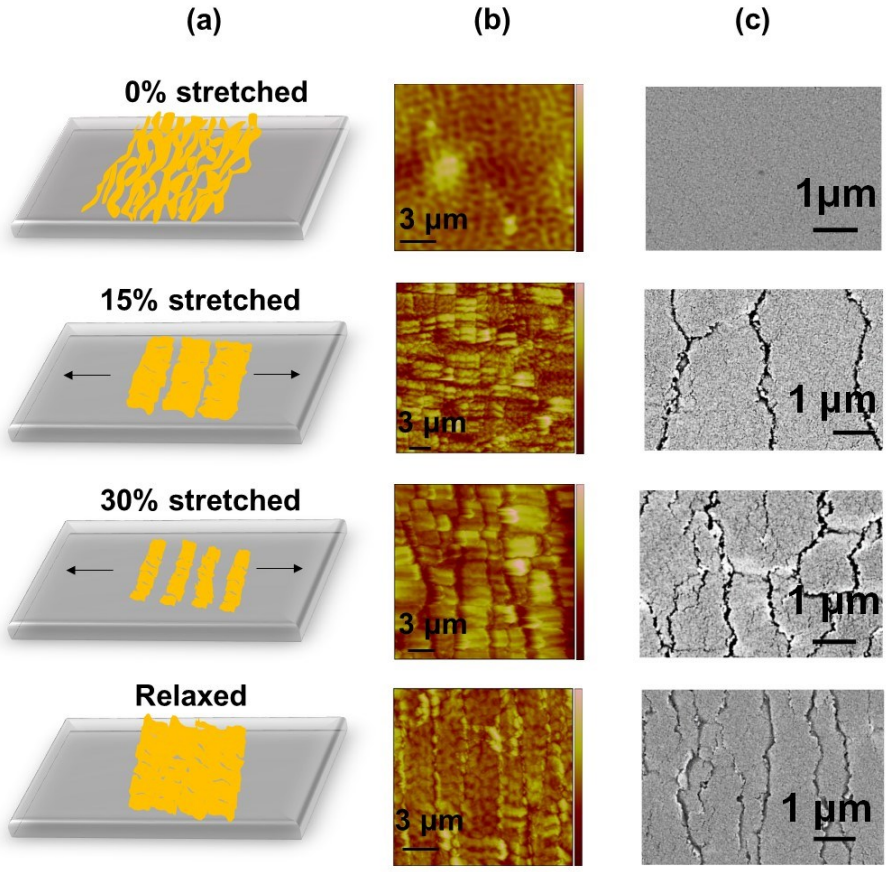

Figure 5-8 (a) Schematic depiction of the Au morphology as a function of strain and the corresponding; (b) AFM; and (c) FESEM images at the indicated strains.

Finally, we attached the bendable bilayer devices to the strain sensors to yield a humidity sensor. Specifically, strong van der Waals forces were used to adhere the uncoated side of a *templated* bilayer device to the uncoated side of the Au-coated PDMS. Therefore, the bending/unbending behavior of the bilayer piece will likewise cause the strain sensor to bend resulting in stretching/unstretching (Au film cracking/uncracking),

and electrical resistance changes. The templated devices were chosen for these experiments as they exhibited more reproducible and predictable bending behavior relative to the untemplated devices. To investigate the humidity response, we connected the assembly to a multimeter (attached onto the gold surface of the strain sensor) and put the setup in a humidity-controlled chamber. As can be seen in the data in Figure 5-9b, at a humidity of 45%, the assembly was flat. In this condition, the resistance of the strain sensor was relatively small. When the humidity was decreased to 35%, the device bent, resulting in an increased resistance. We subsequently lowered the humidity to 5% in 10% increments and measured the resistance. As can be seen in Figure 5-9b, the resistance decreased in a linear fashion with decreasing humidity. When the humidity was increased from 5% to 45% (in 10% increments), the resistance increased in a linear fashion, and closely followed the resistance for the decrease cycle with little hysteresis. Also, we connected the assembly to a circuit composed of a LED and battery and collected the LED light intensity as a function of humidity — this is shown schematically in Figure 5-9a. As can be seen in Figure 5-9b, the light intensity likewise depended on humidity. That is, as the humidity decreased the LED light intensity increased (due to the decreased resistance), while the LED light intensity decreased as the humidity increased (due to the increase in resistance). There was nearly no hysteresis between multiple humidity increase and decrease cycles. This proves that our bilayer self-bending devices can be used as humidity sensors, and could be further developed into sensors for other vapors.

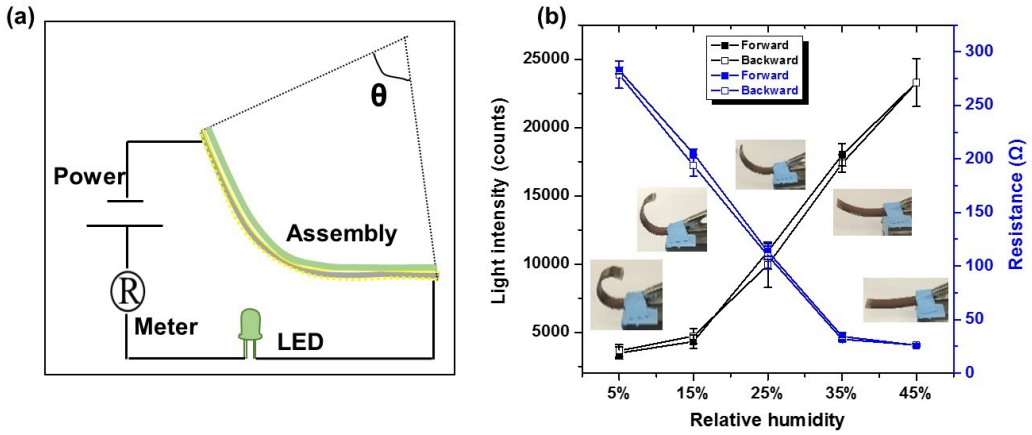

Figure 5-9 (a) Schematic depiction of the experimental setup used to measure resistance and LED light intensity as a function of device bending; (b) Light intensity (left axis) and resistance (right axis) changes induced by the bending of the bilayers coupled to the strain sensors. In all cases, each data point is the average signal obtained from a single device measured three times, while the error bars is the standard deviation.

5.4 Conclusions

In this work we fully characterized the self-bending behavior of humidity responsive polymer-based bilayer devices. We showed that the bending behavior was greatly influenced by the bending history of the materials they were taken from. Specifically, if rectangular bilayer devices were cut from prebent circular devices, they bent in a manner that directly matched the bending behavior of the region they were taken from. From this behavior we proposed that the pDADMAC layer forms both amorphous and crystalline phases — the crystalline phases template in the bending behavior, which is supported by experimental data. Finally, we fabricated strain sensors that could be coupled to the

self-bending materials to yield humidity sensors. While these devices can be used as vapor sensors, they could find utility as soft robotics, and as biomedical devices.

Chapter 6: Reversible Bi-Directional Folding of Hydrogel Actuators

6.1 Introduction

Smart hydrogels are crosslinked networks composed of stimuli responsive hydrophilic polymers, which are highly swellable with water.[317] They can undergo abrupt volume changes in response to changes in their environment, including temperature, pH, ionic strength, chemical, and electricity.[7,213,215,318] Consequently, they play a very important role in practical applications such as sensing,[319,320] drug delivery,[321,322] soft actuators and robotics,[213,259] and artificial muscles.[264,323] Interpenetrating polymer network (IPN) hydrogels are formed by combining two polymers (at least one should be responsive) that have some physical interactions that hold the network together (instead of covalent bonds),[324] as shown in Figure 6-1a. One type of IPN is called a semi-IPN, which is conventionally defined as a combination of two polymers, one of which is chemically crosslinked in the presence of the other linear polymer, which is physically entangled on the network,[325] as shown in Figure 6-1b. Compared with the single network hydrogels, it is possible for components of the IPNs to work together to yield materials with new behavior that is not expected by consideration of the responses of the individual components alone.[326] Most research on IPNs is focused on gaining a better understanding of their fundamental properties (e.g. swelling/deswelling of the system),[327,328] and on

their practical

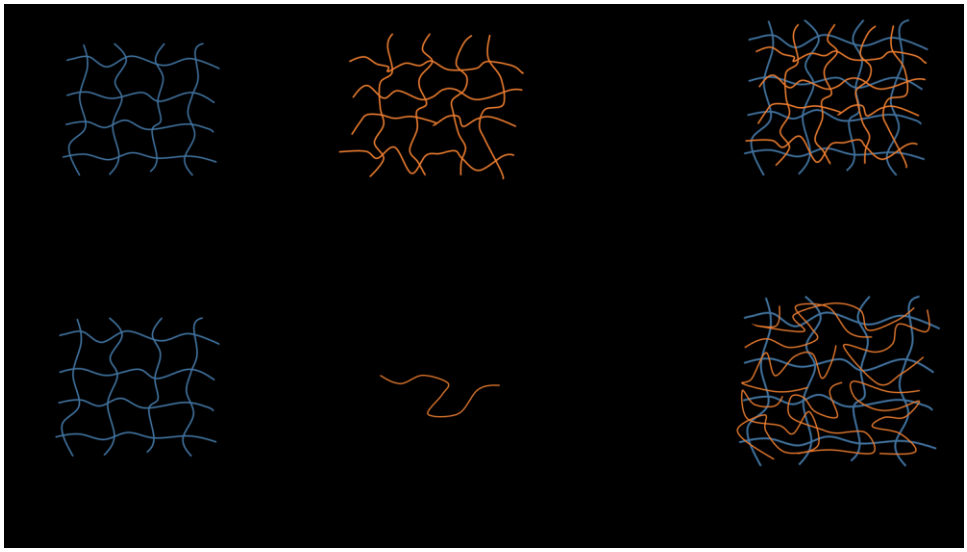

Figure 6-1 Schematic of (a) IPN hydrogel, (b) semi-IPN hydrogel

applications for biomaterials[329] and novel sorbents for separations.[330] Here, for the first time, we describe a novel semi-IPN hydrogel-based actuator composed of two layers. One layer is a poly (*N*-isopropylacrylamide) (pNIPAm)-based hydrogel interpenetrated by a linear poly (diallyldimethylammonium chloride) (pDADMAC), and the other layer is polydimethylsiloxane (PDMS).

PNIPAm is one of the most well-known temperature responsive polymers, which undergoes a coil to globule transition at temperatures above its lower critical solution temperature (LCST) of ~32 ºC.[19] Like linear pNIPAm, pNIPAm-based hydrogels undergo a transition from a swollen to a collapsed state upon heating above pNIPAm's LCST. Due to their thermoresponsivity, they have been applied for cell culturing,[203] drug delivery,[20]

and soft actuators.[190] Introducing ionic groups into neutral pNIPAm networks adds an additional osmotic pressure contribution to the swelling of the network due to the higher concentration of mobile ions within the network as a consequence of the Donnan equilibrium.[331] This renders ionic hydrogel networks responsive to dual stimuli, i.e., responsive to temperature and pH/ionization. For example, by copolymerizing a weak acid with *N*-isopropylacrylamide (NIPAm), a pH and temperature responsive network can be formed.[104] Acrylic acid (AAc) is one of the most commonly studied comonomers used for this purpose, which has a pKa of ~ 4.25. Therefore, AAc becomes deprotonated when pH of the solution is higher than 4.25, which leads to high osmotic pressure and swelling of the pNIPAm-co-AAc hydrogel network. Likewise, the network collapses when the AAc groups are protonated at low pH.

PDADMAC is a strong polycation, which contains permanent positive charges on its backbone. PDADMAC-based gels are able to absorb several hundred times their own volume of water,[332] which makes it a good candidate to induce higher water retention in hydrogels. For example, it has been reported that a series of IPN hydrogels with pDADMAC and other components, such as chitosan[333] and poly (vinyl alcohol),[334] were synthesized and the fundamental swelling dynamics were investigated. This category of hydrogels swell/deswell rapidly and show large-scale volume change in response to external stimuli.

Single-network pNIPAm-based hydrogel bilayer actuators, which rely on volume changes of the stimuli responsive hydrogel layer, have been reported

previously.[205,234,335,336] However, these actuators are limited to one directional deformation, and exhibit low stiffness which makes them too soft for many practical applications. In order to address these limitations, we fabricated semi-IPN hydrogel-based bilayers. In these devices, one layer is composed of pNIPAm-based hydrogel networks semi-interpenetrated with linear pDADMAC. Due to the significantly high water retention of pDADMAC, this semi-IPN hydrogel layer swells to a large extent at a low temperature. Compared with the hydrogel without pDADMAC, it undergoes larger-scale volume change as a result of heating above the LCST of pNIPAm. Secondly, we combine the system with a rigid polymer layer composed of PDMS, which increases the overall stiffness of semi-IPN hydrogel layer. The PDMS layer also serves as a non-water swellable layer, which is dissimilar to the pNIPAm-based hydrogel layer. We chose to construct the bilayer system into a cross-shape, which exhibits bi-directional folding behavior in response to temperature changes. This could be considered as a mimic of some natural actuators, such as jellyfish. Furthermore, we copolymerized AAc with NIPAm in the presence of pDADMAC, and the formed semi IPN hydrogel layer exhibits multi-stimuli responsivity, which enables the cross-shape bilayer devices to deform bi-directionally in response to pH changes. Moreover, we show that the existence of pDADMAC in the hydrogel layer enables our device to deform in a manner that is completely different from devices without pDADMAC. In this work, we show that the bilayers exhibit excellent temperature and pH-responsivity that can be used for temperature and pH controlled biomimetic actuators, manipulators and molecule release

devices.

6.2 Experimental section

Materials: *N*-isopropylacrylamide (NIPAm) was purchased from TCI (Portland, Oregon) and purified by recrystallization from hexanes (ACS reagent grade, EMD, Gibbstown, NJ) prior to use. *N, N′*-methylenebisacrylamide (BIS) (99%), acrylic acid (AAc) (99%), 2-propene-1-thiol (60% GC) and 2,2-diethoxyacetophenone (DEAP) were obtained from Sigma-Aldrich (Oakville, Ontario) and were used as received. Poly (diallyldimethylammonium chloride) solution (pDADMAC) with molecular weights of 100,000 ~ 200,000 (low Mw), 200,000 ~ 350,000 (medium Mw), and 400,000-500,000 (high Mw) (20 wt% in water) were purchased from Sigma-Aldrich (St. Louis, MO). Sylgard 184 silicone elastomer base and Sylgard 184 silicone elastomer curing agent were purchased from Dow Corning Corporation, Midland, MI, USA. Deionized (DI) water with a resistivity of 18.2 MΩ●cm was used. Cr/Au annealing was done in a Thermolyne muffle furnace from Thermo Fisher Scientific (Ottawa, Ontario). Anhydrous ethanol was obtained from Commercial Alcohols (Brampton, Ontario). Cr was 99.999% and obtained from ESPI (Ashland, OR), while Au was 99.99% and obtained from MRCS Canada (Edmonton, AB).

Preparation of pre-gel solution: Three kinds of solutions were made for the fabrication of thermoresponsive bi-directional self-folding bilayers. In solution 1, we firstly mix 12 mL

DI water and 3 mL pDADMAC solution (20 wt%, low M_w), which is used as a solvent. Then monomers mixtures were dissolved in this solvent, with a total monomer concentration of 7.89 mol/L. The monomer mixtures contain 95% (mol%) of NIPAm, and 5% BIS. Then 40 μL DEAP (as a photoinitiator) was added in the solution, followed by covering the container of the solution by aluminum foil and shaking the solution for 1 h. Likewise, in solution 2 and 3, we used pDADMAC solution (20 wt%) with medium M_w and high M_w, respectively. For each solution, we made a control solution with no pDADMAC added.

Additionally, we made three solutions for the fabrication of pH responsive bi-directional self-folding bilayers. In solution 1, we firstly mix 12 mL DI water and 3 mL pDADMAC solution (20 wt%, low Mw), which is used as a solvent. Then monomer mixtures were dissolved in the solvent, with a total monomer concentration of 7.89 mol/L. The monomer mixtures contain 80% (mol%) of NIPAm, 15% AAc, and 5% BIS. Then 40 μL DEAP (photoinitiator) was added in the solution, followed by covering the container of the solution by aluminum foil and shaking the solution for 1 h. Likewise, in solution 2 and 3, we used pDADMAC solution (20 wt%) with medium Mw and high Mw, respectively. For each solution, we made a control solution with no pDADMAC added.

Fabrication of self-folding IPN hydrogel based bilayers: This process is shown schematically in Figure 6-2. Specifically, a PDMS film with a thickness of 0.5 mm was generated by mixing silicone elastomer base and curing agent (from Dow Corning) in a

volume ratio of 10:1. Then the resulting film was rinsed with DI water and ethanol and dried with N_2 gas, and 2 nm of Cr followed by 50 nm of Au were thermally evaporated onto the PDMS at a rate of ~0.2 Å s^{-1} and ~0.1 Å s^{-1}, respectively, using a Torr International Inc. model THEUPG thermal evaporation system. Then the Au-coated PDMS layer was soaked in an ethanol solution of 1-propene-2-thiol overnight at 4 °C, followed by soaking in ethanol for more than 5 h to rinse away the excess 1-propene-2-thiol. Then cross-shaped substrates were cut out of the modified PDMS sheet. The distance between two neighbouring vertexes is 1.25 cm. Then the cross-shaped substrates were put on the surface of a Petri-dish. After deposition of the pre-gel solution on the substrate, the Petri-dish was placed onto a cooling plate (Stir-Kool Model SK-12, Thermoelectrics Unlimited, Inc.), which was supported by recycling cool water through the instrument. The temperature of the cooling plate was set to be ~ 10 °C. Afterwards, the pre-gel solution was covered by a piece of thin Teflon sheet. Then after UV irradiation for 15 mins, photo-initiated polymerization leads to the formation of hydrogels and IPN hydrogels. The formed hydrogel-based bilayers were released, followed by washing away the unreacted monomers by adding and changing DI water in the Petri-dish for several days.

Field emission scanning electron microscopy: The folded bilayer systems were first frozen by immersing them in liquid nitrogen for 10 mins. Then the bilayers were freeze-dried overnight by lyophilization. (FreeZone. 4.5, LABCONCO). Then the dried bilayers were placed on a conductive copper tape coated holder and SEM images

acquired on specific areas using a Zeiss Sigma FESEM, operated at 5 kV.

Crystal Violet (CV) loading and releasing from the bilayer with a polymeric particle encapsulated: Firstly, a bilayer film was generated by mixed 12 mL of DI water and 3 mL of pDADMAC solution (20 wt%, low M_w), which was used as a solvent. Then monomer mixtures were dissolved in the solvent, with a total monomer concentration of 7.89 mol/L. The monomer mixtures contain 80% (mol%) of NIPAm, 25% AAc, and 5% BIS. Then 40 μL DEAP (as a photoinitiator) was added in the solution, followed by covering the container of the solution by aluminum foil and shaking the solution for 1 h. The control solution contained the same components as above except no pDADMAC was present. The fabricated bilayers, which were generated using the same procedure as above, were firstly soaked in a solution of pH 3, which causes the bilayers to be almost flat. Then we placed the bilayer in a bottle containing 15 mL of CV solution (1 mg/mL, pH 6.5) and a polymeric target particle at the bottom. After overnight soaking, the bilayer was completely folded up towards the side of PDMS, and at the same time, the polymeric particle was encapsulated by the bilayer. For CV releasing, a glass vial containing 20 mL pH 6.5 solution was placed on a plate with the temperature set as ~ 25 °C. The solution was stirred continuously at 60 rpm using a magnetic stir bar and flowed through a cuvette in an Agilent 8453 UV-vis spectrophotometer, equipped with an 89090A temperature controller and Peltier heating device, via a peristaltic pump. The pumping speed was kept constant for the whole experiment. Then the CV loaded bilayer with the encapsulated polymeric particle was placed into the solution, and a timer as started. After 30 mins, the

pH of the solution was changed to 3. The absorbance spectrum from the solution was collected every 2 mins.

6.3 Results and discussion

6.3.1 Strategies for design and fabrication of bilayers

It is well known that pNIPAm-based hydrogels have relatively low stiffness.[337] Furthermore, in this work, the semi-IPN hydrogel has a significantly larger water content, which makes it even weaker.[338] In order to make pNIPAm-based hydrogel actuators with high stiffness, we combine a rigid and nonswellable polymer (PDMS) layer with the hydrogel layers.

Our approach depends on differential volume changes in semi-IPN hydrogel layer and the PDMS layer. The active hydrogel layer exhibits significant volume expansion/contraction after exposure to certain stimuli by swelling/deswelling in aqueous solution, whereas the volume of passive PDMS layer remains constant. Consequently, the internal stress generated drives the reversible bi-directional folding of the cross-shaped bilayers. The fabrication process of the hydrogel/PDMS bilayer is shown schematically in Figure 6-2. Specifically, a thin PDMS sheet was coated with Au by thermal evaporation, followed by surface modification with 1-propene-2-thiol, which reacts with Au on the surface of PDMS. Then cross-shaped PDMS layers were cut out of the flat sheet and placed on the surface of the Petri dish. The pre-gel aqueous solution, which contains

NIPAm, or/and AAc, pDADMAC (of three different molecular weights), *N, N'*-methylene-bis-acrylamide (BIS) as crosslinker, and 2, 2-diethoxyacetophenone (DEAP) as photoinitiator, was deposited on the PDMS substrate. To make a thin and homogeneous

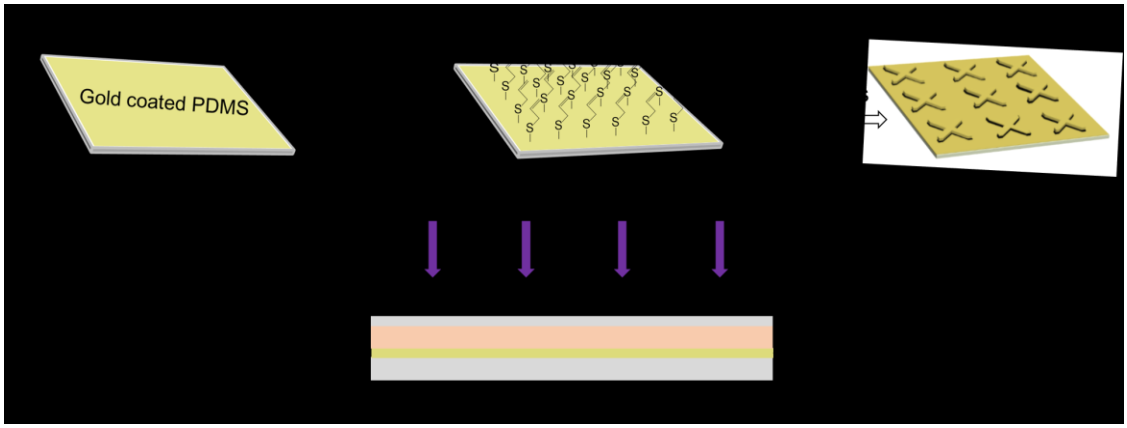

Figure 6-2 a) Schematic illustration of the fabrication process of cross-shaped PDMS substrates; b) the representative cross-section of cross-shaped devices in the process of the adding the hydrogel layer on top of PDMS layers.

hydrogel layer, a thin Teflon sheet (allows light to penetrate through to the monomer solution) was placed on top of the pre-gel solution, as shown in Figure 6-2b. UV irradiation was carried out for 15 mins to initiate the polymerization on a cooling plate, which is set as 10 °C and used to allow polymerization to occur at low temperature to make sure that the formed pNIPAm based hydrogel networks are in a swollen state. As a consequence, the modified molecules (1-propene-2-thiol) on the surface of PDMS are copolymerized with monomers in the pre-gel solution, which serves as a "glue" between

the two layers. Therefore, after removing the Teflon sheet, the thin hydrogel film is left intact on the PDMS layer and the thickness of the hydrogel layer depends on the amount of pre-gel solution deposited. A bilayer product can be obtained after releasing it from the Petri dish. Then they are washed thoroughly with DI water for several days to remove the unreacted monomers and the left pDADMAC, which was not successfully trapped in the hydrogel network.

6.3.2 Thermoresponsive bi-directional self-folding cross-shaped bilayers

To investigate the thermoresponsivity of the bilayer system, we prepared pNIPAm hydrogel/PDMS and pNIPAm-pDADMAC semi-IPN hydrogel/PDMS cross-shaped bilayers. We used pDADMAC with three different molecular weights (100-200 kDa (low Mw), 200-350 kDa (medium Mw), and 400-500 kDa (high Mw)). In order to investigate the combination of the hydrogel layer and PDMS layer, the microstructures of the interface between two layers are observed by scanning electron microscopy (SEM). The bilayer device was freeze-dried before SEM imaging. As shown in Figure 6-3 the hydrogel layer exhibits a microporous network, which results from the sublimation of the frozen water that was formed in the swollen hydrogels before lyophilizing.[339] It clearly shows that crosslinked hydrogel networks are propagated from the surface of PDMS and these two layers are adhered together strongly. Furthermore, the two layers do not separate even after many rounds of folding and unfolding actuation.

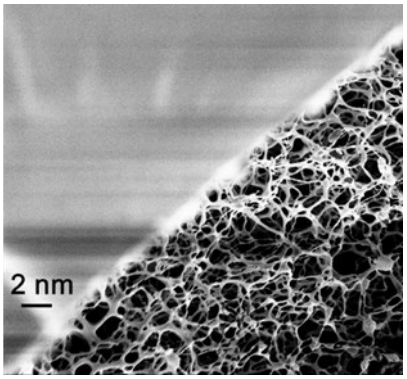

Figure 6 3 The SEM image of the interface of the two layers: the porous side is the hydrogel layer, while the the other side is the PDMS layer.

Effects of pDADMAC in the hydrogel on the temperature stimulated folding behavior of the bilayer system were studied. Figure 6-4a shows that the bilayer, with pDADMAC trapped in pNIPAm hydrogel layer, which is transparent, self-folds towards

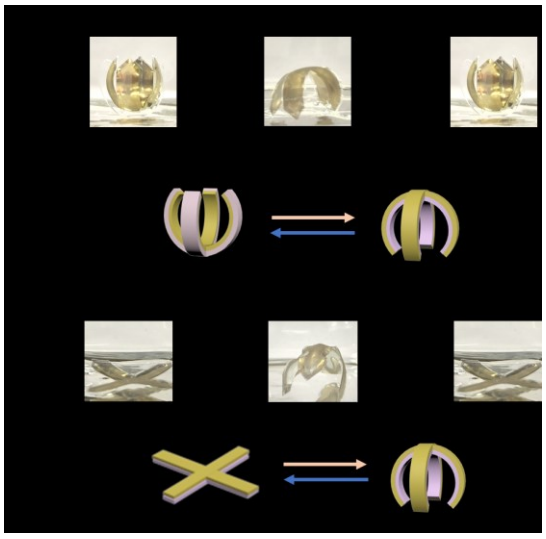

Figure 6-3 a) actuation of the NIPAm-pDADMAC hydrogel/PDMS bilayer system; b) actuation of the NIPAm hydrogel/PDMS bilayer system. In the schematic drawings of the

bilayer systems, the yellow side is the PDMS layer, while the grey side is the pNIPAm-based hydrogel layer.

the side of PDMS into a capsule at low temperature (25 °C) in DI water. When the temperature is increased to 40 °C, the hydrogel layer becomes white as a result of the transition of the pNIPAm-based network from a swollen to deswollen state. This leads to the opening of the capsule and subsequently self-folding of the bilayer in the opposite direction. The bilayers were able to completely fold back to the original conformation when the temperature was decreased to 25 °C within ~ 10 mins. It is worth mentioning that hydrogels containing pDADMAC of three different molecular weights show very similar folding behavior in response to temperature changes. In contrast, as shown in Figure 6-4b, the bilayer system without pDADMAC trapped in the hydrogel layer fail to exhibit bi-directional folding behavior. At low temperature, in the absence of pDADMAC, the mechanical force generated from the volume expansion of the pNIPAm hydrogel layer by swelling is not strong enough to cause the bilayer to bend. Although at high temperature, the strength generated from the shrinking of the hydrogel network could still induce one directional folding of the bilayer system. The thermoresponsive folding behaviour of both bilayer systems in DI water with switching temperature between 25 °C and 40 °C are reversible and repeatable. SEM images were collected to study the changes in the microporous structures of the hydrogel layer in response to temperature. The images in Figure 6-5 (a1, a2, a3) show the pNIPAm-pDADMAC hydrogel layer after the

1st, 2nd, and 3rd cycle of folding at 25 °C, while a1', a2', and a3' show the images of the same hydrogel network after the 1st, 2nd, 3rd cycle of folding at 40 °C. Figure 6-5 (b1, b2, b3) show the SEM images of the microstructures of pNIPAm hydrogel networks after the 1st, 2nd, and 3rd cycle of folding at 25 °C, while

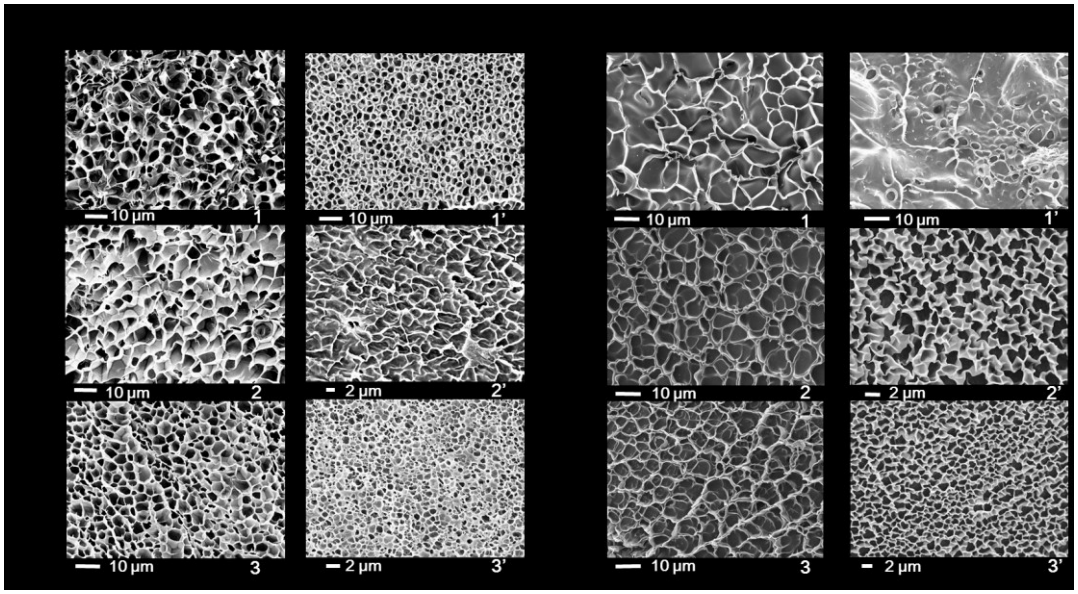

Figure 6-4 a1, a2, a3 are SEM images for the pNIPAm-pDADMAC hydrogel layer after the 1st, 2nd, and 3rd cycle of folding at 25 °C; a1', a2', and a3' are images of the same hydrogel network after the 1st, 2nd, 3rd cycle of folding at 40 °C; b1, b2, b3 are the SEM images of of pNIPAm hydrogel layer after the 1st, 2nd, and 3rd cycle of folding at 25 °C; b1', b2', and b3' are images of the same hydrogel network after the 1st, 2nd, 3rd cycle of folding at 40 °C.

b1', b2', and b3' show the images of the same hydrogel network after the 1st, 2nd, 3rd

cycle of folding at 40 °C. We point out that for all samples were instantaneously frozen in liquid nitrogen and freeze-dried via lyophilization before SEM imaging. In general, we can conclude that the pore sizes of the hydrogel layer (with/without pDADMAC) at 25 °C are much larger than their counterparts at 40 °C, which corresponds with the folding of both types of bilayer systems towards the hydrogel layer at high temperature. Secondly, the structures of the hydrogel layer with pDADMAC at 25 °C are markedly more porous compared with the more compact structures of the hydrogel layers without pDADMAC, which further proves the existence of ionized pendent quaternary ammonium groups in pDADMAC generated high osmotic pressure and the resultant strong repulsion force in the semi-IPN hydrogel network. This explains why the pNIPAm-pDADMAC hydrogel-based bilayers were able to fold towards the PDMS layer at low temperature, while pNIPAm hydrogel based bilayers failed in folding in the same fashion. At last, the changes in pore size of the both hydrogel layers are repeatable and reversible after three cycles of folding and unfolding, which corresponds with the reversible and repeatable folding behaviors of both bilayer actuators.

Figure 6-6 shows the demonstration of pNIPAm-pDADMAC hydrogel/PDMS bilayer as temperature controlled manipulators. When the temperature is decreased from 50 °C to 10 °C the cross-shaped bilayer system folds towards the PDMS side, thus the plastic bead is encapsulated and transferred. When the manipulator with the plastic beads is transferred to a water bath at 50 °C, the capsule opened and the plastic bead is released in the water. The temperature-induced volume swelling and shrinking of the hydrogels is

the driving force for the application of the bilayer system as the manipulator. The encapsulation of the object by the bilayer system, which folds towards the PDMS layer in the water at 10 °C, avoids the hydrogel layer directly contacting the stiff object with the soft hydrogels preventing damage. This is not the case with the bilayer without pDADMAC in the hydrogel layer.

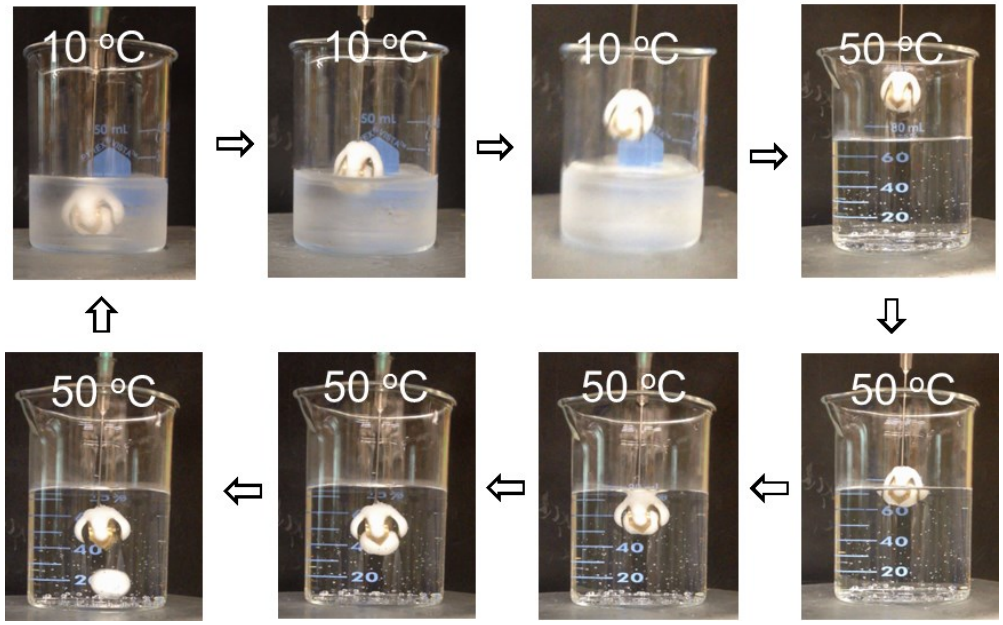

Figure 6-5 The target loading and releasing process in water with different temperatures. (The solution at 10 °C appears cloudy because the beaker was taken out from ice bath)

6.3.3 pH-responsive bi-directional self-folding cross-shaped bilayers

To investigate the pH-responsive behavior of the bilayer system, we prepared pNIPAm-based bilayers composed of 15% AAc (mol%) with and without pDADMAC

(medium Mw). We were interested in understanding the effects of pDADMAC in the hydrogel on the pH responsive folding behavior of the bilayer systems. All the studies in this section were conducted at 25 °C. Figure 6-7a shows that the bilayer system, with pDADMAC trapped in pNIPAm-15% AAc hydrogel layer self-folds toward the hydrogel side of the actuator into a capsule at pH 6.5. Figure 6-7 (a1) shows a photograph of the folded bilayer, and Figure 6-7 (a2) shows the corresponding schematic diagram. When the pH is changed to 3, the bilayer dramatically folds in the opposite direction, as shown in Figures 6-7a1' and 6-7a2'. This bi-directional folding can be repeated many times as the solution pH is switched between 6.5 and 3. In contrast, the bilayer system with only NIPAm and AAc in the hydrogel layer, folds toward the side of the PDMS instead into the capsule at pH 6.5, as shown in Figure 6-7b1 and Figure 6-7b2. When the pH is changed to 3, the capsule opens up to be approximately flat without folding in the other direction.

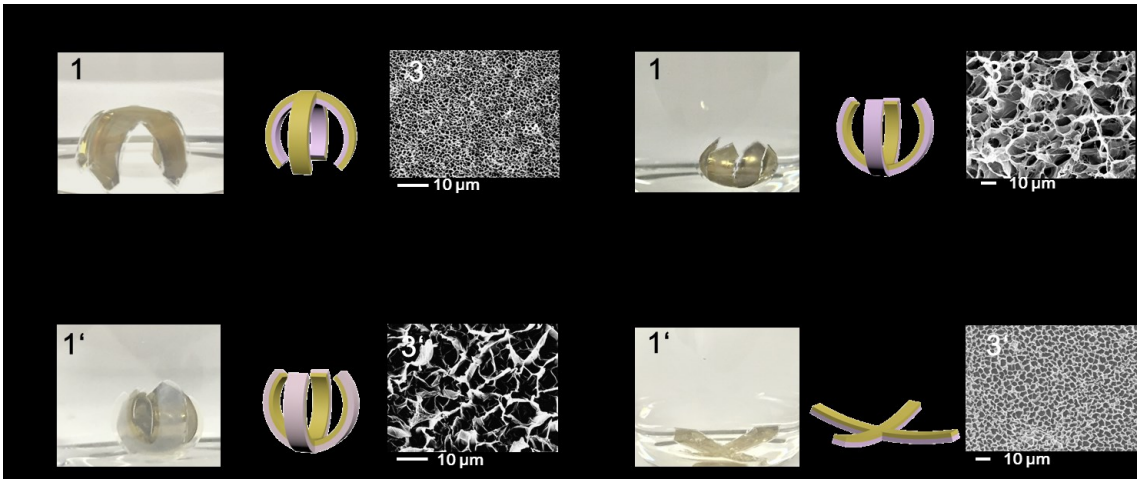

Figure 6-6 A1, a2, a3 are the optical graph, schematic diagram, and SEM image of the

NIPAm-AAc (15%)-pDADMAC hydrogel layer at pH 6.5 respectively; a1', a2', a3' are images for the same hydrogel layer at pH 3.0; b1, b2, b3 are images for the NIPAm-AAc (15%) hydrogel layer at pH 6.5; b1', b2', b3' are images for the same hydrogel layer at pH 3.0.

From the SEM images of the microstructures of NIPAm-15% AAc-PDADMAC hydrogels shown in Figure 6-7a3 (pH 6.5) and Figure 6-7a3' (pH = 3), we propose that the compact pores with small size in Figure 6-7a3 are a result of the strong electrostatic complexes formed between the negatively charged AAc (belongs to the chemically crosslinked hydrogel networks) and the positively charged pDADMAC (belongs to the physically trapped long polyelectrolyte chain) in the hydrogel network, which promotes the shrinking of the hydrogel at pH 6.5 and leads to the folding of the bilayer towards the semi-IPN hydrogel layer. On the other hand, AAc becomes neutral at pH 3. In the absence of the strong electrostatic interactions, the hydrogel network becomes "loose" and pDADMAC recovers its function as a positively charged polyelectrolyte, which allows the hydrogel to absorb a large amount of water. Consequently, the pore sizes of the hydrogel network become much larger at pH 3, as shown in Figure 6-7a3'. The resulting high osmotic pressure promotes the folding of the bilayer towards the PDMS layer. In contrast, the pore size of the NIPAm-15% AAc hydrogel at pH is 6.5 is relatively large due to the osmotic pressure generated by the existence of deprotonated AAc (shown in Figure 6-7b3), which leads to the folding of the bilayer towards the PDMS layer. On the other hand, at pH 3, the protonation of AAc leads to a decreased pore size and shrinking

of the hydrogel network (shown by Figure 6-7b3'), which allows the capsule to open up to be almost flat. In addition, we further proved our hypothesis by trapping pDADMAC with the low Mw and high Mw instead in the pNIPAm-15%AAc hydrogel layer. It was observed that the bilayer with high MW pDADMAC trapped in the hydrogel layer exhibits a similar folding behavior as the one with the medium Mw trapped in response to pH switching between 6.5 and 3.0. However, the bilayer with low Mw pDADMAC trapped shows a small degree of folding towards the PDMS layer at pH 6.5 (the photographs are not shown here), which is different from the other two instances. We hypothesize that this is a result of the low MW pDADMAC being unable to span as much of the network compared to the high Mw pDADMAC, thus the electrostatic interactions formed are not strong enough to induce the shrinking of the hydrogel network at pH 6.5. However, the folding behavior of these three types of bilayer systems is similar at the solution of pH 3. Likewise, at pH 3 the protonation of AAc frees pDADMAC from electrostatic interaction with the negative AAc charges, leading to a larger osmotic pressure in the hydrogel layer and its swelling. Thus the bilayers fold towards the PDMS layer.

6.3.4 Dual stimuli responsive self-folding cross-shaped bilayers

We also investigated the effect of dual-stimuli on the folding behavior of the bilayers, with the NIPAm – 15% AAc - pDADMAC (medium Mw) hydrogel layer as an example.

Figure 6-8a1 and Figure 6-8a2 show photographs and schematic representations of the bilayer structures at pH of 6.5 and temperature of 25 °C. As we expected, the bilayer systems folds toward the hydrogel layer.

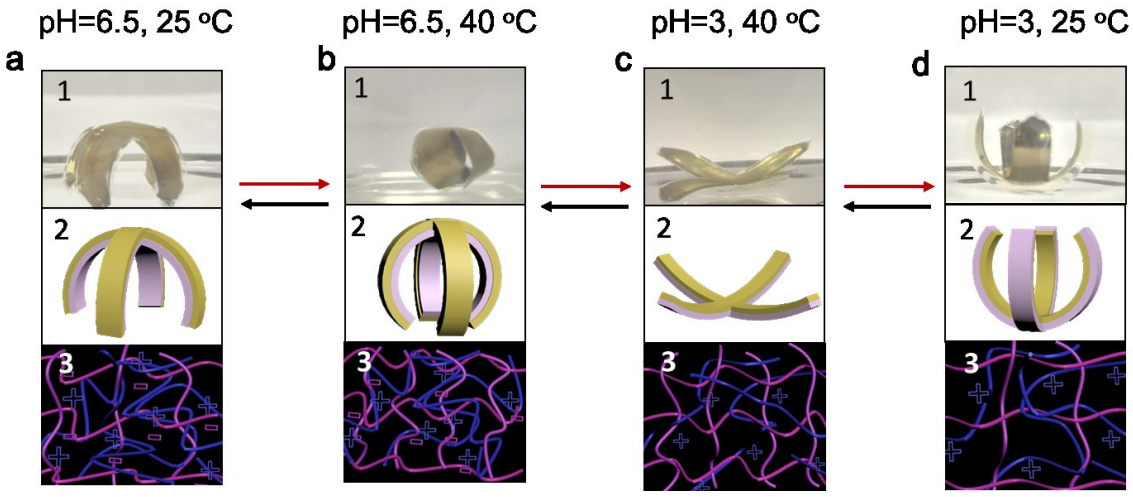

Figure 6-7 Self folded bilayer structures, 1: optical graph, 2: schematic diagram, 3: arrangement of polymer chains, at four combination of temperature and pH.

When the pH is maintained at pH 6.5 and temperature is increased to 40 °C, the bilayer folds toward the hydrogel layer due to the thermoresponsivity of pNIPAm in the hydrogel, which is shown in Figure 6-8b1 and Figure 6-8b2. Furthermore, when the temperature is maintained at 40 °C and the pH is changed to 3.0, we found that the completely folded structure opens up to become almost flat. We proposed that the protonation of AAc allows the positively charged PDADMAC to absorb water and swell, even at elevated temperatures. However, the copolymerization of AAc with NIPAm in the hydrogel increases the LCST of pNIPAm, which maintains the pNIPAm hydrogel network at a

relatively deswollen state compared with the hydrogel network without copolymerized AAc. When the temperature was lowered to 25 ^{o}C, while maintaining pH at 3.0, it fold towards the PDMS instead, due to the swelling of the double complexed hydrogel network. The corresponding schematic diagrams of the arrangement of polymer chains in the hydrogel networks at four different combinations of pH and temperatures are shown in Figure 6-8a3, Figure 6-8b3, Figure 6-8c3 and Figure 6-8d3. The folding states of the bilayer systems can be manipulated in many ways simply by varying pH and temperature in a way that yields the desired structure. On the other hand, the folding states of the bilayer can also be considered as an indicator of the environmental conditions (pH and temperature).

6.3.5 Application: Small molecule release from pH-responsive foldable bilayers

We further studied the ability of the IPN hydrogel-based bilayers to release small molecules in a triggered and controlled fashion. Here, we describe polymeric actuators that actively grab objects and absorb small molecules under a specific environmental condition, and subsequently release both species in a pH triggered fashion. We selected to release the small molecule tris(4-(dimethylamino)phenyl)methylium chloride (Crystal Violet, CV), which is positively charged. The hydrogel layers we investigated were composed of NIPAm-25% AAc (mol%) with and without low Mw pDADMAC. The reason for choosing 25% AAc and low Mw pDADMAC is shown below. Compared with

hydrogels that contain 15% AAc, hydrogel possessing 25% AAc shows higher molecule loading efficiency, as the loading mechanism is based on the strong electrostatic interaction between the deprotonated AAc in the hydrogel network and CV molecules at pH 6.5. Secondly, as mentioned above, pDADMAC (low Mw) in the hydrogel network is not able to form long-range strong electrostatic interaction with deprotonated AAc throughout the hydrogel network. The more free ends of trapped polymer chains renders the interaction between pDADMAC (low Mw) and AAc less stable and more dynamic. Thus when CV molecules are introduced into the hydrogel networks, they are more competitive in binding with AAc in the hydrogel in the presence of low Mw pDADMAC compared with medium Mw species. This leads to enhanced CV loading efficiency of the bilayer (83% for pDADMAC (low Mw) versus 70% for pDADMAC (medium Mw)).

We point out that when loading CV in the bilayer system, the bilayer system with pDADMAC self-folds towards the PDMS layer and gripped the objects (for instance, polymeric beads), as shown in Figure 6-9b1 (the loading process is illustrated in detail in the experimental section). This serves as a proof-of-concept that bilayer has the potential to grab abnormal tissues or cells, transfer them to a location, and release drugs locally. The competitive binding of loaded CV with AAc in the hydrogel renders pDADMAC free in the hydrogel, which leads to the self-folding of the bilayer at pH 6.5. The average loading efficiency of the bilayer with/without pDADMAC (low Mw) trapped in the hydrogel layer is 83% and 97% respectively. The release of CV molecules from both CV-loaded bilayers were evaluated by monitoring the absorbance at 590 nm over time when

exposed them to pH 6.5 and then pH 3.0 solution. As indicated in Figure 6-9a, at pH 6.5 the release of the molecules from both bilayers is very slow because of the favorable electrostatic interactions between CV and hydrogel, as discussed above.

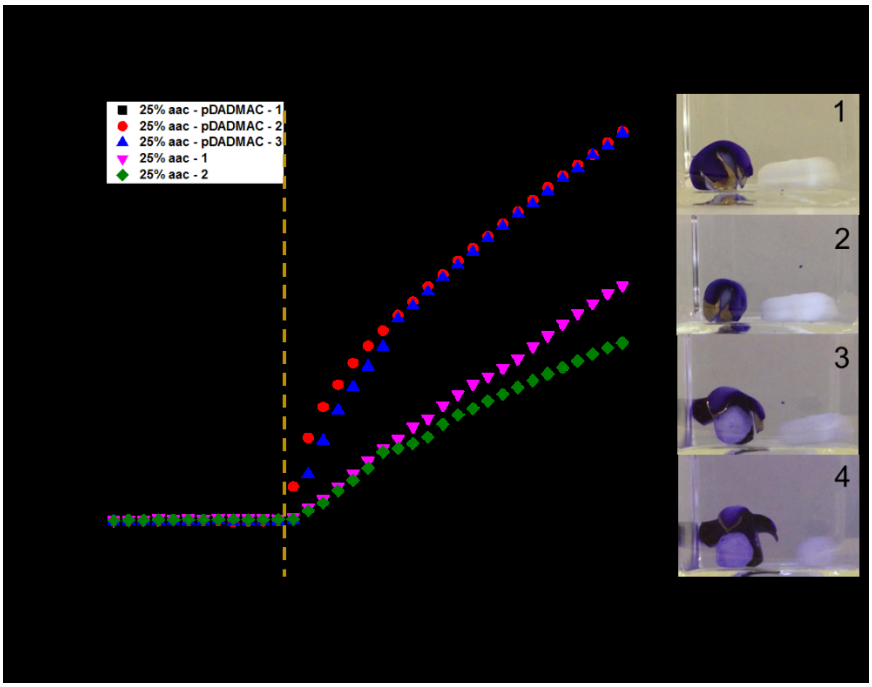

Figure 6-8 a) The releasing profiles of bilayers triggered by pH; b1, b2, b3, b4 represents the releasing of small molecules and as well as opening up of the folded bilayer device.

When the pH is adjusted to 3.0 the bilayers with pDADMAC clearly shows faster releasing rate of CV than the one without pDADMAC. At pH 3.0, the AAc groups are neutralized and the electrostatic interactions holding the CV into hydrogels are destroyed. In the meantime, due to the existence of positively charged pDADMAC (low Mw) with relatively high dynamics of moving inside the hydrogel network facilitates the expelling of CV molecules out of the hydrogel network. As shown in Figure 6-9b2, Figure 6-9b3, and Figure 6-9b4 the folded capsule gradually opens up as more and more CV molecules

are released. In addition, we show that CV molecules can be released from the bilayer system on demand by switching pH of the solution. To accomplish this, we first immersed the CV-loaded bilayers in pH 6.5 solution and monitored the release for a specific period of time. Then we lower the pH of the solution to 3.0 by adding hydrochloric acid (HCl) to induce the fast release of CV molecules, followed by soaking the hydrogel in pH 6.5 solution. This process was repeated and as shown in Figure 6-10, the on-off switching process for releasing can be repeated many times. In the meantime, the bilayers show reversible shape changes as well in responsive to pH changes.

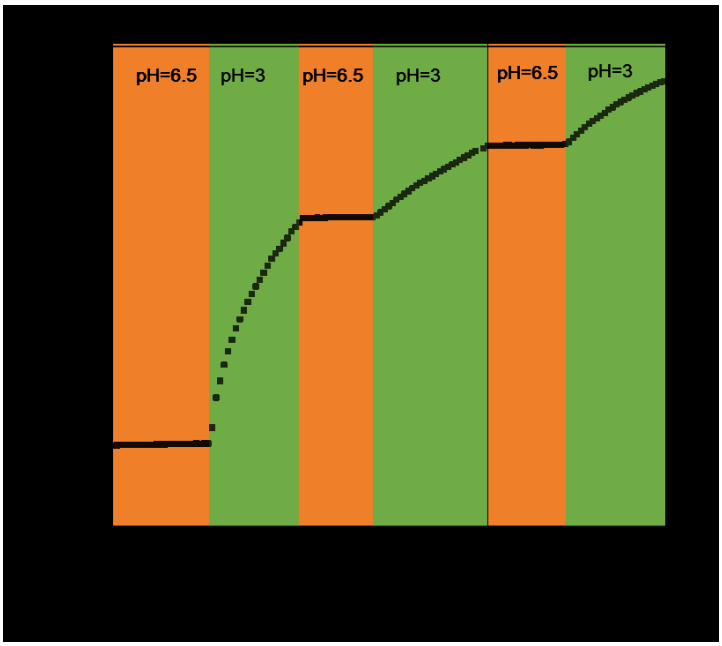

Figure 6-9 Controlled releasing of CV by switching pH.

6.4 Conclusion

In summary, pNIPAm-pDADMAC semi-IPN hydrogels/PDMS bilayers with both

excellent responsive folding property and great elasticity are prepared. For the first time, we show that the existence of pDADMAC enables the bilayer system to fold bi-directionally in response to pH and temperature. The folding property of the bilayer is resulted from the swelling and shrinking of the hydrogel layer with the PDMS layer unswellable. They exhibit reversible and repeatable thermoresponsive and pH-responsive folding/unfolding characteristics. The bilayers are designed as soft grippers and molecule release devices. In addition, the triggered and controlled molecule release from the bilayer system together with the actuation of the bilayer, are highly attractive and promising in biomedical applications.

Chapter 7: Reducing Reagent Responsive Poly (N-isopropylacrylamide) Microgels and Microgel-Based Optical Materials[4]

7.1 Introduction

As outlined in Chapter 1 and Chapter 2, thermoresponsive poly(*N*-isopropylacrylamide) (pNIPAm) based polymers or hydrogels can be endowed with many functional groups for various applications. This Chapter describes pNIPAm based hydrogel particles (microgels), crosslinked with *N, N'*-bis(acryloyl)cystamine (BAC), are prepared using free-radical precipitation polymerization. By coating a single layer of microgels on an Au-coated glass substrate followed by the addition of another Au layer, an optical device (etalon) was fabricated. As mentioned in Chapter 2, the devices were shown to exhibit optical properties that are typical of microgel-based etalons, i.e., they exhibit visual color and unique multipeak reflectance spectra.

Stimuli responsive materials are capable of changing their chemical and/or physical properties in response to specific changes in their environment.[340] As mentioned in Chapter 1, a number of responsivities have been reported previously, including responses

[4] This Chapter has been adapted from a previously published article. Li, X., Gao, Y., Serpe, M. J., *Can. J. Chem.,* 2015, 93, 685.

to: pH,[341] temperature,[96,342] light,[343] and electric field.[344] Ideally, these responses are reversible, i.e., once the stimulus is removed, the responsive material returns to its initial state. These materials have found a number of applications for controlled/triggered drug delivery,[345-347] as antibacterial coatings,[348,349] and for tissue engineering.[350] While all of these responsivities have been previously reported, thermoresponsive materials composed of poly (*N*-isopropylacrylamide) (pNIPAm) are the most widely studied and best understood. Specifically, pNIPAm-based hydrogel particles (microgels) are fully water soluble/swollen (and hydrophilic) in water with a temperature below pNIPAm's lower critical solution temperature (LCST) of ~32 ^{o}C, while it transitions to an "insoluble"/deswollen (and relatively hydrophobic) state when the water temperature is increased to above 32 ^{o}C. This behavior has been exploited for many applications.[351-357,94,358,359]

Previous work in the group has shown that an optical device (etalon) could be fabricated by sandwiching a single layer of pNIPAm-based microgels between two thin metal layers. Using this construct, we have developed optical sensors that change their optical properties in response to glucose,[360] polyelectrolytes,[361] proteins,[362] light,[363] and pH.[364] This is a direct result of the microgel diameter modulating the distance between the two metal layers. Unique to the devices here are their ability to change their optical properties in the presence of thiols. Figure 7-1a is the schematic diagram of the thiol-responsive microgel based etalon. Specifically, in the presence of dithiothreitol (DTT), the microgel crosslinks were reduced, leading to microgel swelling, which ultimately changes the

optical properties of the etalon, as shown in Figure 7-1b. We observed a linear relationship between the shift in the position of the reflectance peaks and the concentration of DTT, which suggests that they can be used to quantify thiols in solution.

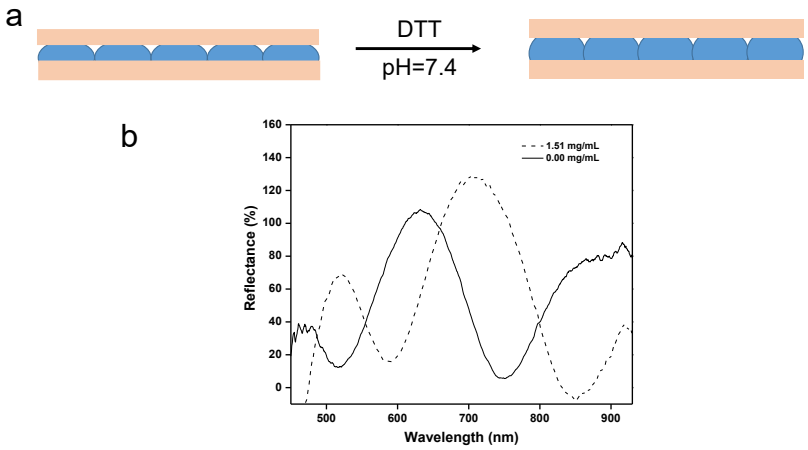

Figure 7-1 (a) Schematic depiction of a microgel based etalon. A layer of pNIPAm-BAC microgels is sandwiched between two Au layers. The microgels swell upon exposure to DTT, which increases the distance between two Au layers. (b) A representative reflectance spectrum from a pNIPAm-BAC microgel-based etalon both before and after DTT exposure.

7.2 Experimental section

Materials. The monomer *N*-isopropylacrylamide (NIPAm) was recrystallized from hexanes and dried in vacuum prior to use. Reagents *N, N'*-bis(acryloyl)cystamine (BAC), *N, N'*-methylene bis(acrylamide) (BIS), ammonium persulfate (APS), dithiothreitol (DTT), methanol, monosodium phosphate were all used as received. All deionized water

was 18.2 MΩ•cm and obtained from a Milli-Q Plus system from Millipore (Billerica, MA). Glass cover slips were 25 mm × 25 mm and obtained from Fisher Scientific. Cr was 99.999% and obtained from ESPI (Ashland OR), while Au was 99.99% and obtained from MRCS Canada (Edmonton, AB). Au annealing was performed in an Isotemp muffle furnace from Fisher Scientific (Ontario, Canada).

Microgel synthesis. A 3-necked round bottom flask was fitted with a reflux condenser, a nitrogen inlet (needle) and temperature probe, and charged with a solution of NIPAm (1.767 mmol) in 20 mL DI water, previously filtered through a 0.2 μm filter. The solution was purged with N_2 gas and allowed to heat to ~70 ºC for ~1 hour. The reaction was initiated with a solution of 0.1 M APS (total concentration 0.4 mM), immediately after addition of 4.63 mM BAC dissolved in 5 mL methanol. The solution was allowed to stir at ~70 ºC for 6 h, then cooled to room temperature and filtered to remove large aggregates. There microgels were then centrifuged at a speed of ~8000 relative centrifugal force (rcf) at room temperature for 35 mins to form a pellet at the bottom of centrifuge tubes. The supernatant was removed and the pellets of microgels were resuspended using deionized water. This process was repeated for six times to remove any remaining monomers and linear polymers. NIPAm-co-BIS was synthesized as previously described.[365]

Etalon fabrication. Etalons were fabricated according to the procedures reported

elsewhere.[365] Briefly, 25 × 25 mm glass coverslips were rinsed with DI water and ethanol and dried with N_2 gas. 2 nm of Cr followed by 15 nm of Au were thermally evaporated onto the glass at a rate of ~0.1 and ~0.25 Å s^{-1}, respectively, using a Torr International Inc. model THEUPG thermal evaporation system (New Windsor, NY). The Cr acts as an adhesion layer to hold the Au layer on the glass. The Au coated substrates were annealed at 250 °C for 3 h and then cooled to room temperature prior to use. Then a previously coated Cr/Au substrate was rinsed with ethanol, dried with N_2, and then placed onto hot plate (Corning, NY) at ~30 °C. A 40 μL aliquot of the concentrated microgels was spread to cover the whole substrate using a micropipette tip. Then the microgel solution was allowed to completely dry on the substrate at ~35 ºC for 2 h. After that, the dry film was rinsed copiously with DI water and soaked in water overnight at ~30 °C. Following this step, the substrate was again rinsed with DI water and dried with N_2 gas, and an additional 2 nm Cr and 15 nm Au overlayer were deposited onto the microgel layer.

Reflectance spectroscopy. Reflectance spectra were collected by a USB 2000+ spectrophotometer, connecting with light source and a reflectance probe from Ocean Optics (Dunedin FL). A Corning PC-420d hot plate (Fisher, Ottawa, Ontario) was used to control the solution temperature and the temperature was also monitored with a thermocouple platinum sensor. The spectra were collected over a wavelength range of 400-1000 nm and analyzed by Ocean Optics Spectra Suite Spectroscopy software.

Particle characterization. The morphology of microgel particles were investigated by Differential Interference Contrast (DIC) images via IX71 inverted microscope (Olympus, Japan). Dynamic light scattering (DLS) was carried out to determine the hydrodynamic diameter of the microgels using a Zetasizer Nano ZS equipped with a 633 nm laser (Malvern, Westborough, MA, USA) and measured in 173° backscatter mode. All measurements of hydrodynamic diameter was repeated three times.

Atomic force microscopy (AFM) tapping imaging. In-liquid height analysis for a BAC crosslinked pNIPAm microgel-based etalons was done in pH 7.4 phosphate buffer solution before and after DTT exposure. The images were obtained using an Asylum Research MFP 3D AFM (Santa Barbara, CA). Images were acquired over a 30 ×30 μm area using a scan rate of 0.50 Hz. For this analysis, a line was scratched into the etalon using a razor blade and the scratch was imaged. Images were first taken in pH 7.4 phosphate buffer solution at 25 °C. Then the sample was treated in 1 mg/mL DTT phosphate buffer solution for at least 2 h. After that, the sample was imaged using the same method at 25 °C. The height was determined using Asylum software.

7.3 Results and Discussion

Free-radical precipitation polymerization was used to synthesize BAC crosslinked pNIPAm-based microgels. As can be seen in the differential interference contrast (DIC)

microscopy image in Figure 7-2a, the microgels are monodispersed with an average diameter of ~900 nm (determined from the microscopy images). In order to examine the BAC crosslinked microgels response to the presence of the reducing agent DTT, we dispersed the microgels in 10 mM phosphate buffer solution (PBS) (pH = 7.4) containing 1 mg/mL DTT and determined their hydrodynamic diameter (D_H) via dynamic light scattering (DLS). As shown in Figure 7-2b, the D_H of microgels in DTT solution is about 100 nm larger than in PBS alone. We attributed this to the DTT reducing the BAC, which reduces the crosslink density, and therefore allows the microgels to swell to a greater degree than before they were reduced. The reduction mechanism is shown in Figure 7-3a. At pH 7.4, the DTT is negatively charged, and the negatively charged thiolate is reactive, which can attack the disulfide bond in the microgel to generate thiols in the microgel and ring oxidized DTT. As a result, the microgels will increase in diameter when the crosslinks are broken, as shown schematically in Figure 7-3b.

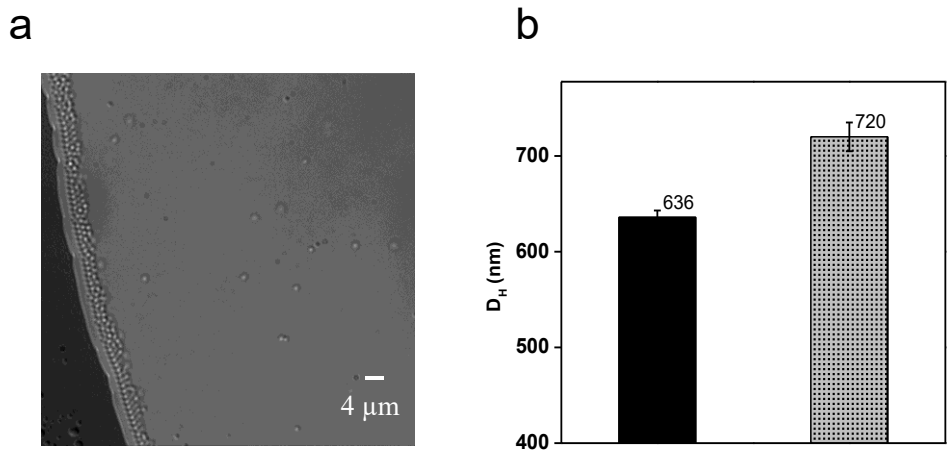

Figure 7-2 (a) DIC microscope image for BAC crosslinked pNIPAm-based microgel

particles; (b) D_H of BAC crosslinked pNIPAm-based microgel particles in the absence and presence of DTT.

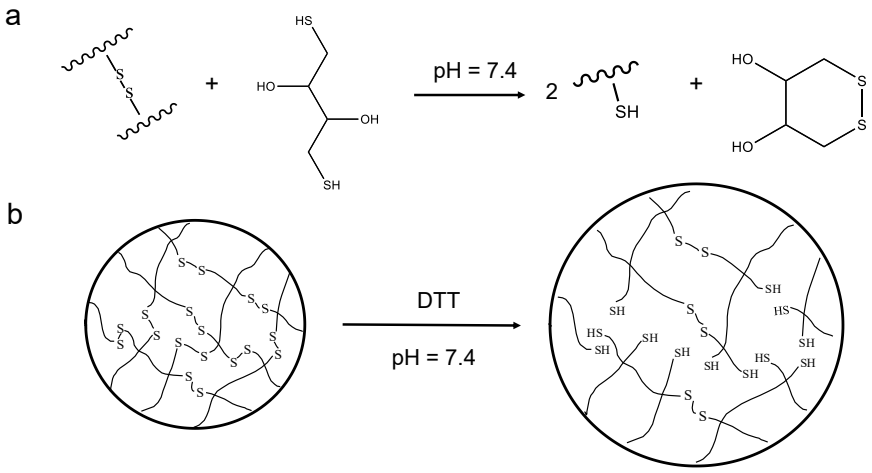

Figure 7-3 (a) The reduction mechanism of disulfide bond by DTT; (b) The proposed microgel swelling behavior after reduction of the microgel's BAC crosslinks.

Following the characterization of the microgels, we went on to show that microgel-based etalons could be fabricated from the BAC crosslinked microgels. Again, a schematic representation of the microgel-based etalon structure can be seen in Figure 7-1a. As we observed in solution above, the microgels increase in diameter when DTT is introduced to the microgels; therefore, we expect similar behavior for the microgels in the etalon. This swelling should result in an increase in the thickness of the dielectric layer, yielding a red shift in the peaks of the reflectance spectrum, as can be predicted from Equation 1. To study these materials, the DTT sensitive etalons were immersed in a 10 mM pH 7.4 phosphate buffer solution at 25 ^{o}C. We exposed our etalons to different

concentrations of DTT, and waited for the etalon response to stabilize, which was ~ 1.5 h. Figure 7-1b shows a representative multipeak reflectance spectrum, and the peaks clearly red shift as the concentration of DTT is increased. Figure 7-4 shows how the position of the pNIPAm-BAC microgel-based etalons reflectance peak depends on the concentration of DTT. In this figure $\Delta\lambda$ represents the reflectance peak wavelength shift of etalons in response to DTT. As can be seen, the etalons show an average cumulative red shift of ~6 nm with 0.19 mg/mL solution. Successive additions gave further red shifts and we observed ~70 nm shift over the range of concentration from 0.00 mg/mL to 1.50 mg/mL. Visibly, we are able to observe the color change of etalons before and after exposing etalons to DTT. A control was also performed using pNIPAm-BIS microgels without disulfide bonds inside in the same manner. As shown in Figure 7-4, they didn't exhibit red shifts after DTT exposure. From the data we can conclude that the cleavage of disulfide bond by DTT can trigger the volume change of the microgel by decreasing the crosslinking density, which results in a red shift of the etalon's spectral peaks. Conclusively, the etalon device can be used as a powerful tool to detect the reducing reagent DTT. In the discussion above, we propose that the DTT is able to reduce the crosslink density of the BAC containing pNIPAm-based microgels, leading to their swelling. We propose that this swelling is capable of changing the optical properties of the microgel-based etalons, which can be used for sensing reducing agents (specifically DTT). To further prove this mechanism, we collected atomic force microscopy (AFM) images of BAC crosslinked pNIPAm microgel-based etalons in buffer without and with

DTT present. From these images, we were able to determine the etalons thickness.

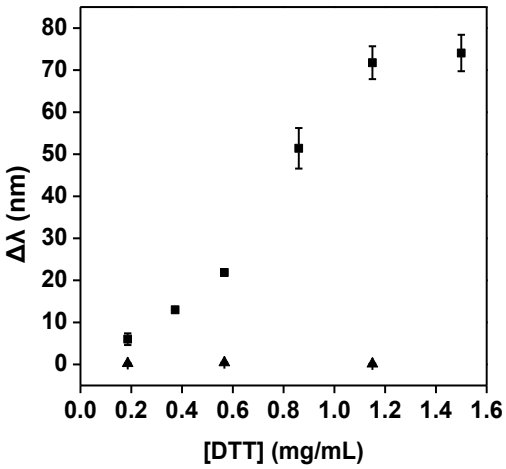

Figure 7-4 The squares represent the position of the etalons reflectance peak after exposure to the indicated amount of DTT; and the triangles represent the response of pNIPAm-BIS (no BAC) microgel-based etalons to DTT. Each point represents the average of three independent measurements from three etalons, and the error bars are the standard deviation for those values.

To accomplish this, an etalon was formed on a substrate, as previously described, and was scratched with a razor blade to remove the etalon from a specific area. The substrate was then imaged in the scratched region to determine the etalons thickness before and after exposure to DTT. Figure 7-5a shows the AFM image for the etalon in the scratched region after soaking in PBS with pH 7.4, and reveals a thickness of ~430 nm, which is expected since previous studies have shown that the thickness of a microgel layer on a Au surface is significantly thinner than expected solely from the solution

diameter. Then the etalon was exposed to 1 mg/mL DTT in the same PBS for 2 h, followed by AFM imaging. Figure 7-5b shows the image for the etalon in the same region as Figure 7-5a, which reveals a thickness of ~520 nm. These data correlate well with the solution data, as well as the red shifts observed in the reflectance spectra.

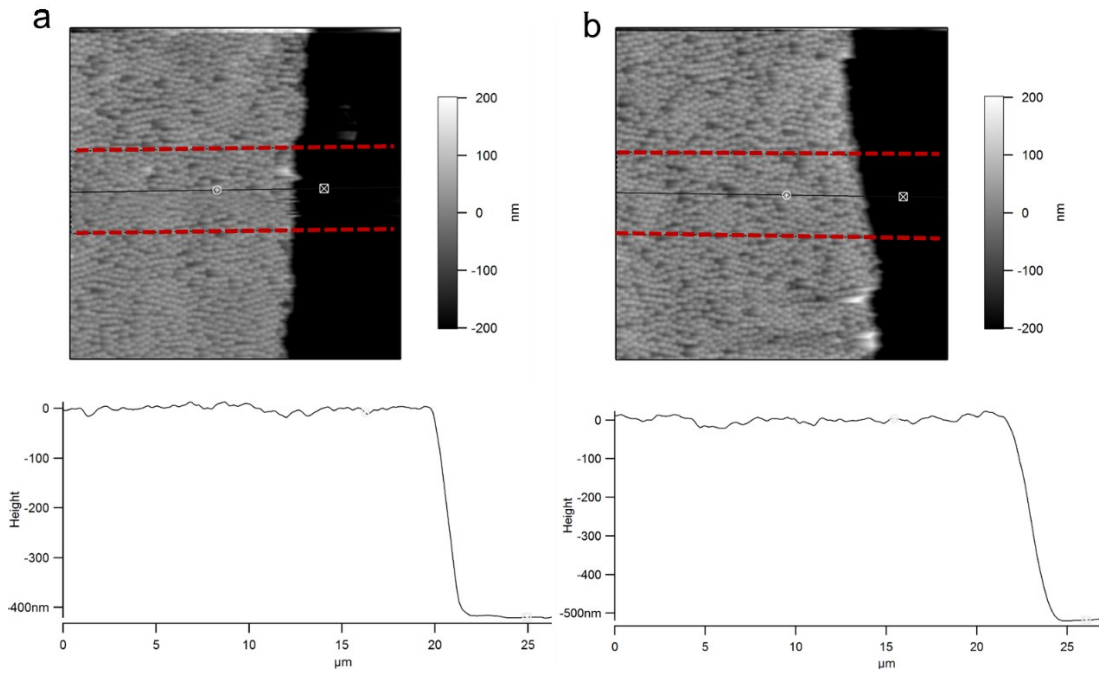

Figure 7-5 AFM images of etalons in (a) pH 7.4 phosphate buffer solution; and (b) the same solution containing 1 mg/mL DTT. The images were taken in a scratched region to allow easy determination of the etalon thickness. The thickness was determined from average thicknesses determined in the step area in the area bounded by the dashed lines. The analysis was carried out at 25 ºC and revealed that the thicknesses were (a) 423 nm ± 9 nm, and (b) 522 nm ± 15 nm.

7.4 Conclusion

In this work, we have shown that BAC crosslinked pNIPAm-based microgels could be synthesized, and etalons made from them. We found that the microgel diameter depended on the presence of DTT, due to the DTT reducing the BAC crosslinks, thereby decreasing the microgels crosslink density, which allows them to swell. Color tunable device (etalons) were subsequently fabricated from these microgels by sandwiching them between two Au layers. These devices exhibit optical properties, specifically multipeak reflectance spectra, which were shown to depend on the presence and concentration of DTT they are exposed to. Specifically, in response to DTT, the BAC crosslinked microgel etalons exhibit a reflectance peak that shifts ~70 nm over the DTT concentration range of 0.19-1.5 mg/mL. Using AFM, we were able to prove that this response was a result of the etalon's cavity thickness increasing, which leads to the observed red shifts. From these results, we believe that thiol/DTT sensors can be fabricated from simple components, and can also have applications for controlled and triggered drug delivery application.

Chapter 8: Conclusion and Future Outlook

8.1 Conclusion and outlook on polymer solids based actuators

The first project in this dissertation demonstrated the study of a novel pNIPAm-co-AAc microgel 'glued' polyelectrolyte-plastic substrate based bilayer actuator. The humidity responsive actuator shows a 'muscle like', being able to lift a mass many times of its own in the air, as described in Chapter 3. Mathematical models are developed to understand the self-folding behavior of the bilayer device. The result of simulation shows that the experimental data fits the built-up model quite well. Accordingly, multiple 3D structures are obtained from the precisely designed 2D planar bilayer sheet, as elaborated in Chapter 4. Subsequently, the shape memory effect (SME) of the bilayer system is studied, as shown in Chapter 5. By a series of characterization of the polyelectrolyte layer, we concluded that the semi-crystallization of the polymer in this layer enables the SME of the device. The 'templated device' is obtained to be assembled with a strain sensor, which could be used as humidity sensors.

We concluded that the humidity-responsive SME of the bilayer system originates from the semicrystallization of the polyelectrolyte layer (pDADMAC). Conventional shape memory polymers (SMPs) includes cross-linked polyethylene, styrene-based polymers, acrylate-based polymers, exopy-based polymers and thioene-based polymers.[366] PDADMAC has not been verified as conventional SMP, and further study on this will be conducted. However, by laminating it with an inelastic polymeric substrate,

its reversible expansion and contraction leads to the reversible (two-way) SEM of the device entirely. In the environment of the relatively low humidity, the drying of the pDADMAC solution on the top layer leads to the self-folding of 2D laminated polymer sheet into 3D structures, which can be considered as the permanent shape. Drying-induced semicrystallization of pDADMAC generates amorphous phase and crystalline phase in this layer, respectively. The crystalline phase, possessing a melting transition temperature T_m, plays the role of 'hard phase', while the amorphous phase, with a glass transition temperature T_g, serves as the 'soft phase'. In a relatively higher humidity environment, water permeates through this layer which leads to the decrease of T_g of the amorphous phase and thus the softening and moving of polymer chains in this phase. It is equivalent to heating the polymer above T_g for the traditional SMP. The internal force generated in the process of forming the permanent shape is released while driving the 3D structure to deform into temporary 2D shape. When the humidity level is reduced to the low level, the crystalline phase directs the temporary 2D shape to self-fold into the permanent shape.

The two-way SME of the device is dependent on the elastic modulus and mechanical strength of the two layers. The crystalline phase in the pDADMAC endowed the bilayer device with strength high enough to handle the mass many times of its own. The two-way SME property of the device enables its application as versatile 3D structure fabrication and sensors.

Polymer based actuators generally requires various properties, such as large strain,

stress, fast response time, and precisely controlled reversible shape changes. These can be tailored by selecting suitable laminating materials, adjusting the thickness, and changing the deformation ratio of the coupling materials. For instance, our device performs large deformation strain, high mechanical stress, and reversible shape changes, but responds to the stimuli (humidity change) in a relatively slow fashion. This can be improved by doping electrothermal or photothermal fillers in the pDADMAC layer, which will accelerates the evaporation speed of water by generating local upon exposure to the stimuli. Furthermore, the study in this part opens the gate for us to design other polymer based actuators. We are on the way to make an electricity responsive conductive polymer based actuators, and some of the work will be illustrated in Appendix C.

8.2 Conclusion and outlook on hydrogel based actuators

The second project is the development of semi-interpenetrated hydrogel based bilayer actuators. The existence of physically trapped polyelectrolyte in the chemically crosslinked pNIPAm based hydrogels enables a significantly large deformation of the device. They show the bi-directional self-folding behavior in response to both temperature and pH in aqueous solution. They are specially designed to be used as grippers and small molecule release devices. The deformation of the device depends on the transport of ions and water across the hydrogel, therefore the actuation speed of macroscopic device is slow. Fabricating the device in small dimensions will significantly

reduce the amount of actuation time. Therefore, miniaturizing the device from mm to μm is the future direction of this project. The mechanical modulus of the device will also be evaluated in order to design structures which are suitable for and bio-mimicking and biomedical applications. For example, we are planning to design pH responsive microgrippers and use them to grasp diseased tissues or cancer cells, and drugs will be released from the device upon triggers.

8.3 Conclusion and outlook on the 1D photonic crystal sensor-etalon

In Chapter 7, reductive reagent responsive microgel based etalons (one type of 1D photonic crystals) are fabricated. The presence of reductive reagents (e.g. Dithiothreitol (DTT)) leads to the breakage of crosslinkers in the microgel network. The resulted decreasing of the crosslink density allows the microgels swell to a larger extent, which leads to the changes of the optical properties (peak shift) of the etalon. The peak shift of the etalon was shown to depend on the concentration of DTT it is exposed to. AFM analysis was carried out to further prove the swelling of the microgels between two Au layers in the presence of DTT. This sensor exhibits easy read-out signals, signal stability, and sensitivity, yet the major issue is lack of selectivity. However, it does give us the general idea that whether the reducing reagents and how much of it exist. This concept of changing crosslinking density of microgels in the etalon can also be used for detecting other analytes. For instance, some of the work related to detecting glucose has been done, which is illustrated in Appendix A. Other than being used as sensors for molecules, the

pNIPAm based etalons can also be applied in environmental chemistry, and some of work has been done for pH and moisture monitoring in soil, which is illustrated in Appendix B. In the future, the properties of the etalon need to be further explored in order to develop new fabrication and modification methods of the device, find diverse applications of this device in sensing and biosensing, and realize their potential in point-of-care diagnostics.

Appendix A: Glucose Responsive Concanavalin A-Pendant Glucose Crosslinked Microgel Based Etalon

A.1 Introduction

A glucose-sensitive microgel was prepared by the application of the glucose sensitive complex formation between a pendent glucose and concavanalin A (ConA) to the crosslinking in the microgel. Glucosyloxyethyl methacrylate (GEMA), being the pendent glucose, and *N*-isopropylacrylamide (NIPAm) were copolymerized in the presence of the crosslinker *N, N*-methylenebisacrylamide (BIS). Subsequently, the penetration of ConA in the microgel network, by soaking microgels in the ConA buffer solution, enables formation of the double crosslinked microgels. The generation of complex between GEMA and ConA has been confirmed.[63,367] The glucose-sensitive etalon was fabricated from the synthesized microgels. The glucose sensitivity is attributed to the increased swelling of the microgel resulted from dissociation of the complex between the ConA and GEMA moieties of the microgel network in the presence of glucose.

A.2 Experimental section

Materials: *N*-isopropylacrylamide was purchased from TCI (Portland, Oregon) and purified by recrystallization from hexanes (ACS reagent grade, EMD, Gibbstown, NJ) prior to use. *N,N*-methylenebisacrylamide (BIS) (99%), and ammonium persulfate (APS) (98+%) were obtained from Sigma-Aldrich (Oakville, Ontario) and were used as received. Glucosyloxyethyl methacrylate (GEMA) solution (5% (w/v) in ethanol was purchased from Sigma-Aldrich and solution (ethanol) was removed prior to use. Deionized (DI) water with a resistivity of 18.2 MΩ●cm was used. Cr/Au annealing was done in a Thermolyne muffle furnace from Thermo Fisher Scientific (Ottawa, Ontario). Deionized (DI) water with a resistivity of 18.2 MΩ●cm was used. Cr/Au annealing was done in a Thermolyne muffle furnace from Thermo Fisher Scientific (Ottawa, Ontario). Methanol (ACS reagent, 99.8% +) was obtained from Sigma Aldrich. Fisher's finest glass coverslips were 25 × 25 mm and obtained from Fisher Scientific (Ottawa, Ontario). Cr was 99.999% and obtained from ESPI (Ashland, OR), while Au was 99.99% and obtained from MRCS Canada (Edmonton, AB).

Microgel synthesis: microgels composed of poly (NIPAm-co-AAc) were synthesized via a temperature-ramp, free radical precipitation as described previously. The monomer mixture, with a total concentration of 112.2 mM, was comprised of 78% (mol%) NIPAm, 21% GEMA, and 1% BIS as the crosslinker. NIPAm (0.88 mmol), BIS (0.11 mmol) were

dissolved in 10 mL deionized water with stirring in a beaker. The mixture was filtered through a 0.2 μm filter affixed to a 10 mL syringe into a 50 mL 3-neck round-bottom flask. The flask was then equipped with a temperature probe, a condenser and a N_2 gas inlet. The solution was bubbled with N_2 gas for ~1.5 h, while stirring at a rate of 450 rpm, allowing the temperature to reach 70 °C. GEMA (0.23 mmol) was first dissolved in 250 μL methonal, and then added to the heated mixture with a micropipette in one aliquot. A 0.078 M aqueous solution of APS (500 μL) was delivered to the reaction flask with a transfer pipet to initiate the reaction The reaction was allowed to proceed for 4h at 70 °C. After polymerization, the reaction mixture was allowed to cool down to room temperature and filtered through a filter paper to remove any large aggregates. The coagulum was rinsed with deionized water and filtered. These microgels (10 mL) were centrifuged at a speed of ~8500 relative centrifugal force (rcf) at 23 °C for ~ 40 minutes to produce a pellet at the bottom of the centrifuge tube. The supernatant was removed from the pellet of microgels, which was then re-suspended to the original volume (10 mL) using deionized water. This process was repeated until the microgels were cleaned a total of six times to remove any unreacted monomer and/or linear polymer from the microgel solution.

Fabrication of ConA included microgel based etalon: Briefly, 25 × 25 mm pre-cleaned glass coverslips were rinsed with DI water and ethanol and dried with N_2 gas, and 2 nm of Cr followed by 15 nm or 15 nm of Au were thermally evaporated onto them at a rate of

~0.2 Å s^{-1} and ~0.1 Å s^{-1}, respectively, using a Torr International Inc. model THEUPG thermal evaporation system (New Windsor, NY). The Au coated glass substrates were annealed at 250 °C for 3 h and then cooled to room temperature prior to use.The coated substrate was rinsed with ethanol, dried with N_2, and then placed onto hot plate (Corning, NY) set to 30 °C. An aliquot (40 μL for each 25 × 25 mm area) of the concentrated microgels was put onto the substrate and then spread toward each edges using the side of a micropipette tip. The microgel solution was allowed to dry completely on the substrate for 2 h with the hot plate temperature set to 35 °C. After 2 h, the dry film was rinsed copiously with DI water to remove any excess microgels not bound directly to the Au. Microgel painted substrate was then placed into a DI water bath and allowed to incubate overnight on a hot plate set to ~30 °C. Following this step, the substrate was again rinsed with DI water to further remove any microgels not bound directly to the Au substrate surface. The microgel painted Au coated substrate was dried with N_2 gas and immersed in 0.1 M tris-HCl buffer solution (pH 7.5) containing 1mg/mL ConA, 1mM $MnCl_2$ and 1mM $CaCl_2$ at 4 °C overnight. Then the substrate was immersed in the buffer solution without ConA to wash off the absorbed ConA on the surface. Then the substrate was dired with N_2 and coated with the top layer of 2 nm Cr and 5 nm Au.

Reflectance spectroscopy: The etalon was kept immersed in 0.1 M tris-HCl buffer (pH 7.5), containing 1 mM $MnCl_2$ and 1 mM $CaCl_2$ until equilibrium was reached at 25 ºC. Reflectance spectra from the etalon were collected by a USB 2000+ spectrophotometer,

connecting with a light source and a reflectance probe from Ocean Optics (Dunedin FL). After that, the etalon was exposed to the buffer solution with different concentrations of glucose. The spectra were collected for etalon socked in each solution over a wavelength range of 400 ~ 1000 nm and analyzed by Ocean Optics Spectra Suite Spectroscopy software.

Atomic force microscopy (AFM) tapping imaging. In-liquid height analysis for ConA-pendent glucose crosslinked pNIPAm microgel-based etalons was done in pH 7.5 tris-HCl buffer solution before and after glucose exposure. The images were obtained using an Asylum Research MFP 3D AFM (Santa Barbara, CA). Images were acquired over a 30 ×30 μm area using a scan rate of 0.50 Hz. For this analysis, a line was scratched into the etalon using a razor blade and the scratch was imaged. Images were first taken in pH 7.4 phosphate buffer solution at 25 ºC. Then the sample was treated in 5 mg/mL glucose phosphate buffer solution for at least 2 h. After that, the sample was imaged using the same method at 25 ºC. The height was determined using Asylum software.

A.3 Results and discussion

The crosslinking structure of the poly (NIPAm-co-GEMA)-ConA microgel are explained by the schematic diagram shown in Figure A-1. ConA is trapped in the

chemically crosslinked p(NIPAm-co-GEMA) microgel network (Figure 1a), and the physical complex was formed between ConA and GEMA moieties, leading to the crosslinking density to a greater extent.

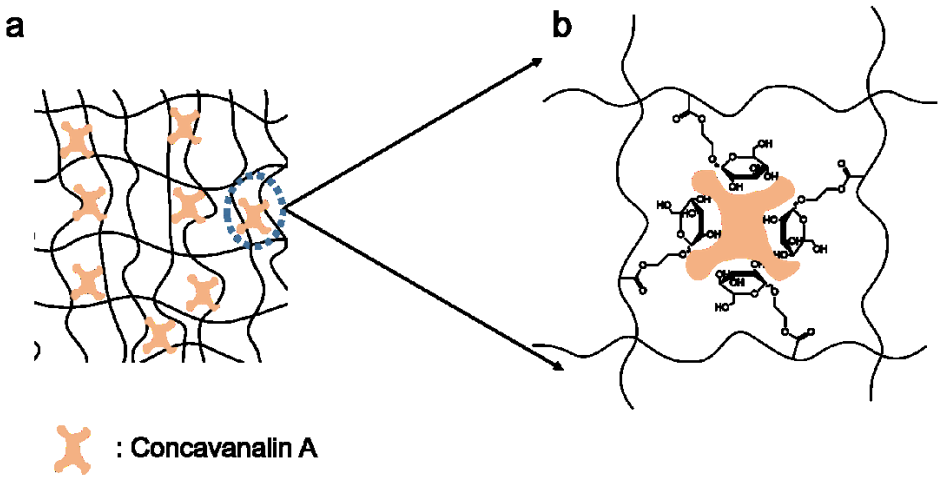

Figure A-1 Schematic diagram of p(NIPAm-co-GEMA)-ConA complexation in the microgel network.

Figure A-2a shows the peak shift of the spectra from the etalon in the presence of glucose solution with different concentrations. In contrast, Figure A-2b is the peak shift of the etalon fabricate microgels which don't contain ConA. There is no response from the control etalon in the presence of glucose.

Figure A-2 a) the positions of the etalons' reflectance peak after exposure to the indicated amount of glucose, b) the response of p(NIPAm-co-GEMA) microgel based etalons to glucose.

Furthermore, we collected atomic force microscopy (AFM) images of ConA included microgel-based etalons in buffer without and with glucose present. From these images, we were able to determine the etalons thickness. To accomplish this, an etalon was formed on a substrate, as previously described, and was scratched with a razor blade to remove the etalon from a specific area. The substrate was then imaged in the scratched region to determine the etalons thickness before and after exposure to glucose. Figure A-3a shows the AFM image for the etalon in the scratched region after soaking in tris-HCl buffer solution with pH 7.5, and reveals a thickness of 1.3 μm. Then the etalon was exposed to 5 mg/mL glucose in the same tris-HCl buffer for 2 h, followed by AFM imaging. Figure A-3b shows the image for the etalon in the same region as Figure A-3a, which reveals a thickness of ~1.9 μm.

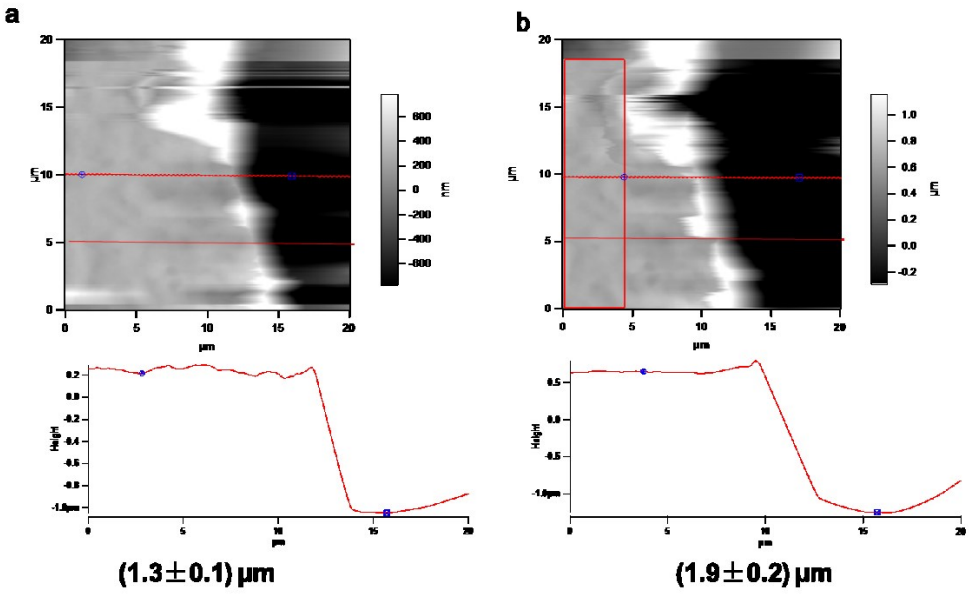

Figure A-3 a) AFM images of etalons in (a) pH tris-HCl buffer solution; b) the same buffer solution containing 5 mg/mL glucose.

A.4 Conclusion and outlook

Part of the work has been done about this project. The etalon fabricated from the ConA entrapped microgels shows the response to the solutions with different concentrations. The experiment needs to be repeated at least two more times. Furthermore, a series of experiment needs to be done to evaluate the loading efficiency of the ConA in the microgels, and select the modified microgels which show the low detection of limit and high sensitivity.

Appendix B: PH and Moisture Monitoring of Soil Using Microgel Based Etalons

In this part, poly(*N*-isopropylacrylamide) (pNIPAm) microgel based etalon is fabricated to monitor the moisture in the soil, and poly(*N*-isopropylacrylamide)-co-acrylic acid (pNIPAm-co-AAc)based etalon is developed to monitor the pH in the soil. The fabrication process was illustrated in other Chapters, which will not be discussed here in detail. Figure B-1 shows the setup of all the instrument used in the experiment. Figure B-1a is the image of the holder for the etalon. The etalon is fixed at the bottom of the holder, and the probe is inserted into the holder until the end of the probe reaches to the place right above the etalon, as shown in Figure B-1b. Then the holder is placed in the soil, and the signals indicating the moisture level or pH of the soil are collected, as shown in Figure B-1c.

Figure B-2 shows the how the position of pNIPAm microgel based etalons' reflectance peak depends on the water mass percentage in the soil. Figure B-3 shows the reflectance peak shift of the pNIPAm-co-AAc microgel based etalon in response to pH in the soil.

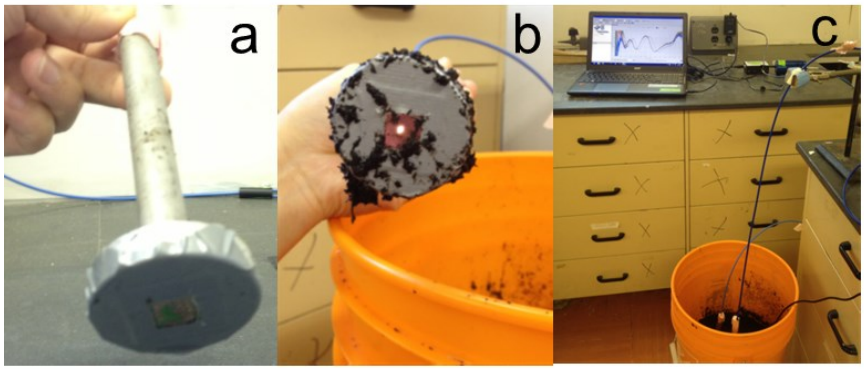

Figure B-1 Images of the setup for the pH and moisture sensing in soil.

Figure B-2 The reflectance peak shift of the etalon in response to moisture percentage in the soil.

Figure B-3 The reflectance peak shift of etalon in response to pH.

Appendix C: Water Soluble Polypyrrole-based Actuators and Their Applications

Materials and polymer synthesis: poly (sodium 4-styrene sulfonate) (SPS) (Mw 70,000) and pyrrole (assay 98%), Horseradish peroxidase (HRP) were purchased from Sigma-Aldrich. Hydrogen peroxide (35 wt%) was obtained from CALEDON LABORATORY CHEMICALS. The synthesis of water soluble polypyrrole was described by Entezami and coworkers.[368] Specifically, a total of 185.5 mg of SPS was dissolved in 50 mL of water (pH 2, adjusted with HCl). This was followed by the addition of 63.5 μL (0.9 mmol) pyrrole and 5.0 mg of HRP to this solution. To initiate the polymerization, 45 mL of 0.02 M hydrogen peroxide was added gradually. The solution was stirred for 12 h to complete the polymerization. The solution becomes darker gradually until to be dark black. This solution was transferred to regenerated cellulose tubes for dialysis for at least 48 h against acidic water solution to remove any unreacted monomers. Figure C-1 shows the structure of the synthesized water-soluble polypyrrole. Figure C-2 is the FT-IR spectra of the SPS-polypyrrole complex.

Figure C-1 The structure of the water soluble SPS-polypyrrole complex.

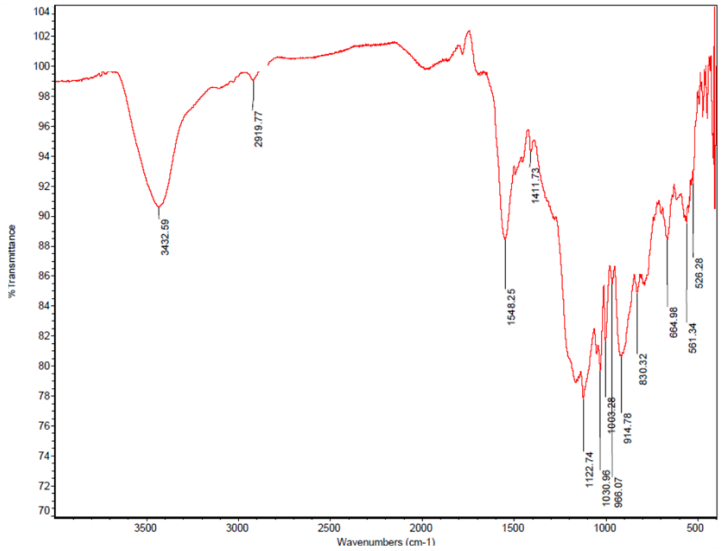

Figure C-2 FT-IR spectra of SPS-polypyrrole complex by casting a film on an AgBr crystal window.

We successfully synthesized the water soluble SPS doped polypyrrole. The future work is to fabricate a novel bilayer system by the layer-by-layer assembly (LBL) technique. For the first layer, we plan to assemble multiple layers of SPS-polypyrrole and poly(diallyldimethylammonium chloride) (pDADMAC), while for the second layer,

multilayers of SPS and pDADMAC will be fabricated.

Bibliography

(1) Gil, E. S.; Hudson, S. M. *Progress in Polymer Science* **2004**, *29*, 1173.

(2) Dimitrov, I.; Trzebicka, B.; Müller, A. H.; Dworak, A.; Tsvetanov, C. B. *Progress in Polymer Science* **2007**, *32*, 1275.

(3) Schumers, J. M.; Fustin, C. A.; Gohy, J. F. *Macromolecular Rapid Communications* **2010**, *31*, 1588.

(4) Ohtake, T.; Tanaka, H. *Polymer Journal* **2015**.

(5) Magnusson, J. P.; Khan, A.; Pasparakis, G.; Saeed, A. O.; Wang, W.; Alexander, C. *Journal of the American Chemical Society* **2008**, *130*, 10852.

(6) Hu, J.; Zhang, G.; Liu, S. *Chemical Society Reviews* **2012**, *41*, 5933.

(7) Roy, D.; Cambre, J. N.; Sumerlin, B. S. *Progress in Polymer Science* **2010**, *35*, 278.

(8) Baltes, T.; Garret‐Flaudy, F.; Freitag, R. *Journal of Polymer Science Part A: Polymer Chemistry* **1999**, *37*, 2977.

(9) Wu, C.; Wang, X. *Physical Review Letters* **1998**, *80*, 4092.

(10) Lau, A. C.; Wu, C. *Macromolecules* **1999**, *32*, 581.

(11) Maeda, Y.; Nakamura, T.; Ikeda, I. *Macromolecules* **2002**, *35*, 217.

(12) Idziak, I.; Avoce, D.; Lessard, D.; Gravel, D.; Zhu, X. *Macromolecules* **1999**, *32*, 1260.

(13) Liu, F.; Urban, M. W. *Macromolecules* **2008**, *41*, 352.

(14) Wu, C.; Zhou, S. *Macromolecules* **1995**, *28*, 8381.

(15) Wu, X. S.; Hoffman, A. S.; Yager, P. *Journal of Polymer Science Part A: Polymer Chemistry* **1992**, *30*, 2121.

(16) Inomata, H.; Goto, S.; Saito, S. *Macromolecules* **1990**, *23*, 4887.

(17) Kaneko, Y.; Nakamura, S.; Sakai, K.; Aoyagi, T.; Kikuchi, A.; Sakurai, Y.;

Okano, T. *Macromolecules* **1998**, *31*, 6099.

(18) Hu, T.; You, Y.; Pan, C.; Wu, C. *The Journal of Physical Chemistry B* **2002**, *106*, 6659.

(19) Schild, H. G. *Progress in Polymer Science* **1992**, *17*, 163.

(20) de las Heras Alarcón, C.; Pennadam, S.; Alexander, C. *Chemical Society Reviews* **2005**, *34*, 276.

(21) Li, G.; Song, S.; Guo, L.; Ma, S. *Journal of Polymer Science Part A: Polymer Chemistry* **2008**, *46*, 5028.

(22) He, E.; Yue, C.; Tam, K. *Langmuir* **2009**, *25*, 4892.

(23) Hu, L.; Chu, L.-Y.; Yang, M.; Wang, H.-D.; Niu, C. H. *Journal of Colloid and Interface Science* **2007**, *311*, 110.

(24) Li, D.; He, Q.; Cui, Y.; Li, J. *Chemistry of Materials* **2007**, *19*, 412.

(25) Su, S.; Ali, M. M.; Filipe, C. D.; Li, Y.; Pelton, R. *Biomacromolecules* **2008**, *9*, 935.

(26) Singh, N.; Bridges, A. W.; García, A. J.; Lyon, L. A. *Biomacromolecules* **2007**, *8*, 3271.

(27) Kim, J.; Singh, N.; Lyon, L. A. *Chemistry of Materials* **2007**, *19*, 2527.

(28) Kumar, G. S.; Neckers, D. *Chemical Reviews* **1989**, *89*, 1915.

(29) Khoukh, S.; Oda, R.; Labrot, T.; Perrin, P.; Tribet, C. *Langmuir* **2007**, *23*, 94.

(30) Sugiyama, K.; Sono, K. *Journal of Applied Polymer Science* **2001**, *81*, 3056.

(31) Mamada, A.; Tanaka, T.; Kungwatchakun, D.; Irie, M. *Macromolecules* **1990**, *23*, 1517.

(32) He, J.; Tong, X.; Zhao, Y. *Macromolecules* **2009**, *42*, 4845.

(33) Yager, K. G.; Barrett, C. J. *Journal of Photochemistry and Photobiology A: Chemistry* **2006**, *182*, 250.

(34) Irie, M. In *New Polymer Materials*; Springer: 1990, p27.

(35) Finkelmann, H.; Nishikawa, E.; Pereira, G.; Warner, M. *Physical Review Letters*

2001, *87*, 015501.

(36) Jiang, H.; Kelch, S.; Lendlein, A. *Advanced Materials* **2006**, *18*, 1471.

(37) Desponds, A.; Freitag, R. *Langmuir* **2003**, *19*, 6261.

(38) Lee, H.-i.; Pietrasik, J.; Matyjaszewski, K. *Macromolecules* **2006**, *39*, 3914.

(39) Brochu, P.; Pei, Q. *Macromolecular Rapid Communications* **2010**, *31*, 10.

(40) Smela, E. *Advanced Materials* **2003**, *15*, 481.

(41) Shahinpoor, M.; Bar-Cohen, Y.; Simpson, J.; Smith, J. *Smart materials and Structures* **1998**, *7*, R15.

(42) Baughman, R. *Synthetic Metals* **1996**, *78*, 339.

(43) Carpi, F.; De Rossi, D.; Kornbluh, R.; Pelrine, R. E.; Sommer-Larsen, P. *Dielectric elastomers as electromechanical transducers: Fundamentals, materials, devices, models and applications of an emerging electroactive polymer technology*; Elsevier, 2011.

(44) MacDiarmid, A. G. *Angewandte Chemie International Edition* **2001**, *40*, 2581.

(45) Kanatzidis, M. G. *Chemical & Engineering News* **1990**, *68*.

(46) Pei, Q.; Inganäs, O. *The Journal of Physical Chemistry* **1992**, *96*, 10507.

(47) Torresi, R.; de Torresi, S. C.; Matencio, T.; De Paoli, M.-A. *Synthetic Metals* **1995**, *72*, 283.

(48) Naoi, K.; Lien, M.; Smyrl, W. H. *Journal of the Electrochemical Society* **1991**, *138*, 440.

(49) Otero, T. F. *Journal of Materials Chemistry* **2009**, *19*, 681.

(50) Otero, T. F. *Journal of Materials Chemistry B* **2013**, *1*, 3754.

(51) Schmidt, C. E.; Shastri, V. R.; Vacanti, J. P.; Langer, R. *Proceedings of the National Academy of Sciences of the United States of America,* **1997**, *94*, 8948.

(52) Lutolf, M.; Hubbell, J. *Nature Biotechnology* **2005**, *23*, 47.

(53) Mano, J. F. *Advanced Engineering Materials* **2008**, *10*, 515.

(54) Schmaljohann, D. *Advanced Drug Delivery Reviews* **2006**, *58*, 1655.

(55) Rapoport, N. *Progress in Polymer Science* **2007**, *32*, 962.

(56) Holtz, J. H.; Asher, S. A. *Nature* **1997**, *389*, 829.

(57) Giljohann, D. A.; Mirkin, C. A. *Nature* **2009**, *462*, 461.

(58) Ito, Y.; Casolaro, M.; Kono, K.; Imanishi, Y. *Journal of Controlled Release* **1989**, *10*, 195.

(59) Chu, L.-Y.; Li, Y.; Zhu, J.-H.; Wang, H.-D.; Liang, Y.-J. *Journal of Controlled Release* **2004**, *97*, 43.

(60) Podual, K.; Doyle, F. J.; Peppas, N. A. *Journal of Controlled Release* **2000**, *67*, 9.

(61) Brownlee, M.; Cerami, A. *Science* **1979**, *206*, 1190.

(62) Tanna, S.; Taylor, M. J.; Sahota, T. S.; Sawicka, K. *Biomaterials* **2006**, *27*, 1586.

(63) Nakamae, K.; Miyata, T.; Jikihara, A.; Hoffman, A. S. *Journal of Biomaterials Science, Polymer Edition* **1995**, *6*, 79.

(64) Miyata, T.; Asami, N.; Uragami, T. *Macromolecules* **1999**, *32*, 2082.

(65) Miyata, T.; Asami, N.; Uragami, T. *Nature* **1999**, *399*, 766.

(66) Zhang, R.; Bowyer, A.; Eisenthal, R.; Hubble, J. *Biotechnology and Bioengineering* **2007**, *97*, 976.

(67) Castellani, O. F.; Martínez, E. N.; Añón, M. C. *Journal of Agricultural and Food Chemistry* **1999**, *47*, 3001.

(68) Jones, D. P.; Carlson, J. L.; Samiec, P. S.; Sternberg, P.; Mody, V. C.; Reed, R. L.; Brown, L. A. S. *Clinica Chimica Acta* **1998**, *275*, 175.

(69) You, Y.-Z.; Zhou, Q.-H.; Manickam, D. S.; Wan, L.; Mao, G.-Z.; Oupický, D. *Macromolecules* **2007**, *40*, 8617.

(70) Cerritelli, S.; Velluto, D.; Hubbell, J. A. *Biomacromolecules* **2007**, *8*, 1966.

(71) Jocelyn, P. C. *Methods in Enzymology* **1986**, *143*, 246.

(72) Oh, J. K.; Siegwart, D. J.; Lee, H.-i.; Sherwood, G.; Peteanu, L.; Hollinger, J. O.; Kataoka, K.; Matyjaszewski, K. *Journal of the American Chemical Society* **2007**, *129*,

5939.

(73) Hoffman, A. S. *Advanced Drug Delivery Reviews* **2012**, *64*, 18.

(74) Ratner, B. D.; Hoffman, A. S.; Schoen, F. J.; Lemons, J. E. *Biomaterials science: an introduction to materials in medicine*; Academic Press, 2004.

(75) Drury, J. L.; Mooney, D. J. *Biomaterials* **2003**, *24*, 4337.

(76) Akiyoshi, K.; Kang, E.-C.; Kurumada, S.; Sunamoto, J.; Principi, T.; Winnik, F. M. *Macromolecules* **2000**, *33*, 3244.

(77) Sanabria-DeLong, N.; Crosby, A. J.; Tew, G. N. *Biomacromolecules* **2008**, *9*, 2784.

(78) Collier, J. H.; Hu, B.-H.; Ruberti, J. W.; Zhang, J.; Shum, P.; Thompson, D. H.; Messersmith, P. B. *Journal of the American Chemical Society* **2001**, *123*, 9463.

(79) Wang, Q.; Schlenoff, J. B. *Advanced Materials* **2015**, *27*, 2077.

(80) Hua, Z.; Chen, Z.; Li, Y.; Zhao, M. *Langmuir* **2008**, *24*, 5773.

(81) Topuz, F.; Okay, O. *Macromolecules* **2008**, *41*, 8847.

(82) Marpu, S.; Hu, Z.; Omary, M. A. *Langmuir* **2010**, *26*, 15523.

(83) Wei, H.; Yu, H.; Zhang, A.-y.; Sun, L.-g.; Hou, D.; Feng, Z.-g. *Macromolecules* **2005**, *38*, 8833.

(84) Garty, S.; Kimelman-Bleich, N.; Hayouka, Z.; Cohn, D.; Friedler, A.; Pelled, G.; Gazit, D. *Biomacromolecules* **2010**, *11*, 1516.

(85) Flory, P. J.; Rehner Jr, J. *The Journal of Chemical Physics* **1943**, *11*, 521.

(86) Wu, C. *Polymer* **1998**, *39*, 4609.

(87) Wu, C.; Zhou, S. *Journal of Macromolecular Science, Part B: Physics* **1997**, *36*, 345.

(88) Dong, L.-c.; Hoffman, A. S. *Journal of Controlled Release* **1991**, *15*, 141.

(89) Mathur, A. M.; Moorjani, S. K.; Scranton, A. B. *Journal of Macromolecular Science, Part C: Polymer Reviews* **1996**, *36*, 405.

(90) Nagaoka, N.; Safrani, A.; Yoshida, M.; Omichi, H.; Kubota, H.; Katakai, R.

Macromolecules **1993**, *26*, 7386.

(91) Zhang, J.; Chu, L.-Y.; Li, Y.-K.; Lee, Y. M. *Polymer* **2007**, *48*, 1718.

(92) Zhao, Y.-L.; Stoddart, J. F. *Langmuir* **2009**, *25*, 8442.

(93) Murdan, S. *Journal of Controlled Release* **2003**, *92*, 1.

(94) Saunders, B. R.; Vincent, B. *Advances in Colloid and Interface Science* **1999**, *80*, 1.

(95) Kawaguchi, H. *Progress in Polymer Science* **2000**, *25*, 1171.

(96) Pelton, R. *Advances in Colloid and Interface Science* **2000**, *85*, 1.

(97) Feher, J.; Filipcsei, G.; Szalma, J.; Zrínyi, M. *Colloids and Surfaces A: Physicochemical and Engineering Aspects* **2001**, *183*, 505.

(98) Lyon, L. A.; Debord, J. D.; Debord, S. B.; Jones, C. D.; McGrath, J. G.; Serpe, M. J. *The Journal of Physical Chemistry B* **2004**, *108*, 19099.

(99) Xu, S.; Zhang, J.; Paquet, C.; Lin, Y.; Kumacheva, E. *Advanced Functional Materials* **2003**, *13*, 468.

(100) Varma, M. V.; Kaushal, A. M.; Garg, S. *Journal of Controlled Release* **2005**, *103*, 499.

(101) De Geest, B.; Dejugnat, C.; Verhoeven, E.; Sukhorukov, G.; Jonas, A. M.; Plain, J.; Demeester, J.; De Smedt, S. *Journal of Controlled Release* **2006**, *116*, 159.

(102) Schmidt, S.; Zeiser, M.; Hellweg, T.; Duschl, C.; Fery, A.; Möhwald, H. *Advanced Functional Materials* **2010**, *20*, 3235.

(103) Gan, T.; Guan, Y.; Zhang, Y. *Journal of Materials Chemistry* **2010**, *20*, 5937.

(104) Sorrell, C. D.; Carter, M. C.; Serpe, M. J. *Advanced Functional Materials* **2011**, *21*, 425.

(105) Sorrell, C. D.; Serpe, M. J. *Advanced Materials* **2011**, *23*, 4088.

(106) Gan, D.; Lyon, L. A. *Macromolecules* **2002**, *35*, 9634.

(107) Kratz, K.; Hellweg, T.; Eimer, W. *Polymer* **2001**, *42*, 6631.

(108) Schmidt, S.; Motschmann, H.; Hellweg, T.; von Klitzing, R. *Polymer* **2008**,

49, 749.

(109) Liu, C.; Qin, H.; Mather, P. *Journal of Materials Chemistry* **2007**, *17*, 1543.

(110) Hu, J.; Zhu, Y.; Huang, H.; Lu, J. *Progress in Polymer Science* **2012**, *37*, 1720.

(111) Lendlein, A.; Kelch, S. *Angewandte Chemie International Edition* **2002**, *41*, 2034.

(112) Behl, M.; Razzaq, M. Y.; Lendlein, A. *Advanced Materials* **2010**, *22*, 3388.

(113) Hu, J.; Yang, Z.; Yeung, L.; Ji, F.; Liu, Y. *Polymer International* **2005**, *54*, 854.

(114) Zhao, Q.; Qi, H. J.; Xie, T. *Progress in Polymer Science* **2015**, *49*, 79.

(115) Peponi, L.; Navarro-Baena, I.; Sonseca, A.; Gimenez, E.; Marcos-Fernandez, A.; Kenny, J. M. *European Polymer Journal* **2013**, *49*, 893.

(116) Ping, P.; Wang, W.; Chen, X.; Jing, X. *Biomacromolecules* **2005**, *6*, 587.

(117) Zhu, G.; Liang, G.; Xu, Q.; Yu, Q. *Journal of Applied Polymer Science* **2003**, *90*, 1589.

(118) Chun, B. C.; Cho, T. K.; Chong, M. H.; Chung, Y.-C. *Journal of Materials Science* **2007**, *42*, 9045.

(119) Liu, T.; Li, J.; Pan, Y.; Zheng, Z.; Ding, X.; Peng, Y. *Soft Matter* **2011**, *7*, 1641.

(120) Brostowitz, N. R.; Weiss, R.; Cavicchi, K. A. *ACS Macro Letters* **2014**, *3*, 374.

(121) Kolesov, I. S.; Kratz, K.; Lendlein, A.; Radusch, H.-J. *Polymer* **2009**, *50*, 5490.

(122) Morshedian, J.; Khonakdar, H.; Mehrabzadeh, M.; Eslami, H. *Advances in Polymer Technology* **2003**, *22*, 112.

(123) Alteheld, A.; Feng, Y.; Kelch, S.; Lendlein, A. *Angewandte Chemie International Edition* **2005**, *44*, 1188.

(124) Lin, J. R.; Chen, L. W. *Journal of Applied Polymer Science* **1999**, *73*, 1305.

(125) Yakacki, C. M.; Shandas, R.; Safranski, D.; Ortega, A. M.; Sassaman, K.; Gall, K. *Advanced Functional Materials* **2008**, *18*, 2428.

(126) Shi, Y.; Yoonessi, M.; Weiss, R. *Macromolecules* **2013**, *46*, 4160.

(127) Meng, H.; Li, G. *Polymer* **2013**, *54*, 2199.

(128) Leng, J.; Lv, H.; Liu, Y.; Du, S. *Applied Physics Letters* **2007**, *91*, 144105.

(129) Goo, N. S.; Paik, I. H.; Yoon, K. J. *Smart Materials and Structures* **2007**, *16*, N23.

(130) Cho, J. W.; Kim, J. W.; Jung, Y. C.; Goo, N. S. *Macromolecular Rapid Communications* **2005**, *26*, 412.

(131) Leng, J.; Huang, W.; Lan, X.; Liu, Y.; Du, S. *Applied Physics Letters* **2008**, *92*, 204101.

(132) Luo, X.; Mather, P. T. *Soft Matter* **2010**, *6*, 2146.

(133) Yu, K.; Zhang, Z.; Liu, Y.; Leng, J. *Applied Physics Letters* **2011**, *98*, 074102.

(134) Jung, Y. C.; Yoo, H. J.; Kim, Y. A.; Cho, J. W.; Endo, M. *Carbon* **2010**, *48*, 1598.

(135) Lu, H.; Gou, J. *Polymers for Advanced Technologies* **2012**, *23*, 1529.

(136) Huang, W.; Yang, B.; An, L.; Li, C.; Chan, Y. *Applied Physics Letters* **2005**, *86*, 114105.

(137) Chen, M.-C.; Tsai, H.-W.; Chang, Y.; Lai, W.-Y.; Mi, F.-L.; Liu, C.-T.; Wong, H.-S.; Sung, H.-W. *Biomacromolecules* **2007**, *8*, 2774.

(138) Lu, H.; Liu, Y.; Leng, J.; Du, S. *European Polymer Journal* **2010**, *46*, 1908.

(139) Zhao, Q.; Dunlop, J. W.; Qiu, X.; Huang, F.; Zhang, Z.; Heyda, J.; Dzubiella, J.; Antonietti, M.; Yuan, J. *Nature Communications* **2014**, *5*.

(140) Chae Jung, Y.; Hwa So, H.; Whan Cho, J. *Journal of Macromolecular Science, Part B* **2006**, *45*, 453.

(141) Hribar, K. C.; Lee, M. H.; Lee, D.; Burdick, J. A. *ACS Nano* **2011**, *5*, 2948.

(142) Koerner, H.; Price, G.; Pearce, N. A.; Alexander, M.; Vaia, R. A. *Nature Materials* **2004**, *3*, 115.

(143) Ohm, C.; Brehmer, M.; Zentel, R. *Advanced Materials* **2010**, *22*, 3366.

(144) Finkelmann, H.; Kock, H.-J.; Rehage, G. *Die Makromolekulare Chemie, Rapid Communications* **1981**, *2*, 317.

(145) Russew, M. M.; Hecht, S. *Advanced Materials* **2010**, *22*, 3348.

(146) Hiraoka, K.; Tagawa, N.; Baba, K. *Macromolecular Chemistry and Physics* **2008**, *209*, 298.

(147) Behl, M.; Kratz, K.; Zotzmann, J.; Nöchel, U.; Lendlein, A. *Advanced Materials* **2013**, *25*, 4466.

(148) Agrawal, A.; Yun, T.; Pesek, S. L.; Chapman, W. G.; Verduzco, R. *Soft Matter* **2014**, *10*, 1411.

(149) Tobushi, H.; Hayashi, S.; Sugimoto, Y.; Date, K. *Materials* **2009**, *2*, 1180.

(150) Vukusic, P.; Sambles, J. R. *Nature* **2003**, *424*, 852.

(151) Parker, A. R. *Journal of Optics A: Pure and Applied Optics* **2000**, *2*, R15.

(152) Lotsch, B. V.; Ozin, G. A. *ACS Nano* **2008**, *2*, 2065.

(153) Lotsch, B. V.; Ozin, G. A. *Advanced Materials* **2008**, *20*, 4079.

(154) Zhang, J.-T.; Chao, X.; Asher, S. A. *Journal of the American Chemical Society* **2013**, *135*, 11397.

(155) Zhang, J.-T.; Chao, X.; Liu, X.; Asher, S. A. *Chemical Communications* **2013**, *49*, 6337.

(156) Matijevic, E. *Langmuir* **1994**, *10*, 8.

(157) Cai, Z.; Liu, Y. J.; Teng, J.; Lu, X. *ACS Applied Materials & Interfaces* **2012**, *4*, 5562.

(158) Im, S. H.; Lim, Y. T.; Suh, D. J.; Park, O. O. *Advanced Materials* **2002**, *14*, 1367.

(159) Arsenault, A. C.; Puzzo, D. P.; Manners, I.; Ozin, G. A. *Nature Photonics* **2007**, *1*, 468.

(160) Finkelmann, H.; Kim, S. T.; Munoz, A.; Palffy-Muhoray, P.; Taheri, B. *Advanced Materials* **2001**, *13*, 1069.

(161) Foulger, S. H.; Jiang, P.; Lattam, A. C.; Smith, D. W.; Ballato, J. *Langmuir* **2001**, *17*, 6023.

(162) Asher, S. A.; Holtz, J.; Liu, L.; Wu, Z. *Journal of the American Chemical Society* **1994**, *116*, 4997.

(163) Hong, W.; Hu, X.; Zhao, B.; Zhang, F.; Zhang, D. *Advanced Materials* **2010**, *22*, 5043.

(164) Hart, S. D.; Maskaly, G. R.; Temelkuran, B.; Prideaux, P. H.; Joannopoulos, J. D.; Fink, Y. *Science* **2002**, *296*, 510.

(165) Temelkuran, B.; Hart, S. D.; Benoit, G.; Joannopoulos, J. D.; Fink, Y. *Nature* **2002**, *420*, 650.

(166) Hwang, K.; Kwak, D.; Kang, C.; Kim, D.; Ahn, Y.; Kang, Y. *Angewandte Chemie International Edition* **2011**, *50*, 6311.

(167) Blanco, A.; Chomski, E.; Grabtchak, S.; Ibisate, M.; John, S.; Leonard, S. W.; Lopez, C.; Meseguer, F.; Miguez, H.; Mondia, J. P. *Nature* **2000**, *405*, 437.

(168) Joannopoulos, J. D.; Johnson, S. G.; Winn, J. N.; Meade, R. D. *Photonic crystals: molding the flow of light*; Princeton University Press, 2011.

(169) Fowles, G. R. *Introduction to modern optics*; Courier Corporation, 2012.

(170) Xu, X.; Goponenko, A. V.; Asher, S. A. *Journal of the American Chemical Society* **2008**, *130*, 3113.

(171) Lee, K.; Asher, S. A. *Journal of the American Chemical Society* **2000**, *122*, 9534.

(172) Debord, J. D.; Eustis, S.; Byul Debord, S.; Lofye, M. T.; Lyon, L. A. *Advanced Materials* **2002**, *14*, 658.

(173) Debord, J. D.; Lyon, L. A. *The Journal of Physical Chemistry B* **2000**, *104*, 6327.

(174) Jones, C. D.; Lyon, L. A. *Journal of the American Chemical Society* **2003**, *125*, 460.

(175) Chen, M.; Zhou, L.; Guan, Y.; Zhang, Y. *Angewandte Chemie International Edition* **2013**, *52*, 9961.

(176) Fenzl, C.; Hirsch, T.; Wolfbeis, O. S. *Angewandte Chemie International Edition* **2014**, *53*, 3318.

(177) Ge, J.; Yin, Y. *Angewandte Chemie International Edition* **2011**, *50*, 1492.

(178) Edrington, A. C.; Urbas, A. M.; DeRege, P.; Chen, C. X.; Swager, T. M.; Hadjichristidis, N.; Xenidou, M.; Fetters, L. J.; Joannopoulos, J. D.; Fink, Y. *Advanced Materials* **2001**, *13*, 421.

(179) Kang, Y.; Walish, J. J.; Gorishnyy, T.; Thomas, E. L. *Nature Materials* **2007**, *6*, 957.

(180) Zhai, L.; Nolte, A. J.; Cohen, R. E.; Rubner, M. F. *Macromolecules* **2004**, *37*, 6113.

(181) Chiappelli, M. C.; Hayward, R. C. *Advanced Materials* **2012**, *24*, 6100.

(182) Islam, M. R.; Serpe, M. J. *Analytica Chimica Acta* **2014**, *843*, 83.

(183) Islam, M. R.; Serpe, M. J. *Analytical and Bioanalytical Chemistry* **2014**, *406*, 4777.

(184) Huang, H.; Serpe, M. J. *Journal of Applied Polymer Science* **2015**, *132*.

(185) Sorrell, C. D.; Serpe, M. J. *Analytical and Bioanalytical Chemistry* **2012**, *402*, 2385.

(186) Zhang, Q. M.; Ahiabu, A.; Gao, Y.; Serpe, M. J. *Journal of Materials Chemistry C* **2015**, *3*, 495.

(187) Zhang, Q. M.; Li, X.; Islam, M. R.; Wei, M.; Serpe, M. J. *Journal of Materials Chemistry C* **2014**, *2*, 6961.

(188) Gao, Y.; Serpe, M. J. *ACS Applied Materials & Interfaces* **2014**, *6*, 8461.

(189) Xu, W.; Gao, Y.; Serpe, M. J. *Journal of Materials Chemistry C* **2014**, *2*, 3873.

(190) Ionov, L. *Advanced Functional Materials* **2013**, *23*, 4555.

(191) Fernandes, R.; Gracias, D. H. *Advanced Drug Delivery Reviews* **2012**, *64*, 1579.

(192) Ikeda, T.; Ube, T. *Materials Today* **2011**, *14*, 480.

(193) van Oosten, C. L.; Bastiaansen, C. W.; Broer, D. J. *Nature Materials* **2009**, *8*, 677.

(194) Behl, M.; Razzaq, M. Y.; Lendlein, A. *Advanced Materials* **2010**, *22*, 3388.

(195) Ahir, S. V.; Terentjev, E. M. *Nature Materials* **2005**, *4*, 491.

(196) Chen, D.; Yoon, J.; Chandra, D.; Crosby, A. J.; Hayward, R. C. *Journal of Polymer Science Part B: Polymer Physics* **2014**, *52*, 1441.

(197) Chung, J. Y.; Nolte, A. J.; Stafford, C. M. *Advanced Materials* **2011**, *23*, 349.

(198) Rodríguez-Hernández, J. *Progress in Polymer Science* **2015**, *42*, 1.

(199) Gracias, D. H. *Current Opinion in Chemical Engineering* **2013**, *2*, 112.

(200) Timoshenko, S. *JOSA* **1925**, *11*, 233.

(201) Ionov, L. *Soft Matter* **2011**, *7*, 6786.

(202) Stoychev, G.; Zakharchenko, S.; Turcaud, S. b.; Dunlop, J. W.; Ionov, L. *ACS Nano* **2012**, *6*, 3925.

(203) Stoychev, G.; Puretskiy, N.; Ionov, L. *Soft Matter* **2011**, *7*, 3277.

(204) Stoychev, G.; Turcaud, S.; Dunlop, J. W.; Ionov, L. *Advanced Functional Materials* **2013**, *23*, 2295.

(205) Bassik, N.; Abebe, B. T.; Laflin, K. E.; Gracias, D. H. *Polymer* **2010**, *51*, 6093.

(206) Ye, C.; Nikolov, S. V.; Calabrese, R.; Dindar, A.; Alexeev, A.; Kippelen, B.;

Kaplan, D. L.; Tsukruk, V. V. *Angewandte Chemie International Edition* **2015**, *127*, 8610.

(207) Wei, Z.; Jia, Z.; Athas, J.; Wang, C.; Raghavan, S. R.; Li, T.; Nie, Z. *Soft Matter* **2014**, *10*, 8157.

(208) Luo, R.; Wu, J.; Dinh, N. D.; Chen, C. H. *Advanced Functional Materials* **2015**, *25*, 7272.

(209) HeeáLee, J.; Stephen, Z. *Journal of Materials Chemistry* **2011**, *21*, 6824.

(210) Wu, Z. L.; Moshe, M.; Greener, J.; Therien-Aubin, H.; Nie, Z.; Sharon, E.; Kumacheva, E. *Nature Communications* **2013**, *4*, 1586.

(211) Kim, J.; Hanna, J. A.; Byun, M.; Santangelo, C. D.; Hayward, R. C. *Science* **2012**, *335*, 1201.

(212) Zhang, X.; Pint, C. L.; Lee, M. H.; Schubert, B. E.; Jamshidi, A.; Takei, K.; Ko, H.; Gillies, A.; Bardhan, R.; Urban, J. J. *Nano Letters* **2011**, *11*, 3239.

(213) Tokarev, I.; Minko, S. *Soft Matter* **2009**, *5*, 511.

(214) Stuart, M. A. C.; Huck, W. T.; Genzer, J.; Müller, M.; Ober, C.; Stamm, M.; Sukhorukov, G. B.; Szleifer, I.; Tsukruk, V. V.; Urban, M. *Nature Materials* **2010**, *9*, 101.

(215) Qiu, Y.; Park, K. *Advanced Drug Delivery Reviews* **2012**, *64*, 49.

(216) Peppas, N. A.; Hilt, J. Z.; Khademhosseini, A.; Langer, R. *Advanced Materials* **2006**, *18*, 1345.

(217) Behl, M.; Kratz, K.; Noechel, U.; Sauter, T.; Lendlein, A. *Proceedings of the National Academy of Sciences of the United States of America* **2013**, *110*, 12555.

(218) Chen, S.; Hu, J.; Zhuo, H. *Composites Science and Technology* **2010**, *70*, 1437.

(219) Chen, S.; Hu, J.; Zhuo, H.; Zhu, Y. *Materials Letters* **2008**, *62*, 4088.

(220) Du, H.; Zhang, J. *Soft Matter* **2010**, *6*, 3370.

(221) Luo, H.; Hu, J.; Zhu, Y.; Zhang, S.; Fan, Y.; Ye, G. *Journal of Applied Polymer Science* **2012**, *125*, 657.

(222) Zhu, Y.; Hu, J.; Luo, H.; Young, R. J.; Deng, L.; Zhang, S.; Fan, Y.; Ye, G.

Soft Matter **2012**, *8*, 2509.

(223) Lee, W. E.; Jin, Y. J.; Park, L. S.; Kwak, G. *Advanced Materials* **2012**, *24*, 5604.

(224) Ma, M.; Guo, L.; Anderson, D. G.; Langer, R. *Science* **2013**, *339*, 186.

(225) Cheng, H.; Liu, J.; Zhao, Y.; Hu, C.; Zhang, Z.; Chen, N.; Jiang, L.; Qu, L. *Angewandte Chemie International Edition* **2013**, *52*, 10482.

(226) Zhang, L.; Liang, H.; Jacob, J.; Naumov, P. *Nature Communications* **2015**, *6*.

(227) Wang, W.; Sun, X.; Wu, W.; Peng, H.; Yu, Y. *Angewandte Chemie International Edition* **2012**, *124*, 4722.

(228) Wei, J.; Yu, Y. *Soft Matter* **2012**, *8*, 8050.

(229) de Haan, L. T.; Verjans, J. M.; Broer, D. J.; Bastiaansen, C. W.; Schenning, A. P. *Journal of the American Chemical Society* **2014**, *136*, 10585.

(230) Shim, T. S.; Kim, S. H.; Heo, C. J.; Jeon, H. C.; Yang, S. M. *Angewandte Chemie International Edition* **2012**, *51*, 1420.

(231) Jamal, M.; Kadam, S. S.; Xiao, R.; Jivan, F.; Onn, T.-M.; Fernandes, R.; Nguyen, T. D.; Gracias, D. H. *Advanced Healthcare Materials* **2013**, *2*, 1142.

(232) He, H.; Guan, J.; Lee, J. L. *Journal of Controlled Release* **2006**, *110*, 339.

(233) Jamal, M.; Kadam, S. S.; Xiao, R.; Jivan, F.; Onn, T. M.; Fernandes, R.; Nguyen, T. D.; Gracias, D. H. *Advanced Healthcare Materials* **2013**, *2*, 1142.

(234) Malachowski, K.; Breger, J.; Kwag, H. R.; Wang, M. O.; Fisher, J. P.; Selaru, F. M.; Gracias, D. H. *Angewandte Chemie International Edition* **2014**, *126*, 8183.

(235) Gultepe, E.; Randhawa, J. S.; Kadam, S.; Yamanaka, S.; Selaru, F. M.; Shin, E. J.; Kalloo, A. N.; Gracias, D. H. *Advanced Materials* **2013**, *25*, 514.

(236) Jager, E. W.; Inganäs, O.; Lundström, I. *Science* **2000**, *288*, 2335.

(237) Ilievski, F.; Mazzeo, A. D.; Shepherd, R. F.; Chen, X.; Whitesides, G. M. *Angewandte Chemie International Edition* **2011**, *50*, 1890.

(238) Felton, S.; Tolley, M.; Demaine, E.; Rus, D.; Wood, R. *Science* **2014**, *345*, 644.

(239) Yoshida, R. *Advanced Materials* **2010**, *22*, 3463.

(240) Morales, D.; Palleau, E.; Dickey, M. D.; Velev, O. D. *Soft Matter* **2014**, *10*, 1337.

(241) Kim, Y. S.; Liu, M.; Ishida, Y.; Ebina, Y.; Osada, M.; Sasaki, T.; Hikima, T.; Takata, M.; Aida, T. *Nature Materials* **2015**.

(242) Kwon, G. H.; Park, J. Y.; Kim, J. Y.; Frisk, M. L.; Beebe, D. J.; Lee, S. H. *Small* **2008**, *4*, 2148.

(243) Hilt, J. Z.; Gupta, A. K.; Bashir, R.; Peppas, N. A. *Biomedical Microdevices* **2003**, *5*, 177.

(244) Smela, E.; Inganas, O.; Lundstrom, I. *Science* **1995**, *268*, 1735.

(245) Baughman, R. H.; Cui, C.; Zakhidov, A. A.; Iqbal, Z.; Barisci, J. N.; Spinks, G. M.; Wallace, G. G.; Mazzoldi, A.; De Rossi, D.; Rinzler, A. G. *Science* **1999**, *284*, 1340.

(246) Smela, E. *Journal of Micromechanics and Microengineering* **1999**, *9*, 1.

(247) Svennersten, K.; Berggren, M.; Richter-Dahlfors, A.; Jager, E. W. *Lab on a Chip* **2011**, *11*, 3287.

(248) Jager, E. W.; Smela, E.; Inganäs, O. *Science* **2000**, *290*, 1540.

(249) Yamada, M.; Kondo, M.; Mamiya, J. i.; Yu, Y.; Kinoshita, M.; Barrett, C. J.; Ikeda, T. *Angewandte Chemie International Edition* **2008**, *47*, 4986.

(250) Nawroth, J. C.; Lee, H.; Feinberg, A. W.; Ripplinger, C. M.; McCain, M. L.; Grosberg, A.; Dabiri, J. O.; Parker, K. K. *Nature Biotechnology* **2012**, *30*, 792.

(251) Takashima, Y.; Hatanaka, S.; Otsubo, M.; Nakahata, M.; Kakuta, T.; Hashidzume, A.; Yamaguchi, H.; Harada, A. *Nature Communications* **2012**, *3*, 1270.

(252) Lima, M. D.; Li, N.; De Andrade, M. J.; Fang, S.; Oh, J.; Spinks, G. M.; Kozlov, M. E.; Haines, C. S.; Suh, D.; Foroughi, J. *Science* **2012**, *338*, 928.

(253) Lendlein, A.; Jiang, H.; Jünger, O.; Langer, R. *Nature* **2005**, *434*, 879.

(254) Beebe, D. J.; Moore, J. S.; Bauer, J. M.; Yu, Q.; Liu, R. H.; Devadoss, C.; Jo, B.-H. *Nature* **2000**, *404*, 588.

(255) Russell, T. *Science* **2002**, *297*, 964.

(256) Osada, Y.; Matsuda, A. *Nature* **1995**, *376*, 219.

(257) Liu, K.; Cheng, C.; Cheng, Z.; Wang, K.; Ramesh, R.; Wu, J. *Nano Letters* **2012**, *12*, 6302.

(258) Wang, Z.; Zhang, J.; Li, J.; Xie, J.; Li, Y.; Liang, S.; Tian, Z.; Li, C.; Wang, Z.; Wang, T. *Journal of Materials Chemistry* **2011**, *21*, 1264.

(259) Wang, E.; Desai, M. S.; Lee, S.-W. *Nano Letters* **2013**, *13*, 2826.

(260) Serpe, M. J.; Yarmey, K. A.; Nolan, C. M.; Lyon, L. A. *Biomacromolecules* **2005**, *6*, 408.

(261) Islam, M. R.; Li, X.; Smyth, K.; Serpe, M. J. *Angewandte Chemie International Edition* **2013**, *52*, 10330.

(262) Islam, M. R.; Serpe, M. J. *Chem. Commun.* **2013**, *49*, 2646.

(263) Islam, M. R.; Serpe, M. J. *Macromolecules* **2013**, *46*, 1599.

(264) Fuhrer, R.; Athanassiou, E. K.; Luechinger, N. A.; Stark, W. J. *Small* **2009**, *5*, 383.

(265) Alben, S.; Balakrisnan, B.; Smela, E. *Nano Letters* **2011**, *11*, 2280.

(266) Yakacki, C. M.; Satarkar, N. S.; Gall, K.; Likos, R.; Hilt, J. Z. *Journal of Applied Polymer Science* **2009**, *112*, 3166.

(267) Fukushima, T.; Asaka, K.; Kosaka, A.; Aida, T. *Angewandte Chemie International Edition* **2005**, *44*, 2410.

(268) Yoshida, R.; Uchida, K.; Kaneko, Y.; Sakai, K.; Kikuchi, A.; Sakurai, Y.; Okano, T. *Nature* **1995**, *374*, 240.

(269) Kopeček, J. *Nature* **2002**, *417*, 388.

(270) Hu, Z.; Zhang, X.; Li, Y. *Science* **1995**, *269*, 525.

(271) Thérien-Aubin, H.; Wu, Z. L.; Nie, Z.; Kumacheva, E. *Journal of the American Chemical Society* **2013**, *135*, 4834.

(272) Kumpfer, J. R.; Rowan, S. J. *Journal of the American Chemical Society* **2011**, *133*, 12866.

(273) Ma, Y.; Zhang, Y.; Wu, B.; Sun, W.; Li, Z.; Sun, J. *Angewandte Chemie International Edition* **2011**, *50*, 6254.

(274) Jaber, J. A.; Schlenoff, J. B. *Macromolecules* **2005**, *38*, 1300.

(275) Sorrell, C. D.; Carter, M. C.; Serpe, M. J. *ACS Applied Materials & Interfaces* **2011**, *3*, 1140.

(276) Chun, I. S.; Challa, A.; Derickson, B.; Hsia, K. J.; Li, X. *Nano Letters* **2010**, *10*, 3927.

(277) Leong, T. G.; Zarafshar, A. M.; Gracias, D. H. *Small* **2010**, *6*, 792.

(278) Cho, J.-H.; Azam, A.; Gracias, D. H. *Langmuir* **2010**, *26*, 16534.

(279) Cho, J. H.; Keung, M. D.; Verellen, N.; Lagae, L.; Moshchalkov, V. V.; Van Dorpe, P.; Gracias, D. H. *Small* **2011**, *7*, 1943.

(280) Bashir, R.; Hilt, J. Z.; Elibol, O.; Gupta, A.; Peppas, N. A. *Applied Physics Letters* **2002**, *81*, 3091.

(281) Singamaneni, S.; McConney, M. E.; LeMieux, M. C.; Jiang, H.; Enlow, J. O.; Bunning, T. J.; Naik, R. R.; Tsukruk, V. V. *Advanced Materials* **2007**, *19*, 4248.

(282) Harris, K. D.; Bastiaansen, C. W. M.; Lub, J.; Broer, D. J. *Nano Letters* **2005**, *5*, 1857.

(283) Yamada, M.; Kondo, M.; Mamiya, J.-i.; Yu, Y.; Kinoshita, M.; Barrett, C. J.; Ikeda, T. *Angewandte Chemie International Edition* **2008**, *47*, 4986.

(284) Islam, M. R.; Li, X.; Smyth, K.; Serpe, M. J. *Angewandte Chemie International Edition* **2013**, *125*, 10520.

(285) Ionov, L. *Advanced Functional Materials* **2013**, *23*, 4555.

(286) Hu, Z.; Zhang, X.; Li, Y. *Science* **1995**, *269*, 525.

(287) Thomsen, D. L.; Keller, P.; Naciri, J.; Pink, R.; Jeon, H.; Shenoy, D.; Ratna, B. R. *Macromolecules* **2001**, *34*, 5868.

(288) Zhu, Y.; Hu, J. L.; Yeung, K. W.; Liu, Y. Q.; Liem, H. M. *Journal of Applied Polymer Science* **2006**, *100*, 4603.

(289) Ji, F. L.; Hu, J. L.; Li, T. C.; Wong, Y. W. *Polymer* **2007**, *48*, 5133.

(290) Xie, T. *Polymer* **2011**, *52*, 4985.

(291) Stroganov, V.; Al-Hussein, M.; Sommer, J.-U.; Janke, A.; Zakharchenko, S.; Ionov, L. *Nano Letters* **2015**, *15*, 1786.

(292) Schwartz, G.; Tee, B. C. K.; Mei, J.; Appleton, A. L.; Kim, D. H.; Wang, H.; Bao, Z. *Nature Communications* **2013**, *4*, 1859.

(293) Takei, K.; Takahashi, T.; Ho, J. C.; Ko, H.; Gillies, A. G.; Leu, P. W.; Fearing, R. S.; Javey, A. *Nature Materials* **2010**, *9*, 821.

(294) Xiao, X.; Yuan, L.; Zhong, J.; Ding, T.; Liu, Y.; Cai, Z.; Rong, Y.; Han, H.; Zhou, J.; Wang, Z. L. *Advanced Materials* **2011**, *23*, 5440.

(295) Yamada, T.; Hayamizu, Y.; Yamamoto, Y.; Yomogida, Y.; Izadi-Najafabadi, A.; Futaba, D. N.; Hata, K. *Nature Nanotechnology* **2011**, *6*, 296.

(296) Kim, D.-H.; Ahn, J.-H.; Choi, W. M.; Kim, H.-S.; Kim, T.-H.; Song, J.; Huang, Y. Y.; Liu, Z.; Lu, C.; Rogers, J. A. *Science* **2008**, *320*, 507.

(297) Kim, D.-H.; Rogers, J. A. *Advanced Materials* **2008**, *20*, 4887.

(298) Sekitani, T.; Someya, T. *Advanced Materials* **2010**, *22*, 2228.

(299) Kim, D.-H.; Lu, N.; Ma, R.; Kim, Y.-S.; Kim, R.-H.; Wang, S.; Wu, J.; Won, S. M.; Tao, H.; Islam, A.; Yu, K. J.; Kim, T.-i.; Chowdhury, R.; Ying, M.; Xu, L.; Li, M.; Chung, H.-J.; Keum, H.; McCormick, M.; Liu, P.; Zhang, Y.-W.; Omenetto, F. G.; Huang, Y.; Coleman, T.; Rogers, J. A. *Science* **2011**, *333*, 838.

(300) Hammock, M. L.; Chortos, A.; Tee, B. C. K.; Tok, J. B. H.; Bao, Z. *Advanced Materials* **2013**, *25*, 5997.

(301) Khang, D.-Y.; Jiang, H.; Huang, Y.; Rogers, J. A. *Science* **2006**, *311*, 208.

(302) Zhong, J.; Zhong, Q.; Hu, Q.; Wu, N.; Li, W.; Wang, B.; Hu, B.; Zhou, J. *Advanced Functional Materials* **2015**, *25*, 1798.

(303) Yan, C.; Wang, J.; Kang, W.; Cui, M.; Wang, X.; Foo, C. Y.; Chee, K. J.; Lee, P. S. *Advanced Materials* **2014**, *26*, 2022.

(304) Wang, X.; Hu, H.; Shen, Y.; Zhou, X.; Zheng, Z. *Advanced Materials* **2011**, *23*, 3090.

(305) Graz, I. M.; Cotton, D. P. J.; Lacour, S. P. *Applied Physics Letters* **2009**, *94*, 071902.

(306) Solovev, A. A.; Sanchez, S.; Pumera, M.; Mei, Y. F.; Schmidt, O. G. *Advanced Functional Materials* **2010**, *20*, 2430.

(307) Smith, E. J.; Liu, Z.; Mei, Y. F.; Schmidt, O. G. *Applied Physics Letters* **2009**, *95*, 083104.

(308) Zakharchenko, S.; Puretskiy, N.; Stoychev, G.; Stamm, M.; Ionov, L. *Soft Matter* **2010**, *6*, 2633.

(309) Stoychev, G.; Zakharchenko, S.; Turcaud, S.; Dunlop, J. W. C.; Ionov, L. *ACS Nano* **2012**, *6*, 3925.

(310) Cendula, P.; Kiravittaya, S.; Mönch, I.; Schumann, J.; Schmidt, O. G. *Nano Letters* **2011**, *11*, 236.

(311) Lu, J.; Wang, X.; Xiao, C. *Carbohydrate Polymers* **2008**, *73*, 427.

(312) Yeo, S. C.; Eisenberg, A. *Journal of Macromolecular Science, Part B* **1977**, *13*, 441.

(313) Hatakeyama, T.; Nakamura, K.; Yoshida, H.; Hatakeyama, H. *Thermochimica Acta* **1985**, *88*, 223.

(314) Nakamura, K.; Hatakeyama, T.; Hatakeyama, H. *Polym J* **1991**, *23*, 253.

(315) Lambricht, N.; Pardoen, T.; Yunus, S. *Acta Materialia* **2013**, *61*, 540.

(316) Gorrn, P.; Cao, W.; Wagner, S. *Soft Matter* **2011**, *7*, 7177.

(317) Koetting, M. C.; Peters, J. T.; Steichen, S. D.; Peppas, N. A. *Materials*

Science and Engineering: R: Reports **2015**, *93*, 1.

(318) Ahn, S.-k.; Kasi, R. M.; Kim, S.-C.; Sharma, N.; Zhou, Y. *Soft Matter* **2008**, *4*, 1151.

(319) Bashir, R.; Hilt, J.; Elibol, O.; Gupta, A.; Peppas, N. *Applied Physics Letters* **2002**, *81*, 3091.

(320) Stieger, M.; Richtering, W.; Pedersen, J. S.; Lindner, P. *The Journal of Chemical Physics* **2004**, *120*, 6197.

(321) Bajpai, A.; Shukla, S. K.; Bhanu, S.; Kankane, S. *Progress in Polymer Science* **2008**, *33*, 1088.

(322) Hamidi, M.; Azadi, A.; Rafiei, P. *Advanced Drug Delivery Reviews* **2008**, *60*, 1638.

(323) Liu, Z.; Calvert, P. *Advanced Materials* **2000**, *12*, 288.

(324) Myung, D.; Waters, D.; Wiseman, M.; Duhamel, P. E.; Noolandi, J.; Ta, C. N.; Frank, C. W. *Polymers for Advanced Technologies* **2008**, *19*, 647.

(325) Kozhunova, E. Y.; Makhaeva, E. E.; Khokhlov, A. R. *Polymer* **2012**, *53*, 2379.

(326) Tominaga, T.; Tirumala, V. R.; Lee, S.; Lin, E. K.; Gong, J. P.; Wu, W.-l. *The Journal of Physical Chemistry B* **2008**, *112*, 3903.

(327) Liu, M.; Su, H.; Tan, T. *Carbohydrate Polymers* **2012**, *87*, 2425.

(328) Chen, J.; Liu, M.; Liu, H.; Ma, L.; Gao, C.; Zhu, S.; Zhang, S. *Chemical Engineering Journal* **2010**, *159*, 247.

(329) Haque, M. A.; Kurokawa, T.; Gong, J. P. *Polymer* **2012**, *53*, 1805.

(330) Dragan, E. S. *Chemical Engineering Journal* **2014**, *243*, 572.

(331) Flory, P. J. *Cornell University Press: London* **1986**.

(332) Wandrey, C.; Hernandez-Barajas, J.; Hunkeler, D. In *Radical polymerisation polyelectrolytes*; Springer: 1999, p 123.

(333) Kim, S. J.; Yoon, S. G.; Kim, I. Y.; Kim, S. I. *Journal of Applied Polymer*

Science **2004**, *91*, 2876.

(334) Kim, S. J.; Yoon, S. G.; Lee, Y. M.; An, K. H.; Kim, S. I. *Journal of Applied Polymer Science* **2003**, *90*, 1389.

(335) Maeda, S.; Hara, Y.; Sakai, T.; Yoshida, R.; Hashimoto, S. *Advanced Materials* **2007**, *19*, 3480.

(336) Yoon, C.; Xiao, R.; Park, J.; Cha, J.; Nguyen, T. D.; Gracias, D. H. *Smart Materials and Structures* **2014**, *23*, 094008.

(337) Wang, J.; Lin, L.; Cheng, Q.; Jiang, L. *Angewandte Chemie International Edition* **2012**, *51*, 4676.

(338) Ma, C.; Shi, Y.; Pena, D. A.; Peng, L.; Yu, G. *Angewandte Chemie International Edition* **2015**, *127*, 7484.

(339) Kang, H.-W.; Tabata, Y.; Ikada, Y. *Biomaterials* **1999**, *20*, 1339.

(340) Theato, P.; Sumerlin, B. S.; O'Reilly, R. K.; Epps, I. I. I. T. H. *Chemical Society Reviews* **2013**, *42*, 7055.

(341) Hoare, T.; Pelton, R. *Macromolecules* **2004**, *37*, 2544.

(342) Lyon, L. A.; Meng, Z. Y.; Singh, N.; Sorrell, C. D.; John, A. S. *Chemical Society Reviews* **2009**, *38*, 865.

(343) Suzuki, A.; Tanaka, T. *Nature* **1990**, *346*, 345.

(344) Tanaka, T.; Nishio, I.; Sun, S. T.; Uenonishio, S. *Science* **1982**, *218*, 467.

(345) Schmaljohann, D. *Advanced Drug Delivery Reviews* **2006**, *58*, 1655.

(346) Ganta, S.; Devalapally, H.; Shahiwala, A.; Amiji, M. *Journal of Controlled Release* **2008**, *126*, 187.

(347) Islam, M. R.; Gao, Y.; Li, X.; Serpe, M. J. *Journal of Materials Chemistry B* **2014**, *2*, 2444.

(348) Cheng, G.; Xue, H.; Li, G.; Jiang, S. *Langmuir* **2010**, *26*, 10425.

(349) Zhou, C.; Li, P.; Qi, X.; Sharif, A. R. M.; Poon, Y. F.; Cao, Y.; Chang, M. W.; Leong, S. S. J.; Chan-Park, M. B. *Biomaterials* **2011**, *32*, 2704.

(350) Lee, K. Y.; Mooney, D. J. *Chemical Reviews* **2001**, *101*, 1869.

(351) Reese, C. E.; Mikhonin, A. V.; Kamenjicki, M.; Tikhonov, A.; Asher, S. A. *Journal of the American Chemical Society* **2004**, *126*, 1493.

(352) Qiu, Y.; Park, K. *Advanced Drug Delivery Reviews* **2001**, *53*, 321.

(353) Wu, C.; Zhou, S. *Macromolecules* **1995**, *28*, 8381.

(354) Hoare, T.; Pelton, R. *Macromolecules* **2007**, *40*, 670.

(355) Gao, J.; Wu, C. *Macromolecules* **1997**, *30*, 6873.

(356) Alexeev, V. L.; Sharma, A. C.; Goponenko, A. V.; Das, S.; Lednev, I. K.; Wilcox, C. S.; Finegold, D. N.; Asher, S. A. *Analytical Chemistry* **2003**, *75*, 2316.

(357) Zhang, J.-T.; Smith, N.; Asher, S. A. *Analytical Chemistry* **2012**, *84*, 6416.

(358) Islam, M. R.; Lu, Z.; Li, X.; Sarker, A. K.; Hu, L.; Choi, P.; Li, X.; Hakobyan, N.; Serpe, M. J. *Analytica Chimica Acta* **2013**, *789*, 17.

(359) Ringsdorf, H.; Simon, J.; Winnik, F. M. *Macromolecules* **1992**, *25*, 7306.

(360) Sorrell, C.; Serpe, M. *Analytical Bioanalytical Chemistry* **2012**, *402*, 2385.

(361) Islam, M. R.; Serpe, M. J. *Macromolecules* **2013**, *46*, 1599.

(362) Islam, M. R.; Serpe, M. J. *Chemical Communications* **2013**, *49*, 2646.

(363) Zhang, Q. M.; Xu, W.; Serpe, M. J. *Angewandte Chemie International Edition* **2014**, *53*, 4827.

(364) Hu, L.; Serpe, M. J. *Journal of Materials Chemistry* **2012**, *22*, 8199.

(365) Sorrell, C. D.; Carter, M. C. D.; Serpe, M. J. *Advanced Functional Materials* **2011**, *21*, 425.

(366) Behl, M.; Lendlein, A. *Materials Today* **2007**, *10*, 20.

(367) Miyata, T.; Jikihara, A.; Nakamae, K.; Hoffman, A. S. *Macromolecular Chemistry and Physics* **1996**, *197*, 1135.

(368) Nabid, M. R.; Entezami, A. A. *Journal of Applied Polymer Science* **2004**, *94*, 254.